Towards Controlling the Growth of Silica-carbonate and Vaterite Microstructures

Alicia McTaggart

A Thesis
in
The Department
of
Chemistry and Biochemistry

Presented in Partial Fulfillment of the Requirements
for the Degree of Master Science (Chemistry) at
Concordia University
Montréal, Québec, Canada

July 04, 2019

CONCORDIA UNIVERSITY

School of Graduate Studies

This is to certify that the thesis prepared

By: Alicia McTaggart

Entitled: Towards Controlling the Growth of Silica-carbonate and Vaterite Microstructures

and submitted in partial fulfillment of the requirements for the degree of

Master of Science (Chemistry)

complies with the regulations of the University and meets the accepted standards with respect to originality and quality.

Signed by the final examining committee:

Dr. Heidi Muchall Chair

Dr. Yves Gelinas Examiner

Dr. Rafik Naccache Examiner

Dr. Louis Cuccia Supervisor

Approved by Dr. Yves Gelinas
Chair of Department or Graduate Program Director

July 2019 André G. Roy
Dean of Faculty

ABSTRACT

Towards Controlling the Growth of Silica-carbonate and Vaterite Microstructures

Alicia McTaggart

Spurred by lessons learnt from the ability of nature to "design" biominerals with a high degree of control over their shape, size, mineral phase and hierarchical assembly over multiple length scales, a multitude of bottom-up research strategies have been geared towards developing self-assembled inorganic materials. The self-assembly route could lead to materials with novel functionality and complexity for applications in fields such as photonics, electronics and photovoltaics. Of particular interest in our labs are biomimetic 3D nanocrystalline composite materials, characterized by long-range orientational order and highly curved surfaces. These composite materials can be synthesized from the coupled reaction of the carbonates of barium, strontium and aragonite-type calcium carbonate with silica in alkaline (pH *ca.* 10–12) environments under the influence of atmospheric CO_2. It has been shown that the complexity of these microstructures can be enhanced under dynamic reaction-diffusion conditions. To replicate this approach, we aim to characterize the effect of changes in solution conditions (*i.e.* pH, CO_2 concentration and temperature) on the growth, structural morphology and the hierarchical organization of silica-carbonate biomorphs. The interaction between the organic and inorganic components of biological systems leads to some of the most beautiful (and often chiral) patterns seen in nature, as demonstrated by snail shells and the chiral narwhal tusk. Attempts to control the handedness of the helices during their formation involved the use of enantiomerically pure amino acids at the molecular level and chiral vaterite crystal templates at the mesoscale, to break the symmetry towards helices of a single handedness. Finally, we aim to show how the size and predominant morphologies of silica-carbonate microstructures was tuned as a function of concentration of Chicago Sky Blue (CSB; a sulphonated azo dye) in addition to its method of incorporation in the crystallization solution. This research also provides indirect evidence for accelerated growth rates of the microstructures from solutions containing dye as demonstrated by an increase in size relative to control experiments without dye during a growth period of 1.5–2 hours. Light and scanning electron microscopies were the principal tools used for the characterization of the as-formed biomorphs.

DEDICATION

I would like to extend special gratitude to my supervisor at Concordia, Dr. Louis Cuccia for being generous with his vast stores of knowledge, guidance, friendship, and photos of his dog, Finnegan, and for always believing in me during the course of my degree. Special thanks as well to Dr. Noorduin for supervising and allowing me to conduct my research stage in his lab at AMOLF, and to Lukas Helmbrecht, his Ph.D. student for his co-supervision. All three worked tirelessly in providing me with excellent feedback and encouragement that were instrumental in putting together this thesis. My fondness for expressos was aided and abetted not only by the many invitations to Louis' Cup, but also by Wim and Lukas who pride themselves on always striving to add more tools to their coffee-making skillsets.

Our summer students Poh Ying, and Mia Stankovich also deserve my thanks for helping to grow chiral vaterite and silica-carbonate microstructures, respectively. Additionally, many thanks to Dr. Wenge Jiang (Dr. Marc McKee Lab at McGill Univeristy) for teaching me his methodology to make chiral vaterite.

There are also a few other people in particular whom I would like to thank. Rolf Schmidt, who was always available to demonstrate the technical details on how to use various instruments and softwares. David Liu (supervisor, Scanning Electron Microscope Facilities at McGill University) and the DeWolf Lab for allowing me to use their microscope.

I am grateful to have been a part of the wonderful community of knowledgeable and helpful scientists, technicians, and other support staff at Concordia University.

Finally, I thank my family for their love, support and kindness. In particular, I dedicate this thesis to my beloved nephew, Adrian Alex Hyde, who will continue to live on in a space and time that exist beyond the fidelity of our memories, dreams, love, and even mortality itself.

Chapter 1. Introduction

Contents

1.1. Growth and form of minerals

The natural world has served as a point of fascination for ages, from life that evolved about 3.6 million years ago, to the plethora of mineralized architectures from both biotic and abiotic origins. In the 18th century, D'Arcy Thompson, a prominent, scientist and mathematician, was primarily preoccupied with relating the form of biological specimens, such as mollusc shells, to a set of mathematical principles that could adequately describe their growth. Much of D'Arcy's work can be found in his famous book "Growth and Form", which continues to serve as a source of inspiration for scientists today.[1] However, the challenges of today's material scientists is not only to understand the growth of structures, specifically minerals in our case, but also to recreate them using the guiding principles of nature.

Minerals can be separated into two categories based on their origins: from living things (biominerals); and from the non-living world (geological minerals). Geological minerals (Figure 1a) are typically characterized by flat planes bound by defined edges, whereas biominerals (Figure 1b) are most often associated with a lack of identifiable facets, and instead display smooth curvature, which is an ambiguous indicator of the presence of life.[2]

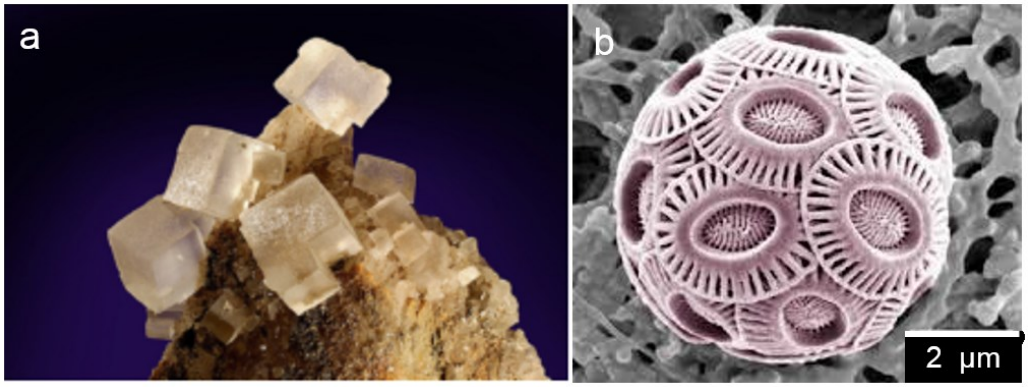

Figure 1. Types of minerals: A) Halite (NaCl), more commonly known as salt is a geological mineral that forms upon the evaporation of ocean water and sometimes leads to the formation of huge deposits of "rock salt"; and B) the secretion of calcium carbonate by a type of marine algae results in elaborate shell-like structures known as a coccolithes, which is an example of a biological mineral. Figure 1a was taken from ref,[3] while Figure 1b) was taken from ref.[4]

1.2. Biomineralization

Biomineralization is the process by which inorganic minerals are produced and secreted in a biological environment leading to the construction of a variety of structures such as teeth, oyster

shells, coral, ivory, sea urchin spines, cuttlefish bone, limpet, magnetic crystals in magnetotactic bacteria, and human bone.[5-8] Multicellular organisms developed the ability to control precipitation *en route* to more intricate mineralized structures after their populations became significantly more diverse about 540 million years ago.[9-10] These complex structures enable living organisms to perform more advanced functions, not limited to hearing, navigation and the protection of embryos in a process called biologically controlled mineralization.[5, 11-12] Biominerals also play key roles in mechanical support and self-protection.[13-16]

1.3. Control of mineral growth

1.3.1. Biominerals

Many minerals exist in nature, including oxides, phosphates, carbonates and silicates,[17] and are often composite materials, since they contain both inorganic and organic components, where the sum of the individual parts are assemblies of intriguing hierarchical shapes and structures.[6, 8, 18] Biomolecules have been implicated in the rigorous control of the structural and morphological organization of the mineral phase in biomineralization processes.[17] Indeed, there are many examples where acidic proteins have been demonstrated to be critical in the evolution of the mineral phase, more specifically its nucleation, growth and assembly.[16, 19-20] Although these principles are not understood entirely, it is generally accepted that they are at least happening. For example, the organic and mineral constituents of biominerals arrange themselves *via* weak, non-covalent interactions into ordered structures in a process known as self-assembly. Not surprisingly, additive-controlled crystallization and self-assembly forms the basis of most mimetic biomineralization (*i.e.* biomimetic) strategies that are focused on efforts to recreate materials with the advantages (*i.e.* unparalleled material properties, highly ordered shapes, green synthesis using simple building blocks)[18] and fidelity seen in nature.[21-22]

1.3.2. Soluble additives: biomineral extracts and analogues

The use of soluble additives in crystallization processes affords an experimentally simple and multifaceted strategy to control polymorph selectivity, and the morphologies and sizes of crystals.[23] Some of the earliest approaches to biomimetic mineralization involved growing crystals in the presence of soluble protein extracts from organisms involved in biomineralization[24-25] and also small molecule analogues of these biomineral-inducing proteins.[26] An example of this was

demonstrated by Mann and co-workers where they used proteins containing several acidic aspartic acid residues to induce the growth of calcite that resembles human otaconia.[26] Nevertheless, the inorganic crystals in many of these studies failed to replicate the unique properties of biominerals, where emphasis was placed on viewing modifications in the morphology of crystals.[27-28] Though more recent research is paving the way to generating more elaborate architectures with similar properties to those seen in biominerals,[22, 29] there is much left to be understood regarding processes that drive the assembly of these materials. This is particularly the case if the precision and functionality found in nature are to be successfully reproduced and maybe even surpassed in the future.

1.4. Calcium carbonate mineralization

1.4.1. Precipitation

One of the most studied model systems for probing the effect of the addition of soluble additives involves calcium carbonate—the most ubiquitous biomineral found in nature. Calcium carbonate precipitation can occur *via* biologically controlled and induced mechanisms, whereas lower lifeforms rely on chemotactic means to mediate the synthesis of this biomineral. The major thermodynamic driving forces for the precipitation of $CaCO_3$ are the synergistic effects of phase-specific supersaturation and pH, where high pH increases the supersaturation of carbonate ion speciation, according to the following equilibrium reaction involving dissolved carbonates (Equation 1):[30]

Equation 1

$$CO_2\,(g) + H_2O\,(l) \rightleftharpoons H_2CO_3\,(aq) \rightleftharpoons H^+\,(aq) + HCO_3^-\,(aq) \rightleftharpoons 2H^-\,(aq) + CO_3^{2-}\,(aq)$$

Furthermore, the presence of CO_2 and H_2O give rise to carbonate ions, which leads to the crystallization of calcium carbonate upon combining with calcium, based on the following reaction (Equation 2):[30]

Equation 2

$$CO_3^{2-}\,(aq) + Ca^{2+}(aq) \rightleftharpoons CaCO_3\,(s)$$

1.4.2. Calcium carbonate polymorphism

Calcium carbonate mineralization is relevant not only in nature, but also has important applications in the paint, plastic, and paper industries,[31] and can cause major scaling problems. Furthermore, $CaCO_3$ exists in several crystal structures, each of which is a unique polymorph. Three biologically-relevant anhydrous polymorphs exist for $CaCO_3$: calcite, aragonite, and vaterite, in order of decreasing thermodynamic stability at ambient temperature.[32] Calcite (Figure 2a) has a rhombohedral crystal structure. The most thermodynamically favoured polymorph at elevated temperatures, aragonite (Figure 2b), crystalizes in the orthorhombic crystal system and constitutes the inorganic component that gives fresh water pearls their luster.[33-34] On the other hand, the presence of vaterite (Figure 2c) in pearls without lustre has been linked to anomalous $CaCO_3$ biomineralization.[35-36] Vaterite typically exists in the hexagonal crystal system and occurs in natural systems typically under extreme conditions regulated by the rigorous control of pH, temperature and pressure. Biologically controlled mineralization of $CaCO_3$ displays clear polymorph selectivity, which typically results in minerals of a single composition. However, in other systems, the nucleation and transition of metastable $CaCO_3$ (*i.e.* amorphous calcium carbonate (ACC) and vaterite) to more stable polymorphs (*i.e.* aragonite, calcite) has been shown to occur *via* dissolution-reprecipitation processes. This results in the formation of minerals of a mixed phase, which is undesirable in relevant applications where the crystal composition, size, morphology and orientation must be controlled in order to optimize the properties of the material.[37]

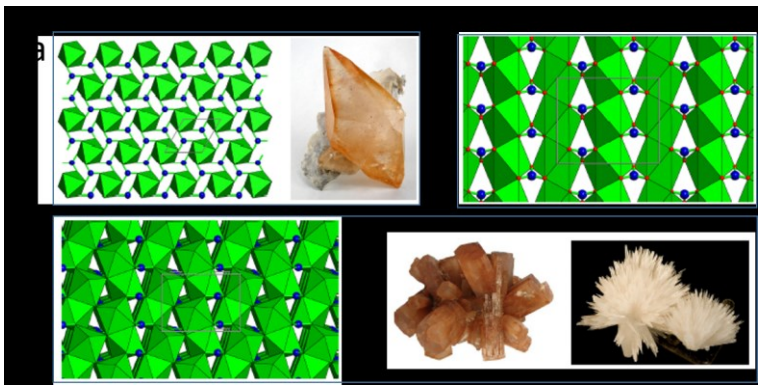

Figure 2. A) The crystal structure of calcite, and a calcite crystal that was taken from Elmwood Mine, Cathage, Tennessee. B) The structure of aragonite accompanied by typical crystal forms, tabular crystals from Tazauta Mine, Sefrou, Morocco (left), and acicular crystals from Transvall, South Africa. C) The crystal structure of vaterite. Blue spheres represent carbon, while the green polyhedra represent calcium-oxygen.[38]

A common strategy used to control different aspects of mineralized structures, such as polymorphism, size, and structural morphology/shape, involves the use of organic macromolecules. This stems from the knowledge obtained from numerous studies where it has been proven that biomolecules are integral in directing the nucleation and assembly of minerals in natural systems.[6, 25, 39-41] In some biominerals, the presence of these biomolecules leads to the development of specific structural properties, like chirality. An object is chiral if it cannot be superimposed on its mirror image. Interestingly, many of the chiral structures in nature, such as gastropod shells, DNA, amino acids and sugars tend towards homochirality.[8, 42-43] For instance, most gastropod shells are right-handed (Figure 3a),[44] which is postulated to originate at the genetic level and its ensuing effect on the expression of certain biomolecules that shape the inorganic minerals (Figure 3b).[45] One type of biomolecule present in shells are amphiphilic chitin nanocrystals that, along with proteins, form nucleation sites for directing the mineralization upon their self-assembly into liquid crystals at the growth fronts of shells.[8, 46] These step-wise processes lead to a spiral pattern that develops from a chitin-calcium carbonate lamellar structure.[47] Mankind's fascination with chiral properties dates back to 1811,[48] and was further enhanced by Louis Pasteur in 1848 when he manually separated sodium ammonium tartrate crystals into their left- and right-handed enantiomorphs based on the asymmetry of the crystal faces.[47]

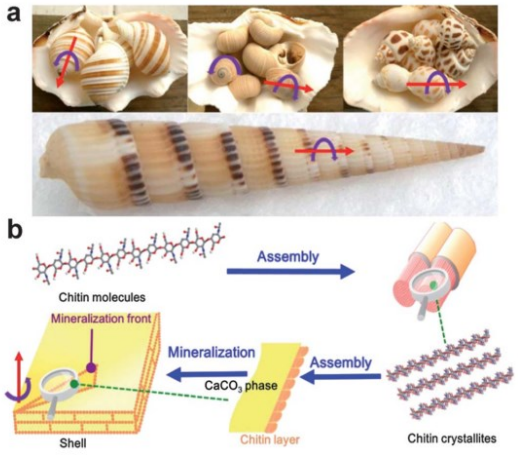

Figure 3. The chirality of gastropod shells and a schematic drawing of the shell mineralization front: A) general gastropod species have right-handed shells; and B) during the natural generation of shell structure β-chitin molecules assemble into supermolecules (chitin crystallites) and their liquid-crystal layers induce the spiral mineralization of calcium carbonate (this scheme is prepared based upon a mechanism proposed by Cartwright *et al.*).[47, 49]

The role of chiral carboxylated organic acids[50-53] on the chiral evolution of calcite crystals has been the subject of several investigations.[26, 50, 54-58] Orme and coworkers[53] used atomic force microscopy and molecular modeling to study calcite growth both in pure water and solutions of enantiopure aspartic acid. Here, rhombohedral calcite growth steps are mirror images about their glide plane in pure water. However, the opposite scenario developed from solutions with chiral aspartic acid, where the exact shape and spacing of the now asymmetric growth steps is dependent on whether L- or D-aspartic acid was used (Figure 4). These results support the conclusion that molecular chirality can sometimes lead to macroscopic chirality, an effect that is attributed to the selective binding of enantiopure amino acids to calcite growth steps. Furthermore, chiral etch pits developed upon the dissolution of the calcite crystals.

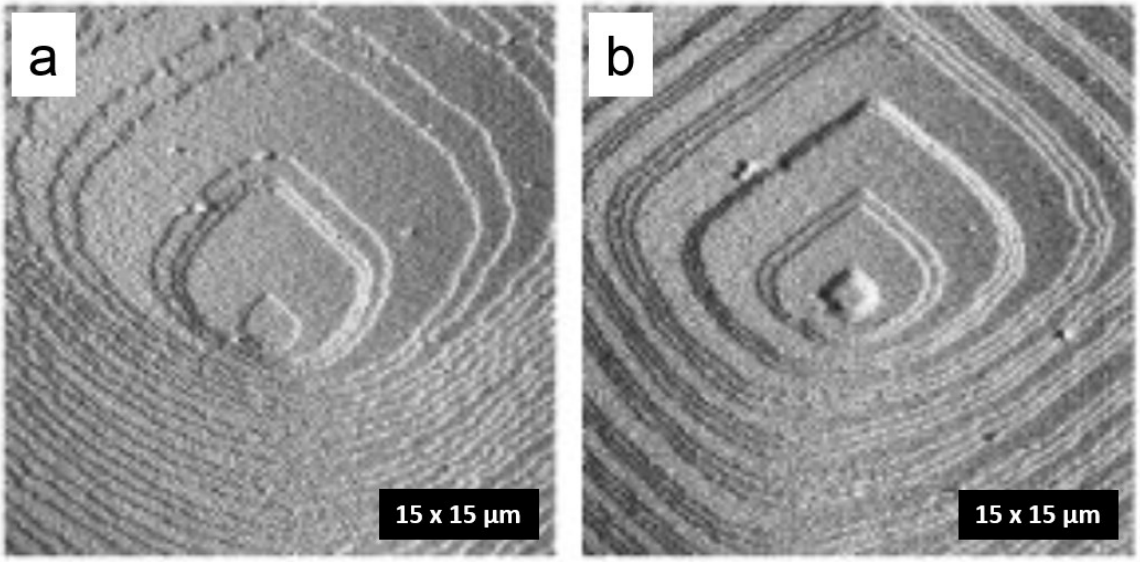

Figure 4. Atomic Force Microscopy of the growth steps in the cleavage face of calcite crystals grown in the presence of: A) L-aspartic acid or B) D-aspartic acid.[53]

Electrochemistry was applied by Kulp and coworkers as a method to control the deposition of calcite that lacks symmetry about its glide plane when grown from solutions containing chiral biomolecules such as enantiopure tartaric acid, maleic acid and aspartic acid.[59] Here the base, generated from the electrochemical splitting of water coupled with bicarbonate ions in the presence of calcium ions, leads to the formation of calcium carbonate according to the equations shown in Figure 5. The handedness of the spiral morphologies correlated with the chirality of the tartaric acid, maleic acid or aspartic acid additive (Figure 5). The handedness of the morphologies is likely

due to the enantioselective binding of the chiral organic molecules to certain chiral planes within the mineral, which produces non-symmetric mirror images.

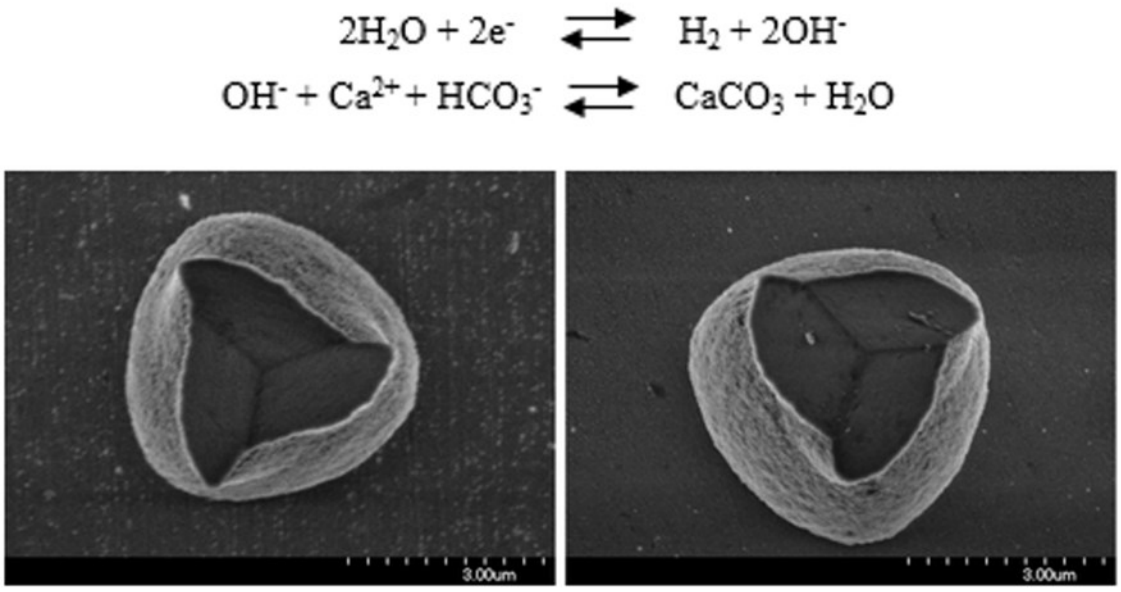

Figure 5. Deposition of chiral calcite possessing spiral-like morphologies by the electrochemical generation of base in the presence of: A) L-tartaric acid or B) D-tartaric acid.[59]

The role of chiral organic molecules in the chiral morphogenesis and polymorph selection of vaterite has also been investigated.[60] In the absence of chiral additive, or racemic preparations of the additive, rhombohedral calcite crystals were the only calcium carbonate polymorph observed at ambient temperature due to its greater thermodynamic stability. However, hierarchical vaterite with chiral spiral morphologies was the predominant polymorph that grew from solutions containing a single enantiomer of aspartic acid (Figure 6). It is proposed that the binding of chiral amino acid stabilises the as-generated nanoparticles and influences their tilt angles over several length scales to produce micron-sized chiral vaterite structures.

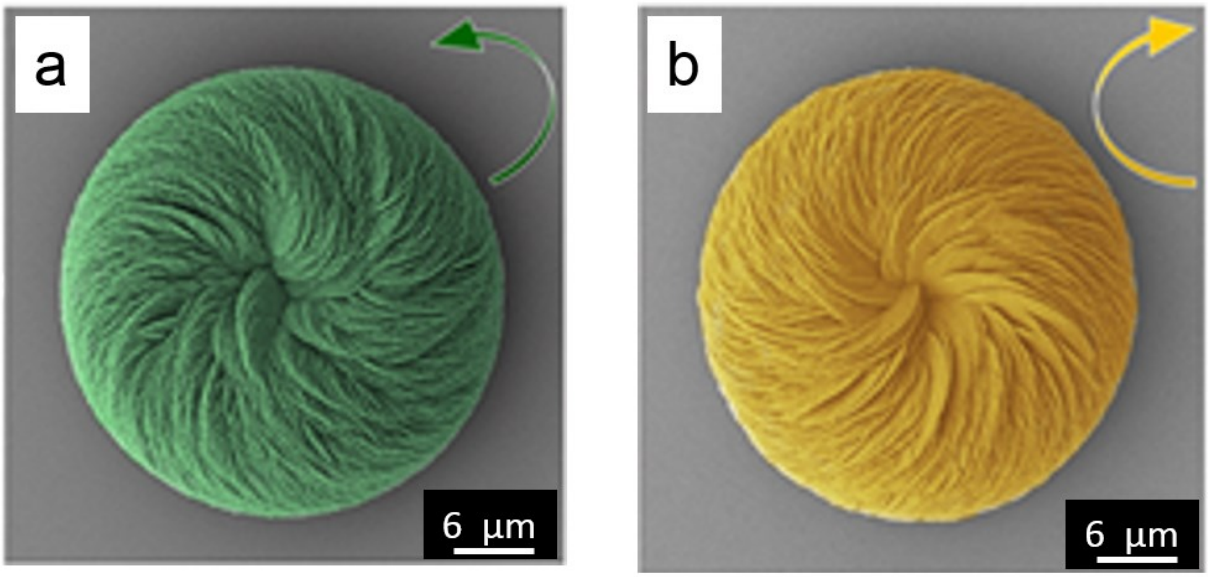

Figure 6. Left- and right-handed spiraling morphologies in vaterite toroids formed at pH 10 from $CaCl_2$-Na_2CO_3 mixtures in the presence of: A) L-aspartic acid or B) D-aspartic acid.[60]

1.5. Barium carbonate mineralization

1.5.1. Structure

While the influence of organic molecules on the mineralization of $CaCO_3$ is a popular choice of study due to inspiration and parallels drawn directly from nature, the role of inorganic additives on barium carbonate ($BaCO_3$) precipitation are far less explored topics of research. $BaCO_3$, another important natural mineral, bears a strong resemblance to aragonite due to its orthorhombic crystal structure.[61] Unlike calcium carbonate, this mineral does not display any sort of polymorphic behaviour, and has important applications in the production of ceramics, optical glass and other barium salts.[62-63] $BaCO_3$ is also used as a precursor in the production of superconductors.[64]

1.5.2. Silica

$BaCO_3$ precipitates from aqueous solutions as small, dendritic crystals. However, these crystals undergo a dramatic transformation to curvilinear structures in the presence of silicates at certain concentrations. Importantly, these structures are composite materials of *ca.* 10–20% silica, with $BaCO_3$ making up the rest. These crystal aggregates are coined as "silica biomorphs" due to their morphological resemblance (curved and non-faceted) to several biological forms.[65-69]

Furthermore, Garcia-Ruiz *et al.*[70-71] established a striking morphological and compositional convergence between silica biomorphs and some samples from the Precambrian Warrawoona Chert Formations of Western Australia, purported to be some of the oldest known putative microfossils in the world (Figure 7). These studies support the findings that the origin of life should not be based solely on structural morphology due to the indistinguishable nature of some of the recovered fossil samples to silica-carbonate biomorphs.[2, 71-72]

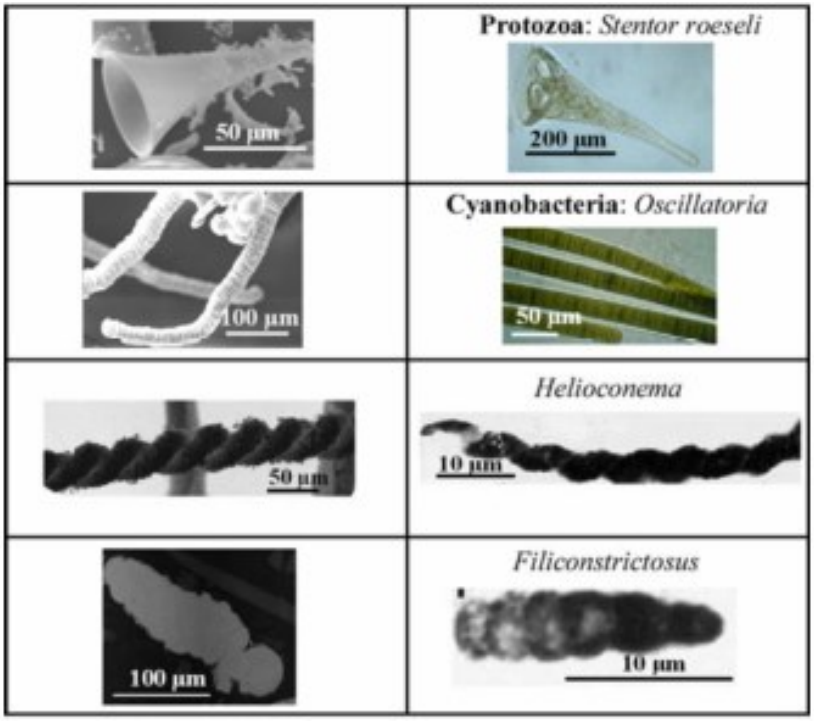

Figure 7. Representations of the morphological similarity of silica biomorphs (on the left) and both modern (Stentor roeseli and Oscillatoria) and ancient (Helioconema and Filiconstrictosus) biological forms.[69]

1.5.3. Synthesis

It has been shown that silica biomorphs can be afforded from simple experimental set-ups involving alkaline silica gel or solution preparations.[69, 73] Both methods require an alkaline earth carbonate (*i.e.* the chloride salts of barium, strontium or calcium at high temperature), a source of carbonate ions (*i.e.* usually atmospheric CO_2), and silica. A typical procedure for synthesising biomorphs involves adding a solution of barium chloride to a silica solution or gel, prepared by diluting commercial sodium silicate in water. In order to prepare the gel, the diluted sodium silicate must be acidified by the addition of HCl and left to equilibrate over days to the required pH (most often 10.5) (Figure 8a). The dissolution of CO_2 in the mixture, *via* the partially covered reaction

flask, creates a local concentration gradient along the solution/gel gas interface and raises the local supersaturation of carbonate and bicarbonate ions, which thus provokes the nucleation of the metal carbonate. Biomorphic structures arise from the coprecipitation and self-assembly of the metal carbonate and silica. Even more elegantly, Noorduin *et al.*[74] developed a method to grow silica-carbonate structures on substrates from solutions of silicate and alkaline earth metal chlorides, which significantly reduced both preparation and reaction times, while allowing for greater control over the evolution of shapes. The microstructures from these reactions show no loss of biomorphic development and character despite significantly diminished reaction times.

1.5.4. Morphology and chirality

The as-formed biomorphs exhibit similar, regular morphologies in both gel and solution, such as "worms", double helicoids, cardioid sheets and globular microstructures (Figure 8b). The racemic helicoids, which grow largest in gels, range from a few to several hundred microns,[69, 73] and are of variable thickness (10 – 60 μm).[69] Garcia-Ruiz *et al.*[66] noted that only left-handed helical braids were precipitated in silica gel to which barium or strontium ions were added in one of their earlier works. Although the number of helicoids was not given and there were no follow-up investigations on these results, it was particularly interesting that braids of only a single handedness were observed in the absence of biological molecules. Instead, the formation and hierarchical nature of these composite materials is believed to originate from various factors not limited to the presence of silica, pH, temperature and fluid dynamics.[2, 65-67, 69, 71, 75]

1.5.5. Organization and shape control

Garcia-Ruiz *et al.*[73] reported that silica concentrations above 300 ppm appear to be a key factor affecting the morphological and organizational outcome of carbonates under alkaline conditions (pH 10.5), where hundreds of carbonate nanorods form and aggregate into complex shapes. However, only dendritic and pseudo-hexagonal twinned carbonate crystals formed at lower silica concentrations. These findings were supported by Bittarello *et al.*[69] who found all the previously mentioned complex shapes precipitated only when the silica concentration of the solution was at least 5000 mgL^{-1} when mixed with $BaCl_2$ of a fixed concentration (100 mM), while dendrites, funnels and sheets were observed at lower silica concentrations.[69] The pH of silica sols decreases fairly slowly both spatially and temporally over the course of days, and even slower in

gels after a month, which suggests that local supersaturation remains constant as well. Furthermore, the observed microstructures formed in these reactions can grow and remain stable for long periods of time, subsequent to their nucleation from "complex" seeds that form when the pH is at least 10.5.

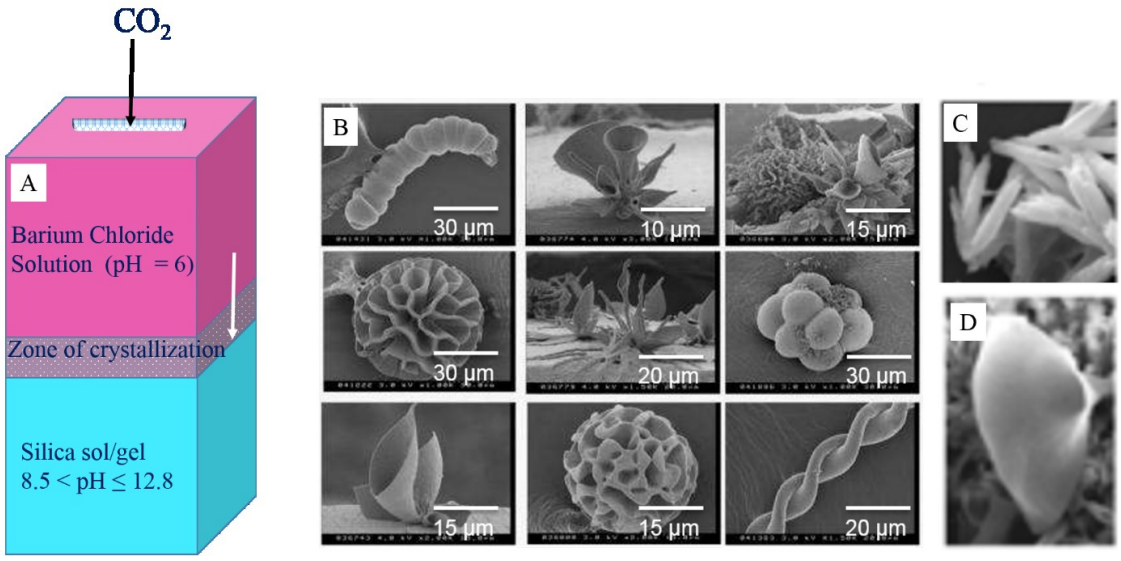

Figure 8. A) Schematic representation of a sample cassette where the diffusion of barium chloride and atmospheric CO_2 in the sol/gel causes the precipitation of biomorphs. B) Typical biomorphic composite silica-carbonate shapes formed under the influence of silica in alkaline sols/gels.[73] Morphological evolution as a consequence of silica content in mixtures of a constant barium carbonate concentration (100 mM): C) large carbonate dendrites formed after two days (silica concentration = 500 mgL^{-1}); and d) funnel-shaped microstructures that precipitated after four days (silica concentration = 4000 mgL^{-1}).[69]

The crystallization of silica biomorphs appears to be related to the fluid dynamics of the conditions under which they are grown (Figure 9).[69] For instance, regular morphologies (*i.e.* leaves and helices) only appear at room temperature in stagnant solutions of metal earth chloride and silicates. This is in direct contrast to stirred solutions or solutions that are warmed above room temperature where microstructures with irregular features develop. These findings imply that the crystallization of silica biomorphs is governed by diffusion-limited processes, where a significant concentration gradient is required to synthesise regular structures such as helicoids that develop at the ends of planar structures.

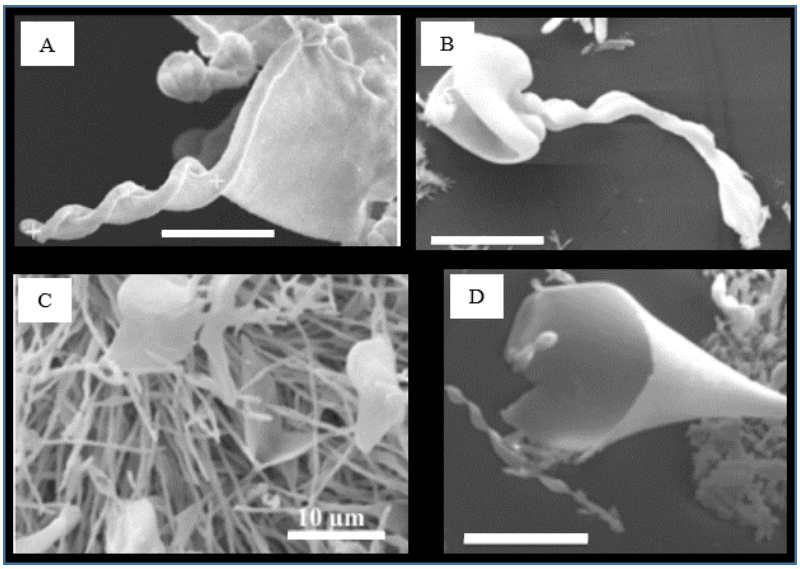

Figure 9. SEM images showing the influence of fluid dynamics on the morphology of silica-carbonate biomorphs: A) a regular helicoid formed in an unstirred solution; B) an irregular helicoid precipitated from a solution that was stirred; C) helical filaments formed when the temperature of the solution was set to 50 ºC; and D) funnel-shaped microstructures formed at high supersaturation in silica sol. Scale bars in the images are 50 µm (A and D), and 20 µm (B).[69]

The presence of multiple concentric bands is a ubiquitous feature of silica-carbonate leaves when viewed with an optical light microscope between crossed polarizers (Figure 10a). It is believed that these patterns are due to the hierarchical arrangement of the nanometric carbonate building blocks within the leaves and other biomorphs such as worms (Figure 10b) and double helices (Figure 10c). These nanometer-sized rods (typically 400 x 40 nm under additive-free conditions)[76] consist of pseudo-hexagonal, twinned single crystals of witherite, strontianite and aragonite. With regard to organization, the rods display orientational but no translational order such that each rod is slightly misaligned with respect to its neighbour and are arranged with their c-axis parallel to the long axis of the biomorph. It is this orientational order that gives rise to the radial pattern of the aforementioned leaves. Several studies suggest that biomorphs are nanoscale composites;[73, 75-77] the outer parts of the carbonate rods are sheathed in many single silica nanospheres (100 nm), which has also been shown to form a "skin" on the outer layer in some recovered silica-carbonate microstructures.[65-68, 71, 73, 75, 78] The presence of a silica skin appears to be more prevalent in crystallization recipes without additives.[76] In direct contrast to this, Kellermeier *et al.*[76] showed that the as-grown biomorphs, although grown in the presence of organic additives, formed outer monodisperse siliceous nanospheres (left of Figure 10d) and carbonate nanocrystallites in the inner core (right of Figure 10d).[76] Interestingly, the composite

nature of these structures can be demonstrated in dissolution experiments where a weak acid dissolves the carbonate nanorods while retaining a hollow silica skin (Figure 11a). Contrasting results develop when the biomorphs are immersed in a weakly basic solution which causes the dissolution of the outer silica skin, and the subsequent exposure of the carbonate nanocrystallites (Figure 11b), whose orientational order can be clearly seen in cross-sections of the untreated microstructures (Figure 11c).

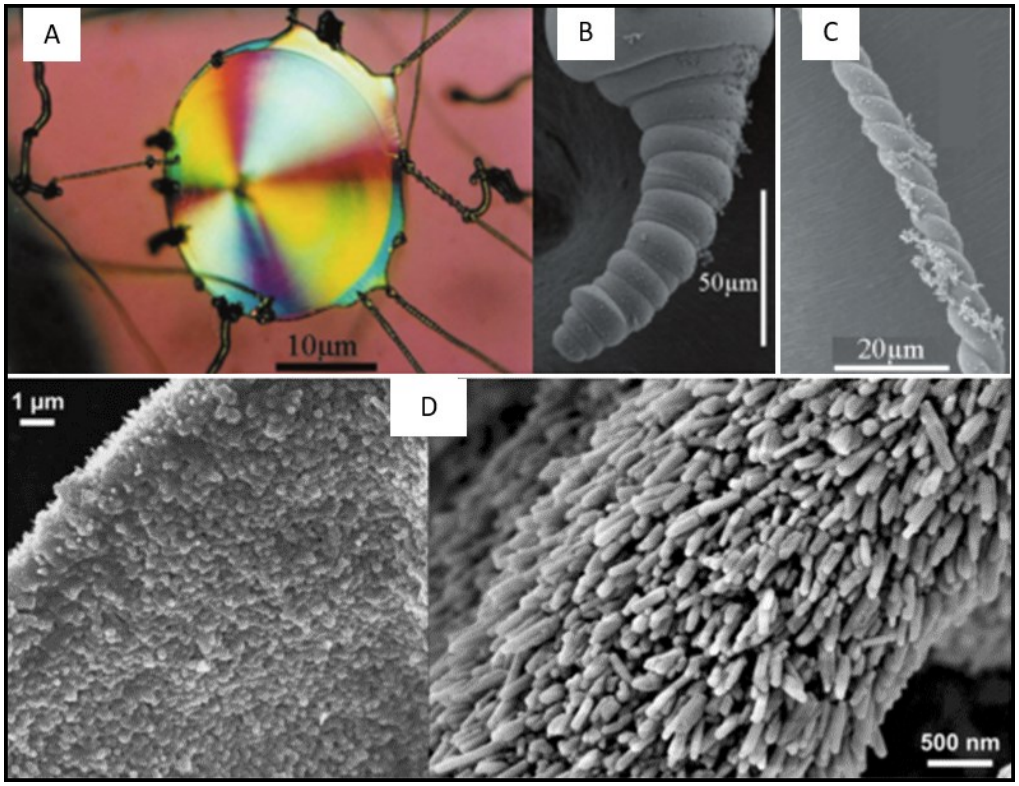

Figure 10. Optical light micrographs with a crossed polarizer and FESEM images depicting: leaf-like, worm-like and double helical silica-carbonate ultrastructures grown under additive-free conditions (A-C);[73] and the outer silica shell (left) and carbonate nanocrystallites (300–400 x 60–100 nm) in the inner core, exposed after dissolution of the shell in 0.1 M NaOH, (right) of biomorphs that were grown in the presence of organic additives for *ca.* six hours (D).[76]

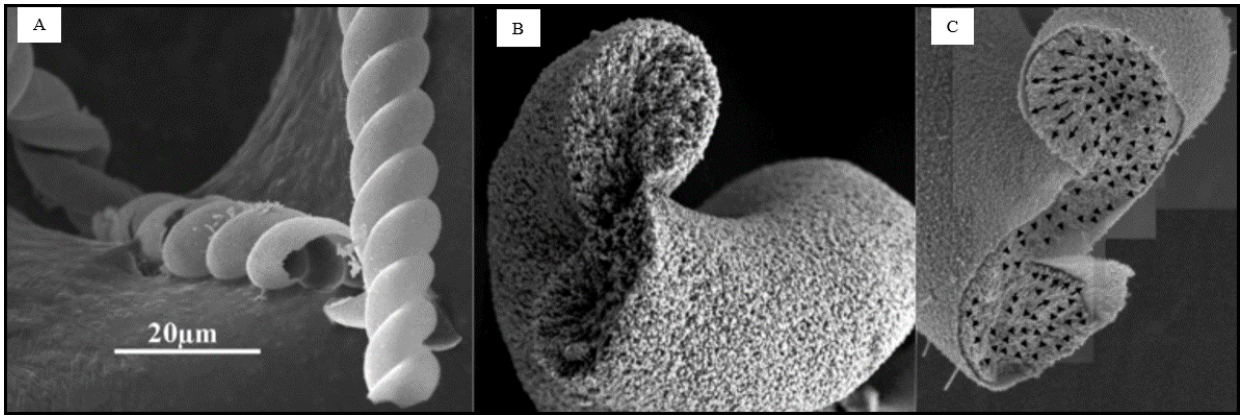

Figure 11. FESEM images showing: a hollow silica skin after dissolution of the carbonate nanorods in weak base (A); carbonate nanocrystallites after immersion and dissolution of the silica skin in dilute acid (B); and orientational order of the carbonate nanocrystals in a cross-section of a helical microstructure (C).[73]

1.5.6. Mechanistic overview

The mineralization of alkaline earth metals in silica-rich environments leads to very intricate ultrastructures with hierarchical textures similar to those found in biominerals, a subject which has been at the forefront of multiple research endeavours directed at understanding the underlying mechanisms governing these processes.[65-66, 68, 73, 76, 78-89] Garcia-Ruiz and coworkers[65-66] first theorised that the formation of biomorphic aggregates might be due to the inextricably linked processes of barium carbonate nucleation and growth, along with the simultaneous precipitation and speciation of polymeric silica. Moreover, it was noted by Voinescu *et al.*[68] that biomorphs only developed in water-ethanol mixtures, where tetraethyl orthosilicate (TEOS) was used as the source of silica, when the volume percentage of ethanol was sufficiently low. Silica polymerization was not unduly promoted so as to significantly outcompete or supress carbonate precipitation. This suggests that there is a certain threshold value of the silica/carbonate ratio that must be maintained, perhaps because of their coupled coprecipitation, in order to form biomorphs. Other theories concerning how the colloidal interaction[73] of silica and carbonate directs the growth and morphogenesis of biomorphs were confined to two basic scenarios: a “top-down” or a “bottom-up” approach. According to the top-down scenario, the evolution of biomorphs with complex shapes is templated by a preformed colloidal silica membrane that develops upon the addition of barium ions to solutions containing silicate species, and whose growth is mediated through cation screening of its negative charge.[73] Taking into account a study conducted by Bittarello *et al.*,[78] the increase in the nucleation frequency and the subsequent miniaturization of certain facets present in witherite, induced by its epitaxial adsorption on the silicate groups in

quartz, gives credence to the notion that the growth of biomorphs could be guided by their silica skin *via* a "top-down" method.[78] In the alternative "bottom-up" theory, the formation of hierarchically-structured silica-carbonate shapes is thought to originate from the interaction of silica species and crystalline barium carbonate nanorods, which self-assemble due to local constraints between crystallites.[73] Moreover, another study suggests that a combination of the two mechanisms in question could not be ruled out according to their findings, which further theorised that local variations in pH and charge are key to the morphological evolution of these curved shapes.[76] It should be noted that the "top-down" theory of biomorph formation was invalidated[79] on the basis that the presence of silica skins is due to the flocculation and formation of colloidal silica *via* a secondary mechanism. It is believed that a significant reduction in bulk pH, after about 7-8 hours of growth, marks the start of this mechanism, which appears to occur subsequent to the morphogenesis of these aggregate, upon which the silica spheres deposit in this latter stage of growth.

The scope of explorations into the nature of the mechanisms of biomorph formation was elevated in later years, when a more sophisticated model[90-91] was proposed and further expanded upon.[79-80, 92-94] With regard to these studies, the growth of biomorphs can be understood on a phenomenological and/or molecular basis.[95] The former mechanism involves the physical morphogenesis of biomorphs, starting from the nucleation and splitting of an alkali earth-metal carbonate seed, and its development to curved, hierarchical superstructures. On the other hand, the molecular basis hinges upon the coupled coprecipitation of carbonate and siliceous species due to an autocatalytic process governed by changes in global supersaturation arising from the pH-dependent solubilities of the reacting species.

1.5.7. Phenomenological model

There are two stages in the phenomenological formation of biomorphs: a fractal stage and a stage characterized by polycrystalline growth.[95] The earliest stage of growth, or the fractal stage, begins with the nucleation of a pseudo-hexagonal carbonate twinned crystal that undergoes continuous splitting *via* a dilation symmetry route due to "poisoning" by polymeric siliceous species. This method of growth accounts for globular shapes such as dendrites, dumbbells, cauliflowers, raspberries and closed spheres. There is very little or no silica incorporated in the crystal lattice of these structures, and the carbonate supersaturation remains relatively unchanged.

Eventually, all the available sites on the carbonate crystal are blocked by siliceous entities, and splitting is no longer possible. However, the crystal may develop a 2D lamina along some point of its structure marking the transition from fractal to the polycrystalline stage of growth, where numerous carbonate nanocrystallites form and interact with silica, thus giving rise to composite structures. The latter process is associated with both radial growth and linear advancement of the lamina, which further develops scroll-like features along its margins that either curl upwards or downwards. In the case where the constant radial velocity is almost equivalent to the tangential velocity throughout the growth period, circular leaf-like structures result. On the other hand, the rate of tangential growth may eventually supersede that in the radial direction, such that the growth fronts move towards a cusp and crash into each other, which then forces the growth fronts to curl upon themselves, thus forming helical structures.

The nature of the curling mechanism[91, 95] is postulated to influence the morphological outcome of silica-carbonate biomorphs. To expand upon this idea, it is proposed that when two growth fronts, with opposite handedness (*i.e.* curl towards the same side of the sheet), are of approximately equal heights and azimuthal/tangential velocities, which when greater than the radial velocity results in cardioids, results in the formation of sheets. However, if all the previously mentioned conditions are met, but the curling of the fronts are of the same sign, a regular double-helicoid forms. Moreover, Noorduin, Kaplan *et al.*[96] have modeled the emergence of biomorphic shapes, where several parameters, including pH-dependent bending deformations, determine the character of helical and other types of microstructures. For example, more regular double helices are formed at lower bending parameters (high pH) compared to higher ones, where an increase in pitch is expected and observed under experimental conditions.

Although it is known how the curling mechanism and development of structures with complex curvature may arise, the presence of leaf-like and helical microstructures nevertheless raises additional questions with regard to why these very different morphologies exist within a given pH range. Recent studies suggest that the morphogenesis of these aggregates is linked to the presence of extrinsic and intrinsic surfaces.[94] It was noted that leaves only form when the initial lamina develop on or close to extrinsic surfaces (*e.g.* solution or gel interfaces, on substrates, on the walls of reaction vessels, *etc.*), whereas helical structures originate far from such surfaces. These results are perhaps indicative of a lower barrier to continue growing on available extrinsic

surfaces in the case of leaves, or on intrinsic surfaces in the case of spirals, which propagate by curling upon themselves. Furthermore, these findings indicate that the morphogenesis of biomorphs may be controlled with micro-patterned substrates in a similar manner to that which was used by Han *et al*. to influence the growth of calcite.[58]

1.5.8. Autocatalytic coprecipitation model

The polycrystalline stage of biomorphic silica-carbonate structures correlates well with a growth mechanism based upon the autocatalytic nature of silica and carbonate coprecipitation under the influence of pH-induced changes, which is opposite for each of the main reactants because of their varying solubilities, on a global scale. Here, the nucleation of carbonate occurs with a decrease in pH, which induces the formation and condensation of silica to silanol. The polymerization and continuous removal of silanol necessitates the rise in local pH, which favours a new carbonate nucleation event. The self-generated process is continuously supported by a feedback mechanism, based upon the hydrogen carbonate/carbonate equilibrium and the decreasing solubility of silica, *via* the slow diffusion of carbon dioxide in a solution/gel of alkali earth-metal chloride and silicate ions. Finally, the subsequent lowering of the pH supplies building blocks to the growing surfaces of the composite. Unsurprisingly, numerous carbonate nanorods are produced in response to the carbonate supersaturation that remains high for many of the important steps of the growth process. The presence of silica has also been implicated in the shape-control,[77, 97] high nucleation frequency and size-confinement of these nanorods *via* a process where the face-selective adsorption[79] of silica provokes a reduction in the interfacial tension with respect to the supersaturated solution.[68, 78]

Initial support for a coupled reaction-coprecipitation process, as the fundamental mechanism involved in the formation and evolution of silica-carbonate microstructures, was mostly based on indirect evidence. For instance, it was expected that such a process would necessitate the formation of a silica sheath around individual nanorods, as suggested in one study.[95] [76] The occurrence of at least some amount of silica on the surface of these nanoparticles was later experimentally verified.[81] According to these findings, preformed barium carbonate ion pairs and/or clusters are stabilised and limited to a small size upon their assembly into nanoparticles due to both their confinement in a silica matrix and the deposition of silica around the nanoparticles, as confirmed by EDX, TEM and STEM measurements.[81] The presence of silica on the rods not

only induced uniformity of the nanoparticles, based on the silica concentration of the solution and silica composition of the rods, but also the blockage of their continued growth, even though the barium and carbonate supersaturation remains high. According to the authors, these events represent the driving force for the formation of biomorphs *via* the autocatalytic model. Furthermore, in analogous experiments,[98] where calcium carbonate was precipitated from solutions of very high supersaturation under the influence of silica, silica shells of concentration-dependent thickness were found on individual amorphous calcium carbonate (ACC) nanoparticles, which could be selectively dissolved to generate hollow silica spheres. This suggests that silica, and its role in a coupled reaction mechanism, cannot be ruled out. Moreover, the epitaxial growth of carbonate on quartz *via* its attachment to the silicate chains present therein, and *vice versa*, gives further credence to this notion.[78, 99] Additional evidence for this postulated mechanism comes from studies which showed that, despite experimental setups that should theoretically favour the outward movement of the locally-higher concentrations of as-generated carbonate and siliceous species away from the active growth region, biomorphs are instead controlled and afforded by surface-localized reactions. These reactions occur independent of diffusion control, as suggested by the zero-order decay of barium ions and steady-state kinetics of growth rates (a few microns/min).[79, 93] Moreover, the model predicted that these reactions should be localized, which was supported by hierarchically-structured material that evolved largely unaffected even at very high stirring rates until a threshold, due to the convergence of hydrodynamic and localized processes, was surpassed.[80] With regard to other indirect support of the localness of the proposed mechanism, Opel *et al.*[85] used a pH-responsive dye with fluorescent properties to identify a zone, extending about 2 microns ahead of the crystallization front, of considerably lower pH in comparison to that of the bulk,[83] though the oscillation of the pH in space and time could not be validated until recently.

The molecular basis for the emergence of silica-carbonate microstructures from nanoscale components was recently supported by concrete evidence gathered using *in situ* fluorescent microscopy with a pH-responsive dye (acridine orange).[86] The results of the study showed that the compositional oscillation in the periodically-banded microstructures are caused by a local autocatalytic process whereby the coupled reaction and co-deposition of silica and alkali earth-metal carbonate causes pH oscillation in a region that is spatially-confined to about 2 microns of the growing crystallization front.[86]

1.5.9. Directed shape control strategies

Inherent in the molecular mechanism of silica-carbonate formation, even *a priori* its proof, were certain clues that suggested the overarching process could be exploited to direct the growth of basic microstructures towards more complex ones. Indeed, Noorduin *et al.*[74] used the synergistic effects of the chemical gradients generated by the feedback-controlled mechanism, and desired reaction parameters, such as CO_2 concentration, pH and temperature, to generate a variety of tailor-made structures. Their model is also supported by findings which suggest there is a dynamic pH-switch that can be manipulated to allow the facile and deterministic transition between each of the as-discovered distinct regimes in which growth of these types of microstructures occur (Figure 12b). In Figure 12a, it can be seen that these three pH-dependant growth regimes are: 11.8-11.9 (regime 1), 11.1-11.3 (regime 2) and 8.5 (regime 3). Since pH is one of the most important factors in the growth of these microstructures, it is perhaps not surprising that these could be sculpted into morphologies that are characteristic of the particular growth regimes: stems, vases and corals (regime 1), helicoids, leaves and globules (regime 2), and regular dendritic $BaCO_3$ crystals (regime 3). Moreover, it is evident that the interplay between the bulk pH and the lowered local pH, set by the reaction in the vicinity of the growth fronts and between neighbouring structures, is heavily influenced by the proximity of the latter to the silica deposition zone. The relationship between these factors provides a basis for understanding why structures characteristically grow away from the vertically-positioned substrates towards the bulk pH in regime 1 or along the substrate in regime 2. Here, the shared feature of these two regimes is morphological evolution in a direction that will avoid the optimum silica precipitation zone, which would otherwise stop the microstructures from growing. The ability of silica to restrict growth only to active barium carbonate growth sites is fundamental to the design of 3D silica-carbonate architectures with enhanced complexity and hierarchy, since shapes can then be assembled onto or grown from other shapes in subsequent reactions (Figure 12c).

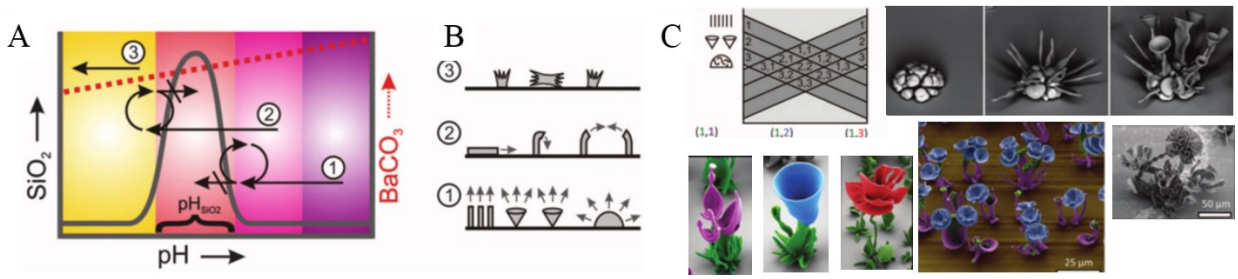

Figure 12. A) pH dependent growth regimes silica-carbonate microstructures. B) Characteristic basic morphologies of each independent growth regime. C) Hierarchical microstructures that were programmed by combining several basic shapes. Reprinted from ref.[74]

1.6. Thesis overview

The objective of this thesis is to explore several aspects of the growth process that leads to the formation of silica-carbonate microstructures with hierarchical textures *via* the bottom-up assembly of alkali earth-metal carbonates (witherite and strontianite) in silica-rich environments at alkaline pH (10-11.9). **Chapter 2** focused on replicating of the work of Noorduin *et al.,* which involved directing the growth of basic microstructures towards more complex, 3D nanocrystalline composite materials that grew on top of or from within previously grown shapes, in sequential growth steps. This involved exploiting the intersection between chemical gradients and predetermined reaction parameters (*i.e.* atmospheric CO_2 concentration, pH and temperature) in order to create the aforementioned hierarchically assembled shapes. The goal of **Chapter 3** is to present findings related to the attempted control of the chirality of helical silica-carbonate shapes using chiral molecular (amino acids) and microscale (vaterite) chiral directing agents. Here, the double helicoids grew from pH-adjusted reaction mixtures to which aliquots of amino acid were added, or on substrates that contain pre-assembled chiral vaterite. **Chapter 4** aims to show how the size and predominant morphologies of silica-carbonate microstructures were tuned as a function of the amount of Chicago Sky Blue, a sulphonated azo dye, incorporated in the crystallization solution. This research also provides indirect evidence for accelerated growth rates of the microstructures from solutions that contained dye, as implied by an increase in size relative to control experiments in the absence of dye during a growth period of 1.5-2 hours. Optical light and scanning electron microscopies were the principle tools used for the characterization of the as-formed microstructures.

Chapter 2. Hierarchical silica-carbonate microstructures

2.1. Introduction

The crystallization of barium carbonate ($BaCO_3$) from solutions at alkaline pH in the presence of silica represents a directed mineralization strategy *via* an inorganic-inorganic approach. The resulting shapes fall outside the purview of classical crystallization methods from which minerals with well-defined facets and geometries arise. Instead, silica-carbonate structures strongly resemble the highly curved surfaces displayed by biominerals formed under the control of organic molecules,[65-69] hence the designation "silica biomorphs" (Figure 13). Biomorphs are formed under conditions far from chemical equilibrium by self-assembly processes, which can be most readily tuned by adjusting the bulk reaction pH.

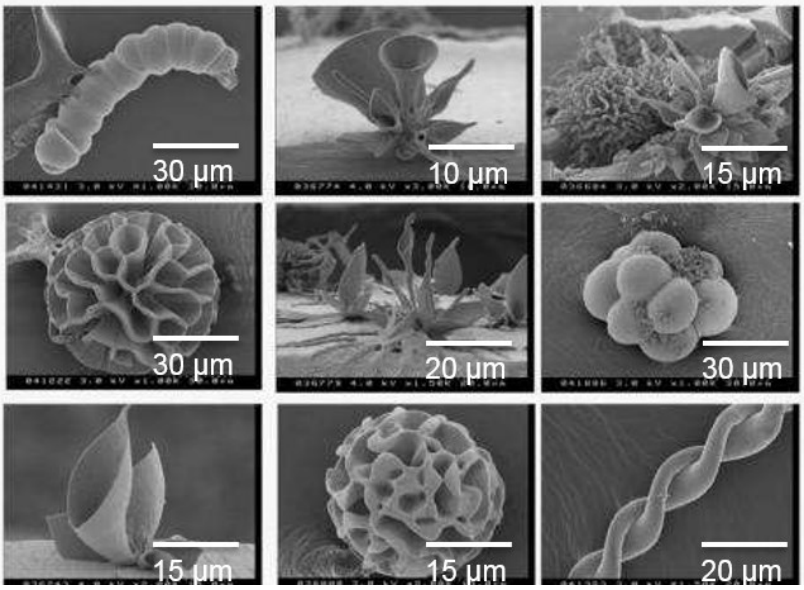

Figure 13. A selection of silica biomorphs resembling biological forms such as caterpillars, flowers and helices. Reproduced from ref[100] (Image credit: Matthias Kellermeier/Stephen Hyde/Juan Manuel Garcia-Ruiz).

The co-mineralization of silica and carbonate has a synergistic effect that originates from their opposite pH-dependent solubilities. In the region of the biomorph growth fronts, barium carbonate precipitation leads to a decrease in pH, which subsequently triggers the polycondensation of silicic acid to silica, thus causing the pH to increase, giving rise to yet another round of barium carbonate crystallization (Figure 14; simplified reaction equations). The coupled

mechanics of this cyclic process implies that each component of the system influences the other as it is being formed, therefore the final assembly of the material can be controlled.

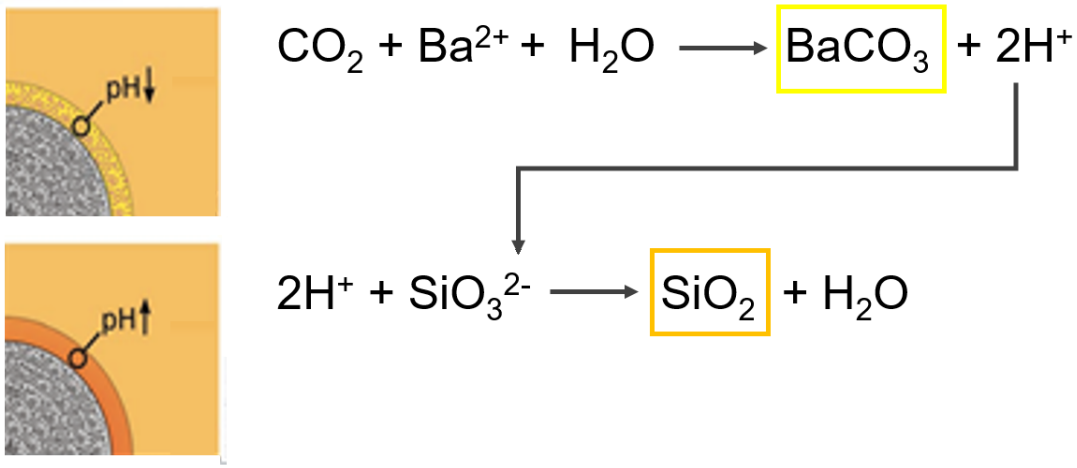

Figure 14. Reaction scheme depicting the pH-controlled coprecipitation of silica and barium carbonate at the front of a growing structure. Reproduced with alterations and with permission from ref.[91]

Noorduin *et al.*[74] devised rationally designed schemes for sculpting a great variety of elementary silica-carbonate shapes in a dynamic reaction-diffusion system (Figure 15a-c). Hierarchical microstructures of enhanced complexity were created by modulating the CO_2 concentration, pH and temperature in mixtures containing sodium metasilicate and barium chloride (Figure 15d-g).

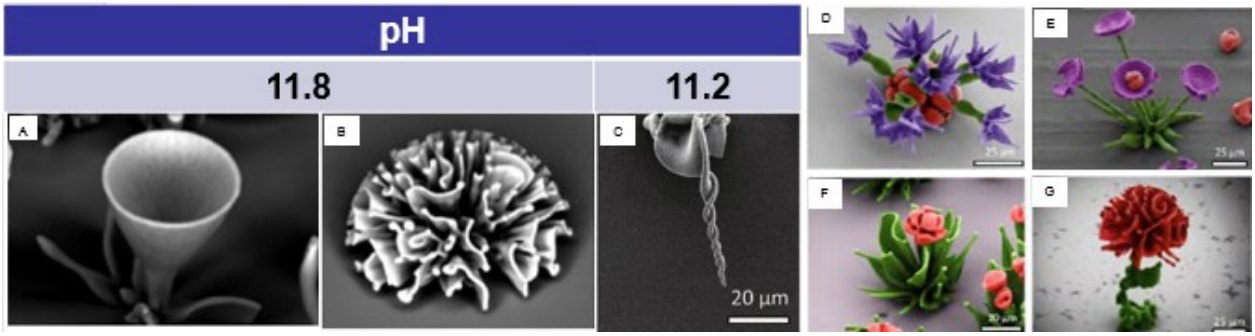

Figure 15. Silica-carbonate microstructures assembled at pH 11.8 and 11.2: A) vase; B) coral; c) double helix; and D-G) hierarchical shapes grown from crevices or stacked on top of each other. Reproduced with permission from ref.[74]

This work investigated the effect of chemical gradients on the shape of silica-carbonate biomorphs in a reaction-diffusion system by careful modulation of the pH, CO_2 concentration and temperature as a route to assemble desired silica-carbonate microstructures in single (basic shapes)

or sequential growth steps (hierarchical shapes). The study of the mineralization of barium and other related carbonates, such as strontium carbonate, sets the stage for the development and transformation to functional 3D materials, whose properties are structure-dependent, *via* means that preserve the underlying shape.

2.2. Results and discussion

2.2.1. Basic shapes

We precipitated silica-carbonate microstructures following the procedure developed by Noorduin *et al.*, [74] in which carbon dioxide diffuses into aqueous solutions of sodium metasilicate and barium chloride. This method circumvents the rigours of preparing gels, as well as allowing for easier control of the initial concentration of the reactants. This facile preparation method requires a simple laboratory setup, and the growth of silica carbonate microstructures (biomorphs) can be confined to 1.5–2 hours. It was found that there are two major pH regions for the evolution of distinct classes of structural morphologies for these nanocomposite materials. In the first regime, where the pH is set to between 11.1–11.3, growth is directed away from the bulk pH, which favours the formation of leaves, helices and globular microstructures. Conversely, at pH 11.8—11.9 can best be described as a regime where the growth of flower-like microstructures occurs. Here, these flowers grow towards the bulk pH, giving rise to stems, vases and corals on a substrate positioned vertically in solution. For successful growth, the commonality between these two pH-induced growth regions is the necessity of avoiding the zone of optimal silica precipitation, which occurs at pH 10.5. This essentially means that the decrease in the local pH must be maintained to the left of this passivating silica deposition zone in regime one, while that of regime two is directed higher, or to the right (Figure 12a). The structures in regime one are able to do so by growing flat along the substrate or by twisting upon themselves as they follow a local growth-induced trail of acid in order to shield themselves from the higher bulk pH. The opposite scenario has been demonstrated for regime two. Active barium carbonate growth sites become covered with silica when the bulk pH approaches 10.5, which inhibits growth. This coprecipitation system thus affords us with a means to design silica-carbonate shapes in a predictable manner based on pH-stimulated responses. Herein, we aim to replicate the growth of these morphologies by tuning the bulk pH.

2.2.1.1. Inward-directed growth of helices, leaves and globules

The formation of microstructures that grow along the substrate or by a twisting mechanism was induced by setting the bulk pH to 11.2. Prior to adjusting the pH, barium chloride was slowly added to a solution of sodium metasilicate in order to avoid the premature precipitation of silica. Fluorescein dye, which was added to facilitate optical confocal microscopy studies, completely dissolved in the pH-adjusted mixture to give a fluorescent green solution. The diffusion of atmospheric carbon dioxide into the mixture increases the carbonate supersaturation and leads to the formation of silica-carbonate microstructures on slides positioned vertically in solution. The results demonstrated herein confirm the presence of double helices, leaves, and globular shapes on a typical optical micrograph at this pH (Figure 16a). Moreover, although distilled water was used, the results suggest that the concentration of extraneous ions was not high enough to disrupt the formation of these shapes. Nevertheless, a switch to deionized water was made in later reactions to rule out the possibility of interference from foreign ions. Dark field microscopy allowed for the chiral characterization of the double helices, where the use of an opaque disc limits most of the light coming from the condenser to only a few scattered beams, which results in a dark background on which a translucent sample appears if it possesses the ability to reflect light. Since this technique is best utilized for studying surface features, in addition to the partially crystalline and translucent nature of these silica-carbonate materials, the chirality of helical microstructures is usually well defined as is exemplified in Figure 16b, where a right-handed double helix is depicted. Polarized light microscopy proved to be another useful technique for the morphological characterization of these microstructures, especially leaf-like shapes. The silica-carbonate leaves were observed as sheets composed of multiple spherical bands emanating from a single nucleus. Each leaf also displayed a prominent Maltese cross that extended from the nucleus to the periphery of the structure when viewed between crossed polarizers (Figure 16c). The banded patterns are a characteristic feature of the leaves, originating from the orientational order of its nanocrystals, which are slightly misaligned with respect to their neighbours. The attractive forces between these nanocrystals leads to their self-assembly into micron-sized structures. Overall, globular aggregates seem to occur more frequently when compared to leaf-like and helical

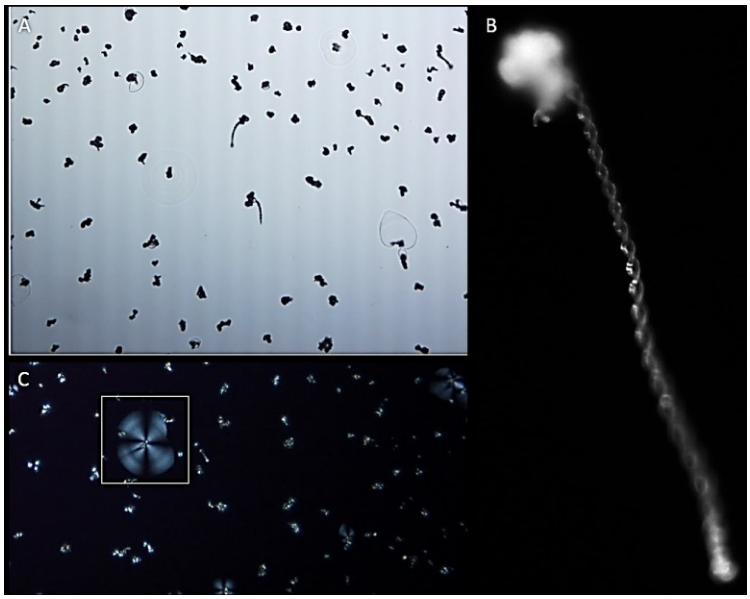

Figure 16. Silica-carbonate microstructures grown in non-degassed aqueous solutions of $BaCl_2$ (19 mM) and Na_2SiO_3 (8.2–8.5.mM), where the former was added to the latter in a 100 mL beaker. The total solution volume was 15 mL, and was adjusted to pH 11.2, prior to the addition of fluorescein dye (1.40 mM). The material precipitated on a clean microscope slide positioned vertically in solution, while a petri dish was used to cover and allow the flow of CO_2 in through the spout of the reaction vessel. After *ca.* two hours, the slide was removed and rinsed twice in distilled water, followed by acetone and finally air dried prior to the morphological characterization of the shapes: A) optical light micrograph showing the morphologies (pH 11.2); B) translucent double helix viewed by dark field optical microscopy; and C) a leaf-like shape displaying a dark extinction pattern when viewed between crossed polarizers of a petrographic microscope.

architectures as can be seen in Figure 17a. This suggests that leaves and helices occur when the barrier to their formation is overcome, perhaps by way of heterogeneous nucleation as noted by Kellermeier *et al.*[94] Nevertheless, a closer examination of the biomorphic shapes reveals that they all must start from a globular aggregate, thereby transitioning from the fractal growth of a barium carbonate seed under the influence of oligomeric silica species to polycrystalline growth.[79] The growth of a leaf is initiated when the radially advancing lamina, extending from the globule, starts to develop folds of opposite handedness but equal heights along its rims. Since radial growth is decreasing as a function of time, this type of growth terminates at an apex when the two folds eventually meet. A helical microstructure could also develop at the apex of a leaf. The growth of helices is similar to that of leaves in that there is also a lamellar component to their growth and curling of its two growth fronts of similar height. However, the lamellae in helices are much smaller and the growth fronts curl in the same sense, most likely in response to the local generation and diffusion of acid, in contrast to those of leaf-like shapes. Another key factor that determines whether leaves or helices will form is the degree of contact with a substrate. In Figures 17b-c and

f, and in general, all the helical microstructures are observed to have grown at some vertical distance away from the substrate, whereas the leaves grow in direct contact with the substrate (Figure 17e). The variation in the different types of helical microstructures, such as double helices (Figures 17b, c and e) and braid-like microstructures (not shown here), can perhaps be explained by differences in growth rates, with curling in the latter expected to occur at a faster rate. Furthermore, the transition of a double helix to a single helix (white box in Figure 17c) represents the stage at which one growth front begins to curl at a much faster rate than the other, most likely due to changes in chemical gradients surrounding the growing tip of the structure. Finally, microstructures with a worm-like appearance seem to arise from a growth front wrapping around itself (Figure 17f).

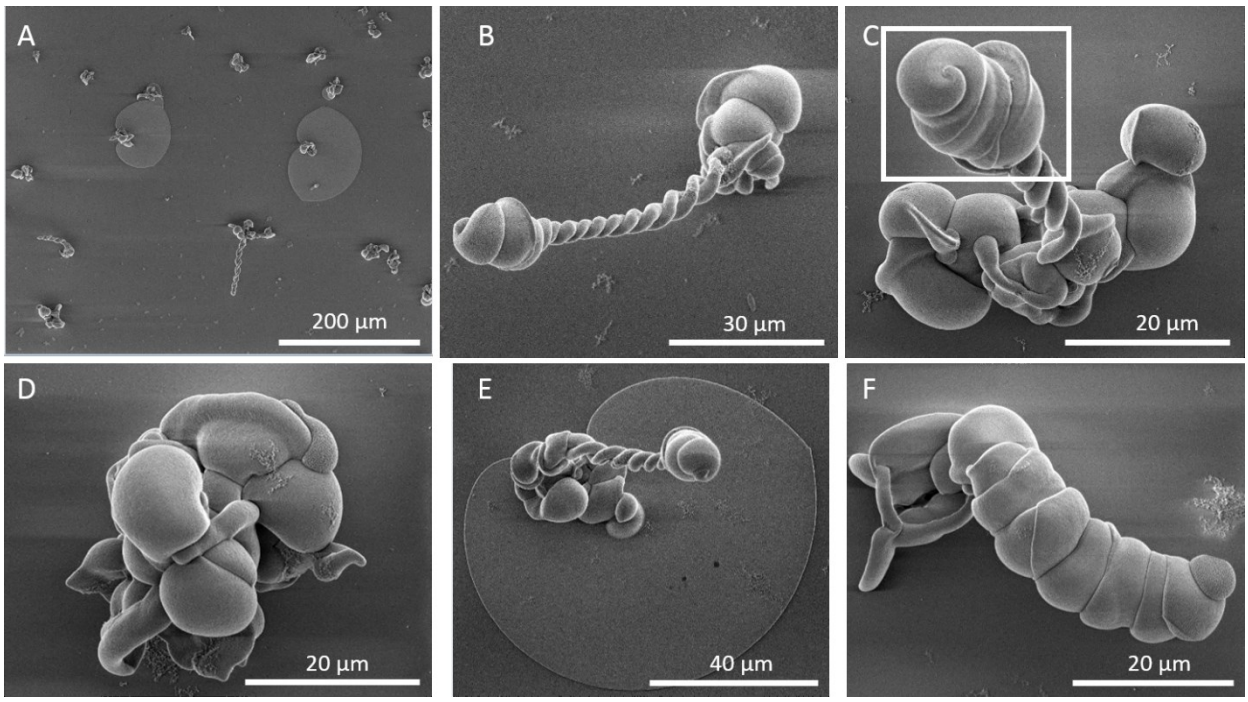

Figure 17. SEM micrographs showing: A) common as-prepared silica-carbonate microstructures upon their precipitation on an uncoated glass substrate from a barium chloride/sodium metasilicate mixture at pH 11.2; B) a left-handed double helix; C) the transition of a right-handed double helix to a single helix of the same chirality (inset of C); D) a globular aggregate; E) a double helix that grew on top of a leaf; and f) a worm/caterpillar-like structure.

These results correlate well with the structural morphologies for silica-carbonate microstructures that have been previously reported by Noorduin *et al.* at pH 11.1–11.3.[74] Moreover, the reaction set-up was tolerant to the use of non-degassed and non-deionized water for

the preparation of solutions, while the incorporation of fluorescein dye had no bearing on the outcome of the shapes that were precipitated from solution on glass substrates.

2.2.1.2. Solution-directed growth of stems, vases and corals

The next set of reactions were conducted at pH 11.8 to verify the importance of the second pH regime for the shaping of silica-carbonate microstructures. The reaction set-up and the preparation of the solutions were maintained as described in section 2.2.1.1, and only the pH was modified. The results demonstrate that the shapes typical for this pH regime were successfully grown under the studied reaction parameters. A field of microstructures terminating in bright and circular rings at their tops were observed by dark field microscopy (Figure 18a). We postulate that the brightness of the tips of these structures suggest that they have an inherent capacity to function as light-directing materials. Bright field microscopy clearly revealed that these shapes are vases that often appear singly or in pairs (Figure 18b). The size of the vases grown in pairs are comparable, so their growth is likely to have been initiated at the same time. Other interesting forms characterized by optical light microscopy were corals (Figure 6c). This type of microstructure is defined by multiple wave-like fronts, and were found growing on parts of the substrate positioned deeper in solution compared to the vases.

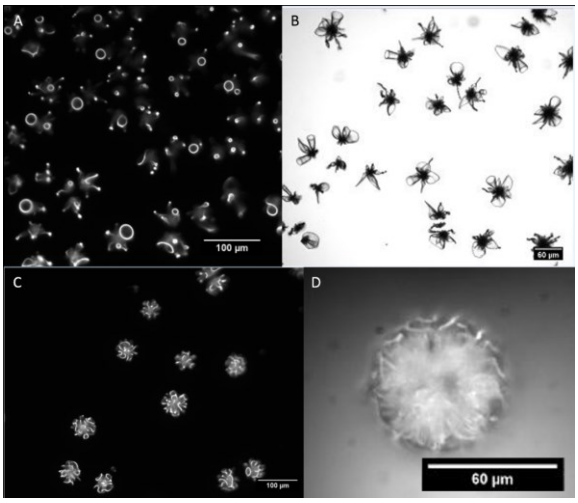

Figure 18. Typical images of vase-like microstructures (A–B) and corals (C–D) crystallized on glass substrates from barium chloride-sodium metasilicate solutions adjusted to pH 11.8, as viewed by dark field (left) and bright field (right) optical light microscopy.

The morphology of the samples was then investigated by SEM. The overarching principle governing the morphology and number of microstructures seemed to be the distance from the air-

water interface, and hence local carbonate supersaturation controlled by the diffusion of CO_2. At the topmost section of the interface, a greater quantity of stems was precipitated on the substrate, which branched from a central point when the carbonate source was switched to strontium (Figure 19a). These stems are of comparable width, except for sections where fluxes in the CO_2 concentration occurred. The higher concentration of CO_2 at the top of the interface leads to the nucleation and growth of more structures, and since they are close to each other, their widths and morphologies are confined to the dimensions of stems. The possibility of patterning these microstructures could be realized by adjusting the CO_2 concentration, simply instigated by removing and replacing the petri dish covering the reaction beaker during unique stages of their growth (Figure 19b). In Figure 7b, the black arrows identify the points in time at which the petri dish was removed, and thus the subsequent thickening of the structures due to greater carbonate precipitation. Perhaps, even more important, this experimental design points to other intrinsic properties governing the size of these stems, since they narrow in order to recover the initial widths set prior to the removal of the petri dish. The stems then make way for the formation of vases, which can be considered as extensions of stems. Here, a stem first forms but, because the lower degree of nucleated structures necessarily need more space to expand laterally, it starts to grow outwards. However, this growing structure then collapses in the middle due to the inability to buffer the build-up of acid within its own walls, thus giving rise to vase-like shapes (Figure 19c). In Figure 19c, the presence of both stems and a vases gives credence to the aforementioned growth theory, as well as highlighting that the passivating effect of silica on the sides of the structures limits growth and deposition of new material to their tops. The other shape (*i.e.* corals) found growing at a greater distance from the vases (*i.e.* further from the air-solution interface) are fewest in number and so have even more space to expand laterally (Figure 19d). Interestingly, these corals resemble many incompletely formed vases which suggests the accumulation and inefficient buffering of acid within the walls of each unit of the overall structure, which are thus steered away from each other to minimise exposure to acid. The effect of the local diffusion and exchange of acid is perhaps best illustrated in cases where two neighbouring structures in close proximity grow away from each other, such that they develop a certain asymmetric characteristic to their growth (Figure 19e).

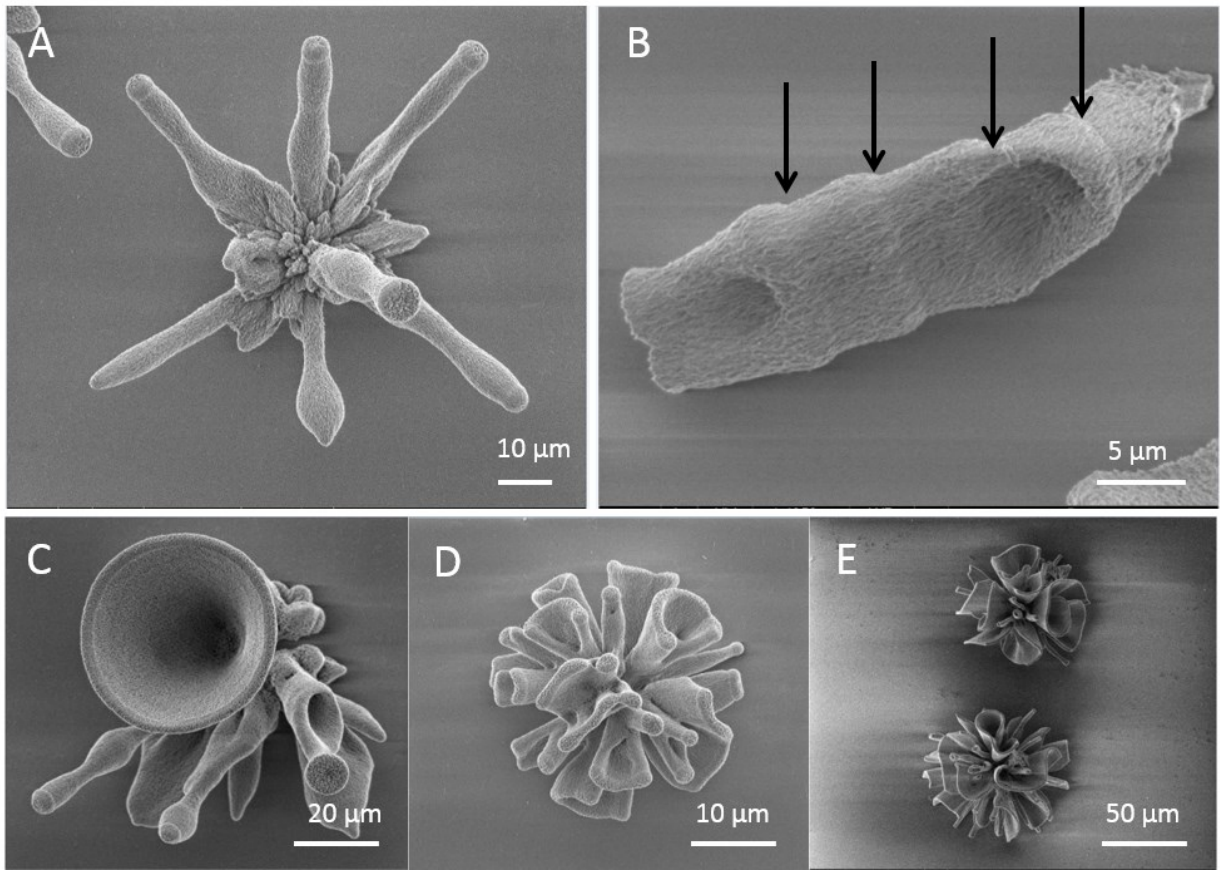

Figure 19. Examples of silica-carbonate microstructures that exhibit characteristic morphologies and features when grown from alkali earth metal chloride-sodium metasilicate solutions at pH 11.8, as observed by SEM: A) similar strontium carbonate stems diverging from a central point; B) a patterned barium carbonate stem where the black arrows depict the closed position of the petri dish; C) a vase; D) a coral; E) and two corals showing that growth is restricted in the region between neighbouring microstructures at pH 11.8.

2.2.2. Hierarchical microstructures

The results discussed in sections 2.2.1 and 2.2.2 demonstrate that it is possible to control the basic morphogenesis of silica-carbonate microstructures by defining the initial pH and with careful modulation of the CO_2 concentration. Furthermore, growth is directional, not only in how these structures grow in the two different pH regimes, but also in terms of where on the structure it occurs. That is, growth seems to occur preferentially at the tips or tops of the structures as opposed to the sides, where silica deposition prohibits growth. These factors then give rise to simple methods of designing new shapes based on the hierarchical assembly of silica and carbonate at the active growth sides of previously grown microstructures. These carbonate growth sites could also be present deep within the structures themselves, such that additional shapes can be inserted

within these sites. Here, we will use these basic principles to assemble hierarchical microstructures in conjunction with controlling other parameters such as the addition of salt, temperature and variation in the alkali earth metal ion source.

2.2.2.1. Stacked barium carbonate shapes

The effect of stacking $BaCO_3$ shapes on top of each other was investigated by transferring the substrate from a first solution, to which NaCl was added, to another under different growth conditions. NaCl can be utilized to change the ionic strength of solutions, though its effect may not be very significant as Noorduin *et. al*[74] noted that NaCl only promoted a slight thickening of the silica-carbonate microstructures. To better understand how temperature can be used to guide the evolution of these shapes, the second solution was cooled down to about four ºC in an ice bath. It can be seen that the first reaction resulted in the formation of 2D semi-circular and circular shapes and vases (Figure 20a). However, when the acid from the first reaction was removed by washing, and the substrate moved into a second 4 ºC solution, the thickening of the outer perimeters of the first set of structures became readily apparent (Figure 20b). This effect can be attributed to the growth of further silica-carbonate shapes from active carbonate growth sites formed in the prior reaction. SEM was used to further investigate the morphologies of the thickened microstructures (Figure 20c). Although there were several vastly different morphologies observed in this reaction, a few false-colored images could best be used to represent the delineation between the first and the second reaction for most of these structures. In particular, it can be seen in Figure 20g that the first reaction produced vases (green), while the second one lead to the assembly of globules on the top walls of the vases (red). The formation of the globular crystals, suggesting wall thickening, perhaps due to the enhanced precipitation of carbonate influenced by the greater CO_2 availability and hence carbonate supersaturation at the lowered temperature. The thickening of the walls of the microstructures also occurred in corals (Figure 20d, pink). Whereas some parts of the coral structures are terminated with lilypad-like structures (Figure 20d–e). This lilypad-like characteristic might have already been present from the first step or could conceivably have developed upon the pinning of the solution meniscus on previously grown structures. With regard to the latter hypothesis, the structures would be forced to grow laterally in a 2D fashion in solution in order to have access to new building materials in the form of carbonate and silica. Finally, hybrid shapes composed of spicules on the bottom and vases on the top were also

characterized by SEM. The vase component of the hybrid shapes is very likely to have occurred under the constraint of a competitive growth mechanism between neighbouring parts of the structures, where only some parts of the spicules evolved into vases in the second step. This is not surprising, since this solution-directed regime dictates that structures move away from each other in order to limit the exchange of acid and continue to successfully grow. Furthermore, active carbonate growth sites seem to be present within these vases from which thick, stem-like microstructures grew. The combined effect leading to the formation of the hybrid spicules, vases and stems is a hierarchical shape reminiscent of a calla lily.

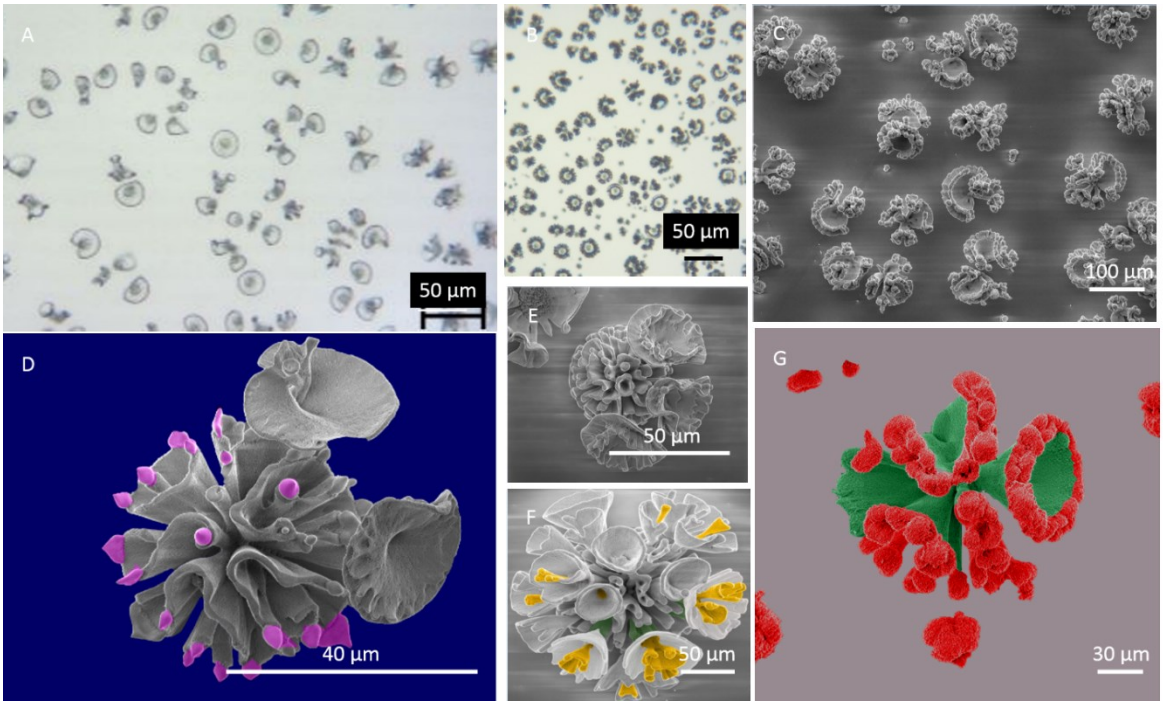

Figure 20. Optical light microscopy (A–B) and SEM (C–G) images illustrating a route to hierarchically-assembled silica carbonate microstructures from two distinct growth steps: A) circular and fan-like barium carbonate structures which grew in the first step, where NaCl was added to the reaction solution that was adjusted to pH 11.8; B–C and g) thickening of the rims of the previously grown and washed structures upon being placed in a barium chloride/sodium metasilicate solution that was adjusted to pH 11.8 and four ºC in the second reaction step; D, F and G) false colour images highlighting the deposition of material from the second step (pink, yellow and red) onto active barium carbonate growth sites that were preserved from the first reaction (green and white); and D–E) lilypad-like features, where the meniscus of the second solution might have pinned onto the structures grown in the previous step, which forced growth to occur in 2D instead of 3D.

2.2.2.2. Accessing core $BaCO_3$ growth sites

To further expand on the concept of designing hierarchical shapes stemming from the insertion and growth of structures from deep-lying sites present within previously grown microstructures, the temperature was first reduced to the temperature of an equilibrated ice-water bath (4 ºC) in the first step and subsequently grown as normal, albeit with increased CO_2 exposure lasting for five minutes in the second step. The reduction of the temperature afforded globular spheres whose appearance can also be attributed to augmented carbonate deposition and fractal splitting of the initial seed, as well as subsequent passivation from silica precipitation, similar to the origins of the globules mentioned above (Figure 21a). Although carbonate deposition increases at lower temperatures, other temperatures, such as 10 or 15 ºC, would presumably have afforded similar globular spheres. Upon performing the second step, there was a noticeable difference in the structures, where barium stems inserted into existing crevices within the original spheres, and subsequently opened into vases when a CO_2 pulse was applied (Figure 21b). To verify this hypothesis, SEM was used to visualize the microstructures, which showed stems and vases emanating from globular spheres (Figure 21c). Once again, the proximity of a stem to its nearest neighbours seems to dictates whether or not it transitioned into a vase. Simply put, a high concentration of CO_2 causes these structures to grow rapidly in a relatively short period of time, so a reduction of the exposure time leads to the formation of smaller, more uniform vases.

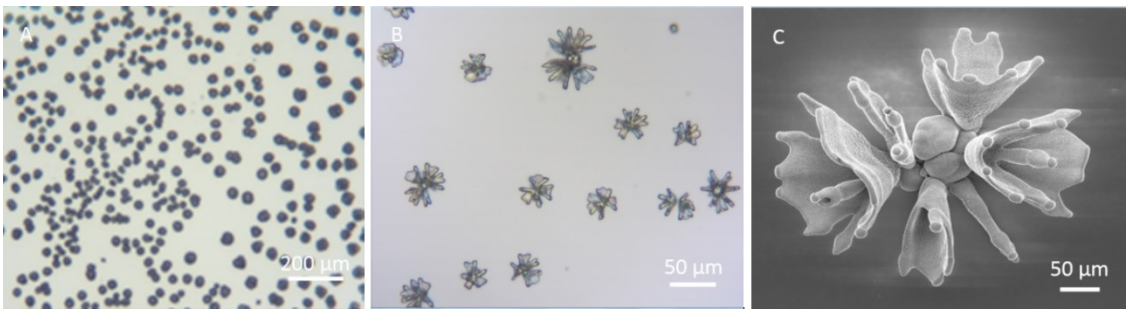

Figure 21. Optical light microscopy (A–B) and SEM (C) images evidencing the assembly of complex silica-carbonate microstructures in two reaction steps: a) globular barium carbonate aggregates grown from a reaction solution where the pH was adjusted to 11.8 at 4 ºC; B) structures showing a transition in the morphological profile of the previously grown microstructures upon being placed in a strontium chloride (19.1 mM) and sodium metasilicate (8.2–8.7 mM) solution that was adjusted to pH 11.8 and maintained at room temperature for *ca.* two hours; and C) scanning electron micrograph depicting one of the as-grown structures subsequent to the termination of growth in the second step, where strontium carbonate stems grew from active growth sites present within the crevices of the globular aggregate, which were further shaped into crude vases upon the opening of the lid of the beaker for *ca.* five minutes.

2.2.2.3. Strontium and barium carbonate microstructures (effects of pH)

The library of hierarchical microstructures could further be expanded by switching the metal ions in the carbonate from barium to strontium. This is a rational approach in the design process since barium and strontium carbonates are both orthorhombic, so they are therefore expected to form similar structures. However, there are observable differences which may be due to variations in ionic radius (219 versus 253 pm with respect to strontium and barium), electron shell structure of the respective metal ions, or crystal habits of these metal carbonates. Furthermore, the solubility of strontium carbonate and barium carbonate at 25 ºC per 1000 g of water were reported to be 0.396 x 10^{-4} g/mL and 0.90 x 10^{-4} g/mL, respectively.[101] Indeed, strontium carbonate vases that were taller than previously shown barium carbonate vases (section 2.2.1.2) were observed at pH 11.8 in the first step. Here, small uniform barium carbonate vases, sprouting from the strontium carbonate vases, originated in the second step, also at pH 11.8 (Figure 22a).

Underscoring the importance of pH in creating steep chemical gradients necessary for the formation of basic and hierarchical shapes, additional standard or curious microstructures could also be obtained. For example, at pH 11.8, flower-like barium carbonate shapes could be assembled on helices grown at pH 11.2 (Figure 22c). As shown in figure 22b, flowers eventually evolved at the tips of the fibrillated stems diverging from a central point. This is a rather strange phenomenon, which suggests that these structures grew from low to high pH. This could have been due to the diffusion and eventual homogenization of base within the bulk solution, thus changing the microenvironment of the structures over the course of the reaction. The morphology of these structures also implies a higher silica content present within the fibrillated sections, which decreases over time to allow carbonate growth to evolve into flowers, free from the passivating constraints of silica deposition.

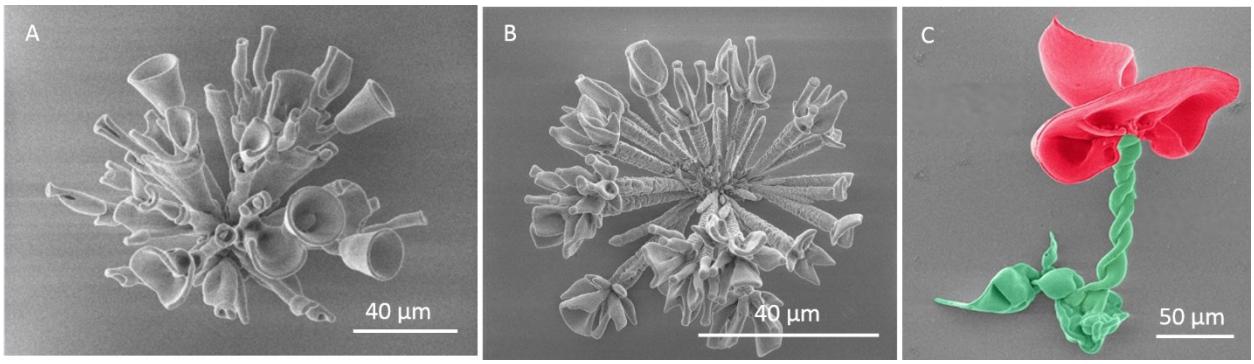

Figure 22. SEM images of hybrid silica-carbonate microstructures: A) tall strontium carbonate vases (first step, pH 11.8) into which shorter barium carbonate stems and vases insert in the second growth step (pH 11.8); B) one-pot synthesis of fibrillated stems (lower pH) decorated with barium carbonate crystals (higher pH); and C) false-coloured microstructure of a flower (red, pH 11.8) that was deposited on top of a double-helix (green, pH 11.2) in a separate growth step.

2.3. Conclusions

The design of both basic and hierarchical micron-sized silica-carbonate structures were realized with control over such parameters as initial bulk pH, CO_2 concentration, temperature and the utilization of different carbonate alkali-metal sources. The structures were characterized by optical light microscopy and scanning electron microscopy.

Distinct classes of microstructures were precipitated based on the initial pH of non-degassed barium chloride and sodium metasilicate mixtures. At pH 11.2, these microstructures either grew flat along the glass substrate to form leaves, or from an interface situated along a globule located at some vertical distance from the substrate. The latter gave rise to various types of helical microstructures such as worms, double helices, and single helices found at the tip of the double helix. The emergence of these types of microstructures is consistent with a solution-shielding effect, as they either twist or grow flat to remain at a local pH on the periphery of the optimum pH for silica deposition. On the other hand, shapes such as stems, vases and corals were afforded at pH 11.8, since growth towards the higher bulk pH favours the enhanced deposition and growth of carbonate, relative to silica, due to their opposite trends in pH-induced solubilities.

The predictable nature of the direction of growth and the types of microstructures obtained in each regime provided a straightforward approach to the design of hierarchical shapes based on sequential stacking of different shapes. It was shown that fresh material will deposit on top of the walls of these structures, leading to wall thickening. The effect of lowering the temperature from

room temperature to 4 ºC is to enhance carbonate deposition and induce the growth of cauliflower-like aggregates. These aggregates were either used to decorate vases, or to provide additional sites for inserting stems that grew from carbonate growth sites present within their crevices. The as-grown stems were further shaped into vases by increasing the exposure of the reaction solution to CO_2. When the reactions were conducted first at pH 11.2, then at 11.8, flower-like shapes with helical stems resulted. The reactions also tolerated the formation of shapes from hybrid alkali metal ion sources (*i.e.* strontium and barium). For instance, tall strontium carbonate vases containing barium carbonate vases were made in two separate growth stages, both at pH 11.8.

2.4. Experimental

2.5.1. Materials and method

Analytical grade barium chloride dihydrate ($BaCl_2 \bullet 2H_2O$), strontium carbonate hexahydrate ($SrCl_2 \bullet 6H_2O$) and sodium metasilicate (Na_2SiO_3) from Sigma Aldrich, and L-aspartic acid from Alfa Aesar were used without further purification. All samples were prepared fresh with distilled water. Microscope slides (75 x 25 x 1 mm) were purchased from Thermo Fisher Scientific and were either used thus or cut to desired dimensions (55 x 25 x 1 mm). The slides were cleaned by soaking in Hellmax^{TM} cleaning agent for at least two hours. The slides were subsequently rinsed in distilled water, air dried and stored in a clean, covered beaker.

Optical light microscopy of the samples was carried out on a Leitz Laborlux 2 Pol S petrographic light microscope equipped with an Axiocam 105 color camera that interfaced with a Zeiss light software program. SEM images were obtained using an FEI Inspect F50 FE-SEM operating at 1–2 keV acceleration voltage in order to minimize charging of the samples (*N.B.* without sputter coating).

2.5.2. Experimental conditions for the microstructures shown in Figures 16–19 (helices, leaves, stems, corals and vases)

Distilled water (100 mL) was added to sodium metasilicate (0.130 g, 1.07 mmol) in a 100 mL beaker and the resulting mixture was stirred magnetically for 10 minutes until the solid completely dissolved. An aqueous solution of $BaCl_2$ (3 mL, 0.0755 g, 0.309 mmol, 103 mM) was delivered dropwise from a 5 mL syringe to an aliquot of the sodium metasilicate (12 mL, 0.127

mmol, 10.65 mM) solution contained in a 100 mL beaker while swirling. Fluorescein (7 mg, 0.0211 mmol) was subsequently added and the pH of the resulting light fluorescent green solution was adjusted to either pH 11.2 (helices and leaves) or 11.8 (stems, vases and corals) with 1 M NaOH and/or HCl solutions. The final concentrations of fluorescein, Na_2SiO_3 and $BaCl_2$ were 1.41, 8.52 and 20.6 mM, respectively. A clean glass slide was positioned vertically in the solution and the beaker loosely covered with a petri dish in order to allow the flow of CO_2 in through its spout. After *ca.* 2 hrs, the substrate was removed and rinsed in water contained in a 250 mL beaker for about 1–2 minutes in order to stop the reaction and to remove any loose precipitate not adhered to the slide. Finally, the slide was rinsed for 30 secs in acetone, then air dried. Optical light microscopy and SEM were subsequently used to visualize the as-prepared aggregates.

2.5.3. Experimental conditions for the microstructures shown in Figures 20 and 21 (hierarchical shapes)

In order to make the structures in figure 20, a slide was transferred from the first solution, to which NaCl (14 mg, 0.35 mmol) was added, to a second solution (without NaCl) that was cooled down to *ca.* 4 ºC in an ice bath (rinsing in distilled water in between). Aside from these modifications, the protocol in section 2.5.2 was followed for preparation of the $BaCl_2$, Na_2SiO_3 and fluorescein solutions, and the subsequent reactions at pH 11.8.

The microstructures in figure 21 were prepared by lowering the temperature to 4 ºC in the first step and subsequently grown as normal, albeit with increased CO_2 exposure lasting for 5 minutes in the second reaction. In order to access the barium carbonate growth sites present in the core of the microstructures from the first step, the slide with the as-prepared globular spheres was transferred to a second solution that contained strontium chloride (3 mL, 0.0489 0.0824g, 0.309 mmol) and Na_2SiO_3 (12 mL, 0.127 mmol, 10.65 mM). The reaction was subsequently conducted at room temperature for *ca.* 2 hours. During this growth period, the petri dish was removed after *ca.* 1.5 hours for about 5 minutes in order to increase the flow of CO_2 into the solution. The petri dish was subsequently restored to its previous position during the rest of the growth period.

2.5.4. Experimental conditions for the microstructures shown in Figures 22 (effect of tuning the alkali earth metal ion and pH)

Briefly, the silica-carbonate microstructures in figure 22a were prepared at pH 11.8 by adding $SrCl_2$ (3 mL, 0.0484 g, 0.309 mmol) to Na_2SiO_3 (12 mL, 0.127 mmol, 10.65 mM) in a 100 mL beaker in the first step, after which the shapes were grown and washed according to the steps outlined in section 2.5.2. In the second growth step, the slide with the strontium microstructures was placed in a 100 mL beaker containing Na_2SiO_3 (12 mL, 0.127 mmol, 10.65 mM) and $BaCl_2$ (3 mL, 0.0755 g, 0.309 mmol, 103 mM). The pH was adjusted to 11.8 and the reaction was conducted at room temperature according to the protocol established in section 2.2.1.1.

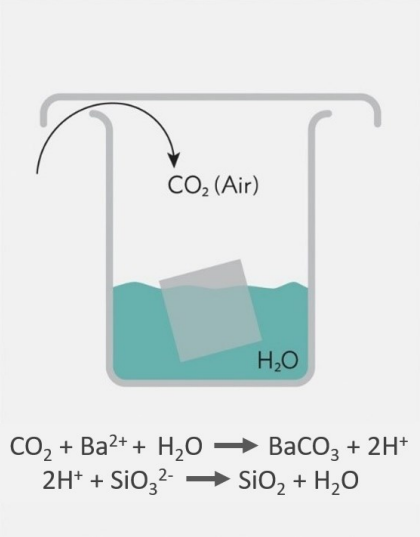

Figure 23. Experimental setup for the growth of silica-carbonate microstructures

Chapter 3. Amino-acid induced chiral vaterite microstructures

3.1. Attempts to control the chirality of $BaCO_3$ microhelices with enantiopure L-aspartic acid

3.1.1. Introduction

The interaction between the organic and inorganic components of biological systems leads to some of the most beautiful (and often chiral) patterns seen in nature, as is nicely demonstrated by snail shells and the chiral narwhal tusk (Figure 24).[47, 49] Moreover, at the molecular level, important examples of homochirality in nature include D-sugars and L-amino acids. The scope of such studies has been extended towards the transfer of chirality over multiple length scales, namely from the molecular to the micron scale, which is in and of itself quite fascinating. Remarkably, the molecular chirality of an amino acid was templated onto the macroscopic chirality of calcite by Orme *et al*.[53] In our model system, the formation of the right- and left-handed microhelices (Figure 25) occurs with an equal distribution under the dynamic diffusion of CO_2 into a solution of barium chloride and sodium metasilicate at pH 11.2. To control the handedness of the helices during the formation we investigated molecular chiral directing agents to break the symmetry towards helices of a single handedness. At the molecular scale, the influence of enantiomerically pure aspartic acid on the self-assembly was studied.

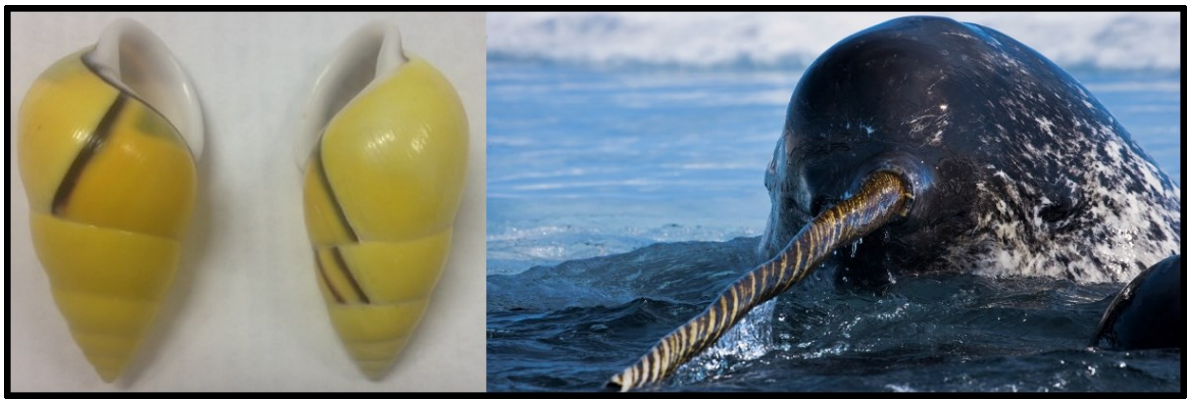

Figure 24. Examples of chiral structures that are found in nature: the snail shell (*Amphidromus perversus*; left) and the narwhal tusk (right)[102]

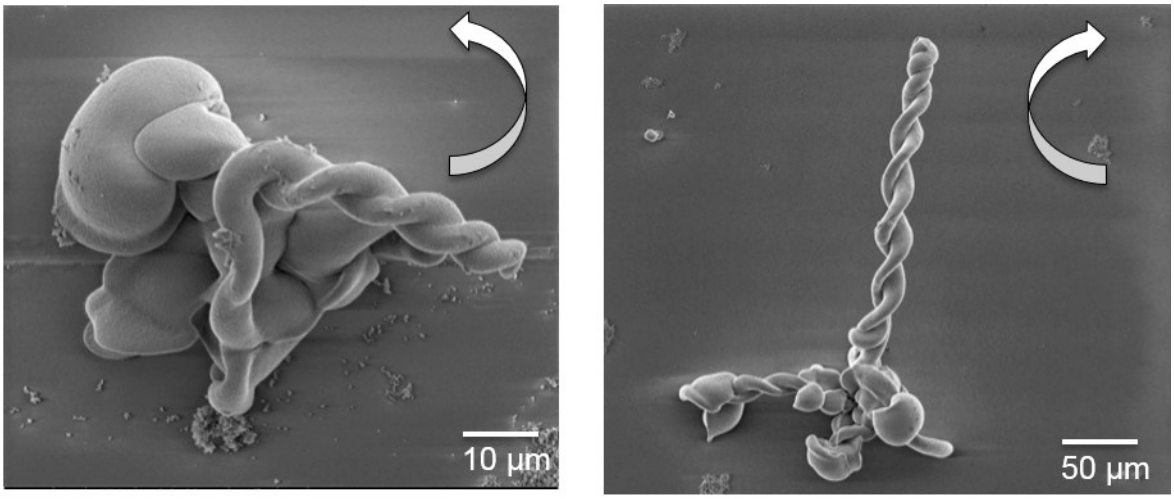

Figure 25. Left- and right-handed microhelices precipitated from the interaction of silica and barium carbonate in a dynamic CO_2-diffusion system at pH 11.2 after *ca.* two hours

3.1.2. Results and discussion

3.1.2.1. Effect of L-aspartic acid on the chirality of silica-carbonate microstructures

In order to investigate its effect on the growth of silica-carbonate microhelices at pH 11.2 over a reaction period of 2 hours, L-aspartic acid (0–3 mM) was incorporated into solutions of Na_2SiO_3, and $BaCl_2 \bullet 2H_2O$. A baseline ratio of the number of right- and left-handed microhelices was first established in control experiments without amino acid. Here, a total of 125:123 left- to right-handed microhelices were counted from 6 separate experiments (Figure 26). Subsequently, the effect of L-aspartic acid on the chirality of these microstructures was investigated.

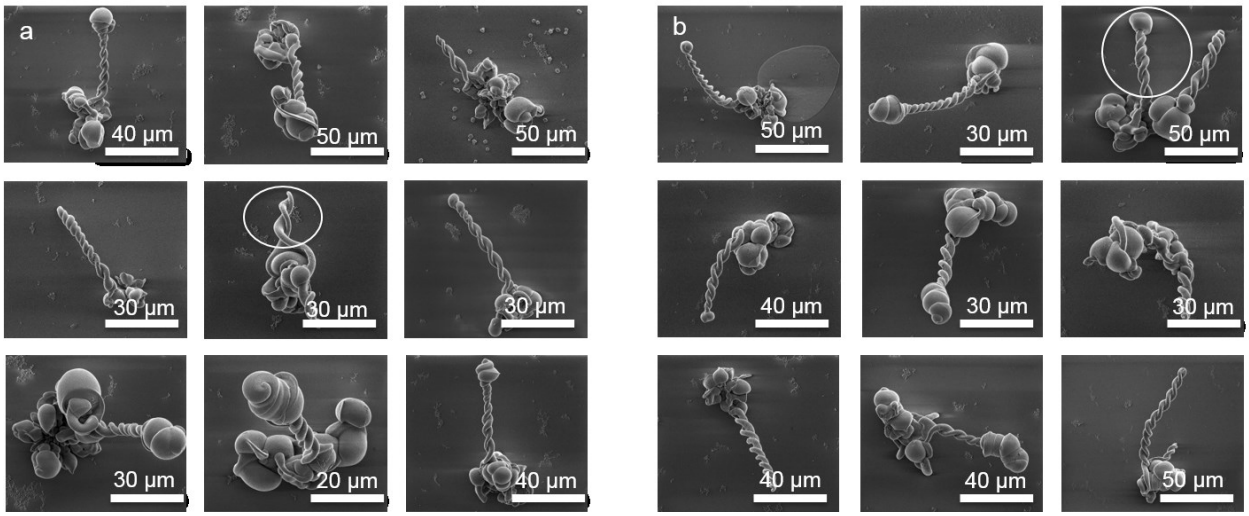

Figure 26. SEM images of representative: A) right-handed double spirals and B) left-handed double spirals in the absence of additive.

Initially, a solution of the additive dissolved in water was added to a mixture of sodium metasilicate and barium chloride. However, this approach was abandoned due to the low solubility of the amino acid at neutral pH, and the consequent significant dilution of the other reactants, which might be one of the possible reasons why these reactions yielded no crystal growth. In order to overcome these challenges, the additive was first dissolved in an equimolar or slight excess of NaOH solution (0.12 M), then was combined with the $BaCl_2$, which was subsequently added to the sodium metasilicate. Based on the results, this latter method seems to be a good approach to avoiding excessive precipitation of silica at the onset of the reaction, while still generating helices and other regular morphologies at pH 11.2 as visualized by polarized light microscopy and SEM. The results suggest that concentrations above 3 mM of the additive suppress the growth of the helices. Nevertheless, growing the biomorphs in the presence of lower concentrations of L-aspartic acid did not lead to any observed dominance of one handedness of the microhelices over the other (Figure 27, 3 mM additive). Both left- and right-handed double helices are shown in Figure 27 from the latter experiments in which 31:25 counterclockwise to clockwise double helices were counted. Similar results were obtained at 23 and 45 µM homochiral L-aspartic acid. It should be noted that although a slight excess in the number of counterclockwise helices relative to clockwise ones, and vice versa, may be observed, this is purely random, and does not follow a trend given the use of only L-aspartic acid . However, a statistically equivalent population of helices is expected to result as the number of experiments increases.

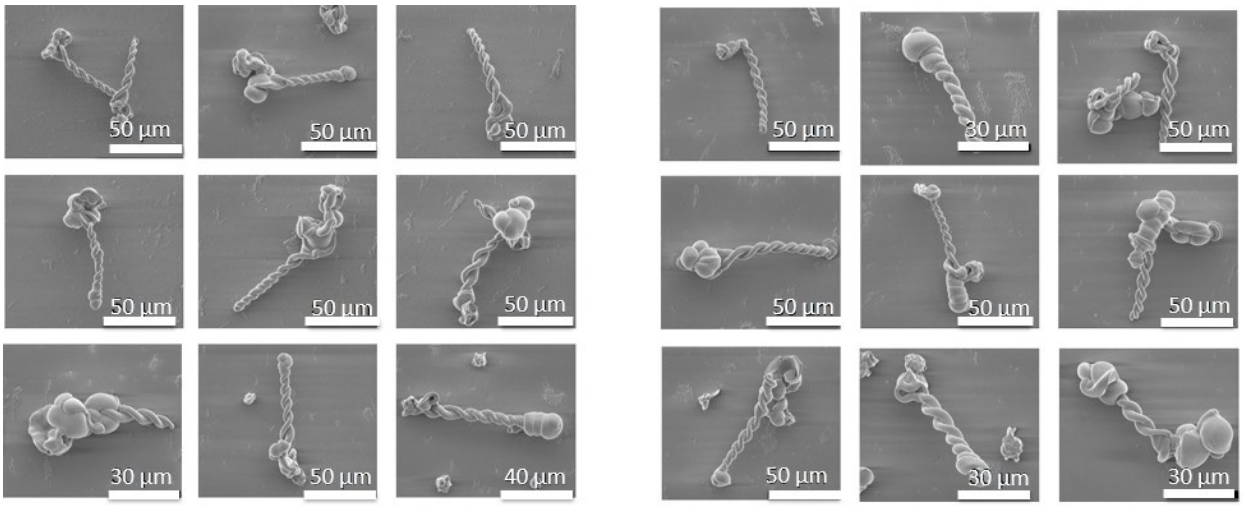

Figure 27. SEM images of: A) right-handed double helices; and B) left-handed double helices that were grown with L-aspartic acid (3 mM).

Other structures displaying multiple colours in a spherically-banded pattern, as observed by polarized light microscopy, were also observed at the highest point of the solution-air interface in samples that contained amino acid. These structures displayed a maltese cross in addition to colours characteristic of interference patterns. Although the exact nature of the interaction(s) of these amino acids with silica-carbonate microstructures is unknown, we can imagine several scenarios depending on the concentration of the former. At low concentrations of the amino acid, the interaction with the mineral might not be strong enough to influence the assembly of the carbonate and silica. On the other hand, too high of an amino acid concentration could lead to significant binding to the mineral, thus preventing the type of interaction between carbonate and silica that is necessary for the formation of helices. Interestingly, there might not be an ideal balance between the ratio of amino acid to carbonate and silica, as there are two distinct processes that need to be taken into consideration in these reactions. First, the double helices develop on a micron scale from two twists that approach each other with the same sign, a process which is purely random, hence the racemic nature of the helices. On the other hand, the use of the amino acid involves a molecular-scale component that might mean that the two systems will never overlap in such a way as to influence the micron-scale chirality of the double helices, due to the vastly different scales on which these interactions are expected to develop. Furthermore, the amino acid would have to direct the formation of the curved surfaces even prior to their approach and subsequent transformation to double helices, which may in itself negatively upset the local balance

struck between the carbonate and silica, and possibly even oligomeric silica species, necessary for the occurrence of these structures in the first place.

3.1.2.2. Conclusions

In conclusion, we show that the use of enantiopure amino acids does not control the handedness of silica-carbonate double helices, although there are known examples involving the transfer of chirality from aspartic acid to some micron-sized $CaCO_3$ architectures. Indeed, this might not even be a feasible method to affect self-assembly of silica and carbonate into homochiral structures, as we have much to learn about the underlying interactions and reaction mechanisms of these additives with composite materials as opposed to single crystals.

3.2. Amino-acid induced chiral vaterite microstructures

3.2.1. Introduction

Calcium carbonate ($CaCO_3$), one of the most ubiquitous biominerals in nature, exists as three anhydrous polymorphs: calcite, aragonite and vaterite, with the latter being the most thermodynamically unstable. In many common $CaCO_3$ architectures, macromolecules direct the composition and assembly of the mineral phase, thus forming very elaborate materials. In the case of the snail shell, the as-formed structure displays chirality, forming either a left- or right-handed spiral. Chiral symmetry breaking of these $BaCO_3$ microhelices is of fundamental interest due to their potential use for optical applications. In the literature, most strategies geared towards controlling chirality, especially of $CaCO_3$, have been centred on the use of biological molecules. For example, Orme *et al.*[53] used aspartic acid to induce the formation of chiral crystal habits in calcite crystals.[1] More recently, Jiang *et al.*[60] demonstrated the transfer of chirality from L- and D-aspartic acid, as well as L- and D-glutamic acid, to vaterite toroids. To date, comparable strategies to direct the handedness of $BaCO_3/SiO_2$ helices with amino acids have not been achieved. We believe that twisted chiral crystal morphologies, namely the vaterite polymorph of $CaCO_3$, could be explored as templates to direct the handedness of $BaCO_3/SiO_2$ helices at the microscale. As a first step towards controlling the chirality of $BaCO_3/SiO_2$ helices with chiral vaterite templates, we focused on attempts to synthesise chiral vaterite using the direct mixing method (Jiang *et al.*), as well as two other similar methods (the ammonium carbonate and the atmospheric CO_2-gas

diffusion methods). While these studies are geared towards providing a first step in the future design of novel functional materials with enhanced properties, it is our hope that they will also foster a better understanding of growth and chirality in biomineralization processes.

3.2.2. Synthesis of vaterite: Jiang *et al.* method

Jiang *et al.*[60] noted that while solutions with enantiomerically pure aspartic or glutamic acid formed round chiral vaterite (Figure 6) as the main $CaCO_3$ phase, control reactions without amino acid resulted in the formation of rhombohedral calcite and achiral hexagonal vaterite. Here, we controlled the $CaCO_3$ polymorphism with a slight modification in this protocol in order to decrease the vaterite growth induction time. Chiral vaterite was synthesised at pH 10.5 from solutions of $CaCl_2 \bullet 2H_2O$ and Na_2CO_3 to which homochiral aspartic acid was added. The observed nucleation density varied as a function of concentration. When the $CaCl_2 \bullet 2H_2O$ and Na_2CO_3 concentrations were both 1.5 mM, fewer chiral vaterite toroids of a more discrete nature formed on the glass substrates as observed by optical light microscopy (Figure 28a–b). In contrast, an increase in the concentration of $CaCl_2 \bullet 2H_2O$ from 1.5 to 2.5 mM corresponded to a noticeably greater population of vaterite toroids (Figure 28c–e). The fact that the vaterite toroids grew in close contact can also be attributed to the enhanced nucleation density of the structures in the latter case.

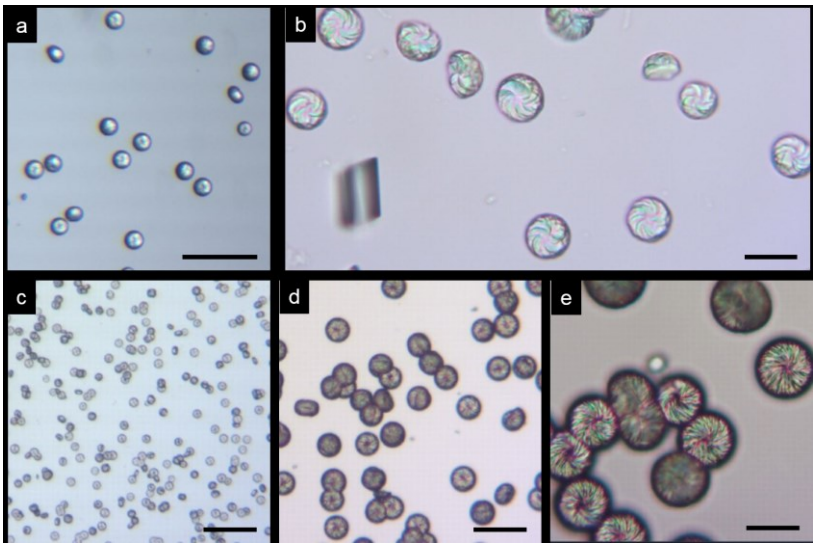

Figure 28. Optical light microscopy images of chiral vaterite toroids that were grown on glass slides at pH 10.5 from solutions containing 20 mM homochiral L-aspartic acid, $CaCl_2$ and Na_2CO_3. The concentrations of $CaCl_2$ and Na_2CO_3 were 1.5 and 1.5 mM (A, 1 day and B, 3 days), and 2.5 and 1.5 mM (D, 1 day and D–E, 4 days), respectively. The scale bars in the images are 200 microns (A), 20 microns (B–E).

We further explored the effect of pH in addition to concentration in another series of experiments. The findings suggest a lower concentration of $NaCO_3$ (1.5 mM) to $CaCl_2$ (2.5 mM) was also favourable for growing chiral vaterite at pH 11 (Figure 29a–c). However, when this ratio was reversed while maintaining the same pH, the chiral spherical vaterite toroids were overgrown with other vaterite morphologies (Figure 29d–e).

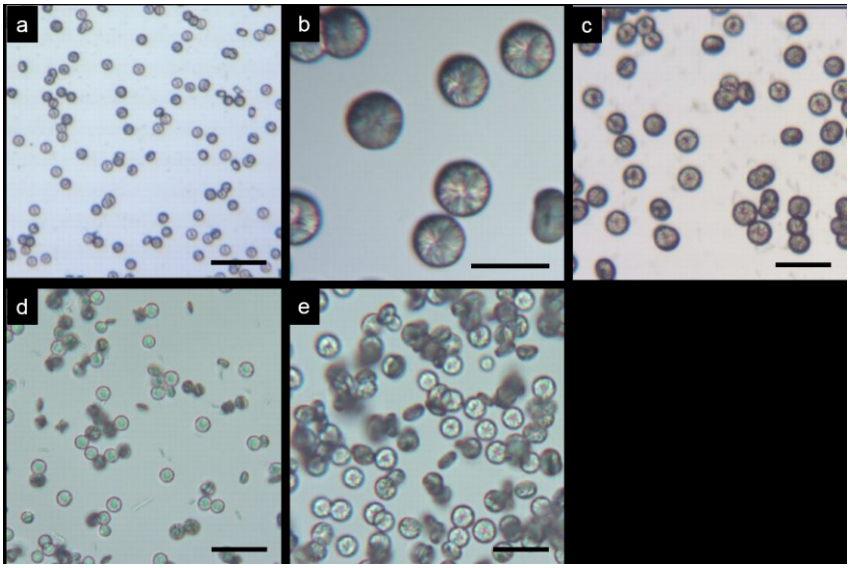

Figure 29. Optical light microscopy images of chiral vaterite toroids that were grown on glass slides at pH 11 from solutions containing 20 mM homochiral L-aspartic acid, $CaCl_2$ and Na_2CO_3. The concentrations of $CaCl_2$ and Na_2CO_3 were 1.5 and 2.5 mM (A–B, 1 day and c, 4 days), and 2.5 and 1.5 mM (D, 90 minutes and E, 1 day), respectively. The scale bars in the images are 20 microns (A, C–E) and 200 microns (B).

In other studies, we discovered that several other factors influenced the polymorphic behaviour and growth induction time of $CaCO_3$. For example, equal volumes (50 mL) of sodium carbonate and calcium chloride- L-aspartic acid solutions were mixed. Here, the concentration ratio of $CaCl_2 \bullet 2H_2O$ to Na_2CO_3 was set to 1:5 mM, while the pH of the calcium chloride-aspartic acid solution was increased from 3.5 to 6.8 before adding to the carbonate solution (pH 10). These conditions induced the formation of both mature and metastable vaterite with roughened textures after about 4 hours at pH 10.5 (Figure 30). On the other hand, when the calcium chloride to carbonate concentration was inverted to 5 and 1 mM, respectively, chiral vaterite mostly formed after one day (not shown). However, significantly more calcite was formed at both concentrations.

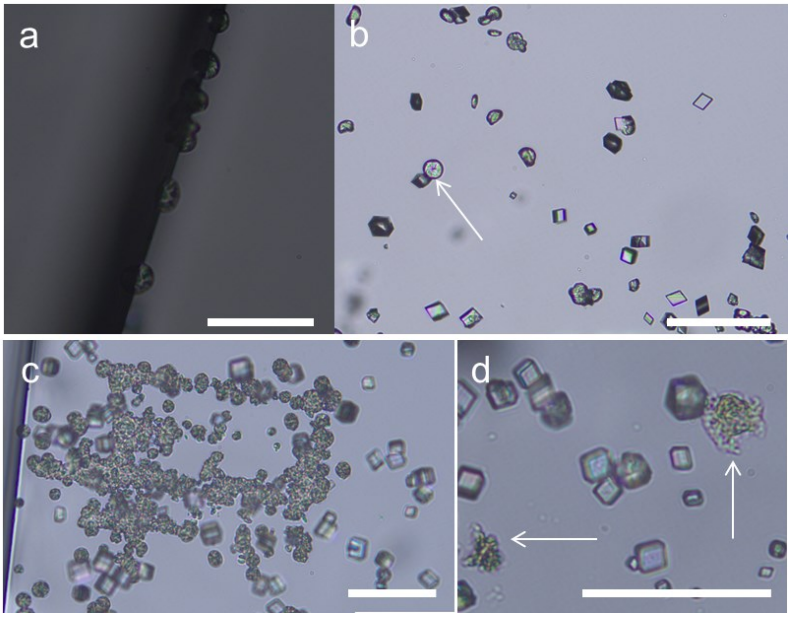

Figure 30. Optical microscopy of calcite and vaterite crystals from solutions of $CaCl_2$ (1 mM) and $NaCO_3$ (5 mM) containing L-aspartic acid (20 mM) at pH 10.5 precipitated on glass at different times: A) *ca.* 2 hours; B) *ca.* 4 hours; and C–D) *ca*. 24 hours. The white arrows point to vaterite toroids which have a very different appearance after 24 hours due to possible dissolution of the crystals. Scale bars in the images are all 100 microns.

Irrespective of whether the pH was adjusted to 10.5 or 11, the nucleation density of the as-grown chiral vaterite toroids was controlled by tuning the $CaCl_2$ concentration. A concentration of 2.5 mM resulted in a greater amount of structures grown on the substrates compared to the lower concentration of 1.5 mM. Other unexpected morphologies, such as high aspect ratio rods, were grown when the pH was adjusted to 11. In direct contrast to these results, increasing the initial pH of the calcium chloride-aspartic acid solution (*i.e.* from 3.6 to 6.8) and either the carbonate or the calcium concentration (*i.e.* 1 or 5 mM) lead to a faster induction time/formation of calcium carbonate in general. However, both ratios gave rise to significant populations of calcite, as well as fewer chiral vaterite toroids of variable stability and texture.

3.2.3. Synthesis of amino-acid induced chiral vaterite: Ammonium carbonate method

The synthesis of achiral $CaCO_3$ from $CaCl_2$ solutions in the presence of ammonium carbonate is well-described in the literature.[103] Here, the decomposition of the ammonium

carbonate produces ammonia and carbon dioxide. The ammonia increases and buffers the pH of the reaction upon its diffusion into the crystallization solution. The synergistic effect of both the presence of an organic compound, homochiral aspartic acid in this case, and the as-produced ammonium species could also play a role in polymorph selection based on the initial ammonia threshold concentration, though a systematic study of the latter was not conducted. Variations of the ammonium carbonate method were used to prepare chiral vaterite from mixtures of $CaCl_2 \bullet 2H_2O$ (0–1.5 mM) and Na_2CO_3 (0–2.5 mM) in the presence of L-aspartic acid (20 mM). The role of temperature (room temperature versus 60 ºC) was investigated in these reactions. A method to synthesise vaterite from the diffusion of atmospheric CO_2 into solutions of $CaCl_2$ was also developed in our lab.

3.2.3.1. Variation 1: Synthesis of vaterite from 1 mM $CaCl_2 \bullet 2H_2O$ and 2.5 mM Na_2CO_3 (room temperature followed by 60 °C)

In variation 1, the effect of temperature (*i.e.* room temperature versus 60 °C) on the precipitation of calcium carbonate *via* the ammonium carbonate diffusion method was studied at a 1:2.5 calcium to carbonate ratio. The progress of the crystallization was followed first at room temperature, then at 60 °C for the same solution. The solutions, in 100 mL beakers, along with freshly ground ammonium carbonate (4–6 g) were kept in a small desiccator. After 12 hours at room temperature, the reaction was deemed to be progressing too slowly based on the lack of precipitate detected at this time. Therefore, the desiccator was placed in a 60 °C oven overnight in order to possibly speed up the precipitation and growth of calcium carbonate. Following a heat exposure time of 6–7 hours, both spherical chiral vaterite (Figure 31a), irregular vaterite (Figure 31b), as well as immature chiral vaterite (Figure 31c) were formed. The surface of the calcite crystal shown in Figure 31c displayed etched characteristics. (Figure 31d). After a day in the oven, the majority of the $CaCO_3$ phase formed on the slides was chiral vaterite (Figure 31e). However, the entire slide (glass and aluminium), including the vaterite toroids, were covered by the deposition/accretion of many rod-shaped crystals (Figure 31f). Indeed, the crystallization solution became milky white in appearance during a heat exposure time of greater than 12 hours. The precipitated material was either due to aluminum hydroxide from aluminum ions and water under

the influence of ammonia gas, or to secondary $CaCO_3$ nucleation, although this hypothesis was not independently verified by carrying out comparative studies in the absence of aluminium substrates.

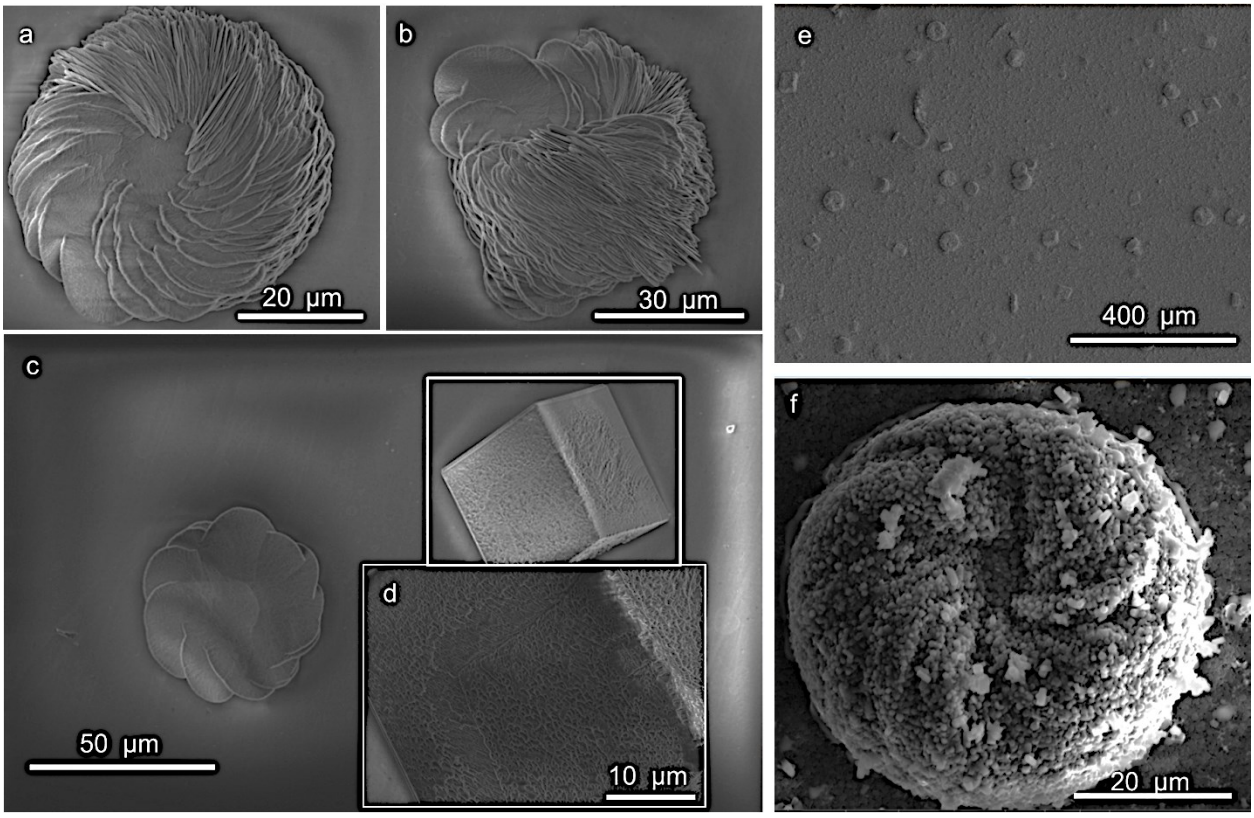

Figure 31. SEM images showing $CaCO_3$ precipitated from a solution of $CaCl_2$ (1 mM) and $NaCO_3$ (2.5 mM) containing L-aspartic acid (20 mM) at pH 10.5. The reaction vessel was first left undisturbed for 12 hours at room temperature in a closed desiccator containing a vial of freshly crushed ammonium carbonate, before being placed in an oven at 60 °C. Slides were removed and viewed after selected times spent in the oven: A–D) 6–7 hours; and E–F) one day.

The above results suggest that the higher temperature increased the precipitation and growth of calcium carbonate, including a majority of chiral vaterite. However, longer exposure time (> 12 hours) in the oven at 60 ºC, while in the presence of aluminium, might be unfavourable due to the precipitation and accretion of a large quantity of possible secondary calcium carbonate particles on the substrates.

3.2.3.2. Variation 2: Synthesis of vaterite from 1 mM $CaCl_2 \bullet 2H_2O$ and 2.5 mM Na_2CO_3 (room temperature followed by 60 ºC)

Since it was shown that temperature reduces the time taken for chiral vaterite formation and precipitation, the viability of eliminating the 12 hour period at room temperature, and instead subjecting the reaction to heat immediately after the preparation of the solutions and insertion into the desiccator was investigated. The solutions were prepared as described in section 3.2.2.1 in a 100 mL beaker, which contained $CaCl_2$ (1 mM), $NaCO_3$ (2.5 mM) and L-aspartic acid (20 mM), and was placed in a closed desiccator (15 cm diameter) with freshly ground ammonium carbonate. The desiccator was immediately placed inside an oven at 60 ºC, which was considered to be the start of the reaction. However, these conditions favoured the crystallization of achiral vaterite (Figure 32a-b) on glass substrates after 13 hours. The vaterite crystals, with diameters ranging from 28–61 microns, appeared flat (inset of Figure 32b), and did not form the tilted platelets that are characteristic of chiral vaterite even after 2 days.

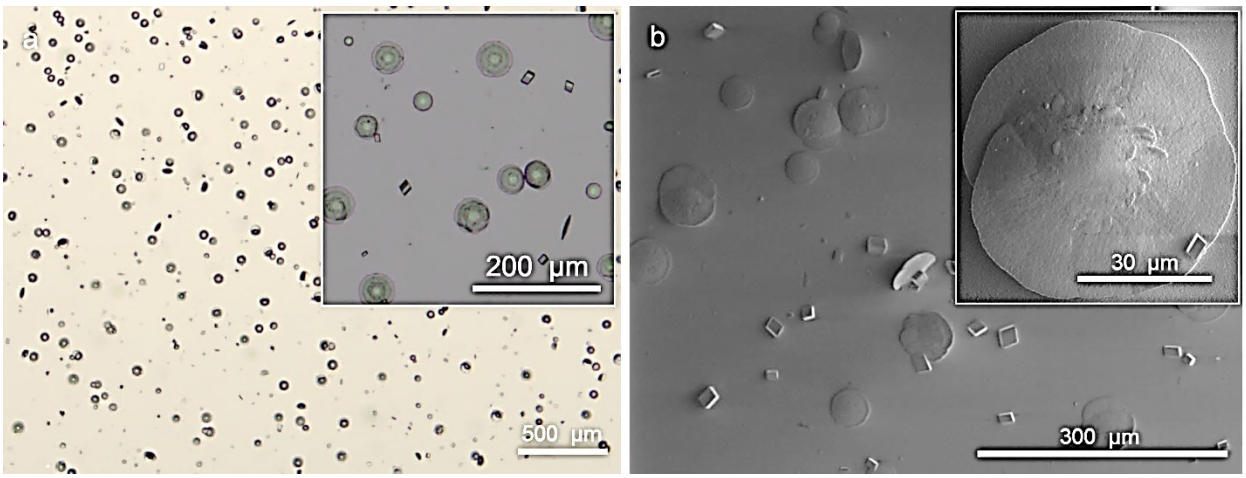

Figure 32. Optical light microscopy (A) and scanning electron microscopy (B) images of vaterite precipitated on glass from a solution of $CaCl_2$ (1mM) and $NaCO_3$ (2.5 mM) containing L-aspartic acid (20 mM) at 60 °C in the presence of ammonium carbonate after *ca.* 13 hours.

These findings confirm that while heat speeds up the reaction, it also leads to the uncontrolled crystallization of vaterite by way of a mechanism that disfavours chiral control of the final structures. This is perhaps not surprising given that heat enhances the production of carbon

dioxide. Therefore, exposing the desiccator to a high temperature of 60 ºC at the onset of the reaction is not a viable option for the synthesis of chiral vaterite.

3.2.3.3. Variation 3: Synthesis of vaterite from $CaCl_2 \bullet 2H_2O$ (with or without Na_2CO_3 at room temperature)

The formation of vaterite was subsequently investigated solely at room temperature due to the problematic nature of the prior reactions at 60 ºC. Flat vaterite microstructures were obtained at all concentrations of $CaCl_2$ and $NaCO_3$ even after several days in the presence of ammonium carbonate (Figure 33). These experimental observations support the finding that homochiral aspartic acid in the solutions favours the crystallization of vaterite. However, the amino acid concentration might not be high enough to support the formation of chirality-inducing platelets, in most cases, under these conditions. Chiral vaterite was only precipitated when the $NaCO_3$, $CaCl_2$, and L-aspartic acid concentrations were 0, 1.5 and 20 mM, respectively (Figure 33b).

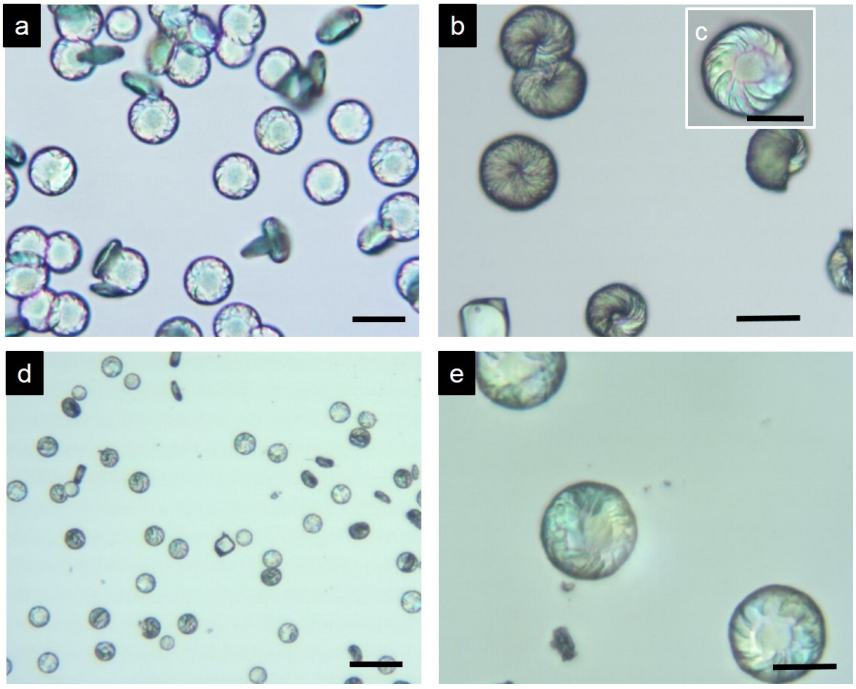

Figure 33. Vaterite toroids were prepared by the ammonium carbonate method and grown on glass slides from solutions of varying concentrations of $NaCO_3$, $CaCl_2$ and L-aspartic acid, which were respectively: 1.5, 1.5 and 20 mM, after three days (A, solution 1); and 0, 1.5 and 20 mM, after five days (B–C, solution 2) and 0, 0.75 and 20 mM (D–E, solution 3). The scale bars in the images are 20 (A, D), 50 (C), and 100 microns (B, E).

3.2.4. Synthesis of vaterite: the diffusion of atmospheric CO_2 method

Experimental conditions where atmospheric CO_2 flows into reaction solution of $NaSiO_3$ and Ba/$SrCl_2$ provide a useful method for dynamically sculpting silica-carbonate microstructures as they grow. This observation provided the basis for growing $CaCO_3$ from atmospheric CO_2, which would potentially not only provide the chiral vaterite for further reactions but also opens up the future possibility of assembling vaterite possessing even greater hierarchical organization and interesting morphologies.

Here we developed a method for growing chiral vaterite from solutions of $CaCl_2 \bullet 2H_2O$ (1.5 mM) and L-aspartic acid (20 or 40 mM) at pH 10.5. The presence of Na_2CO_3 (1.5 mM; control reaction only) and the diffusion of atmospheric CO_2 into all relevant solutions provoked the precipitation of chiral vaterite on glass coverslips (Figure 34). No noticeable effect was detected upon increasing the amino acid concentration from 20 to 40 mM.

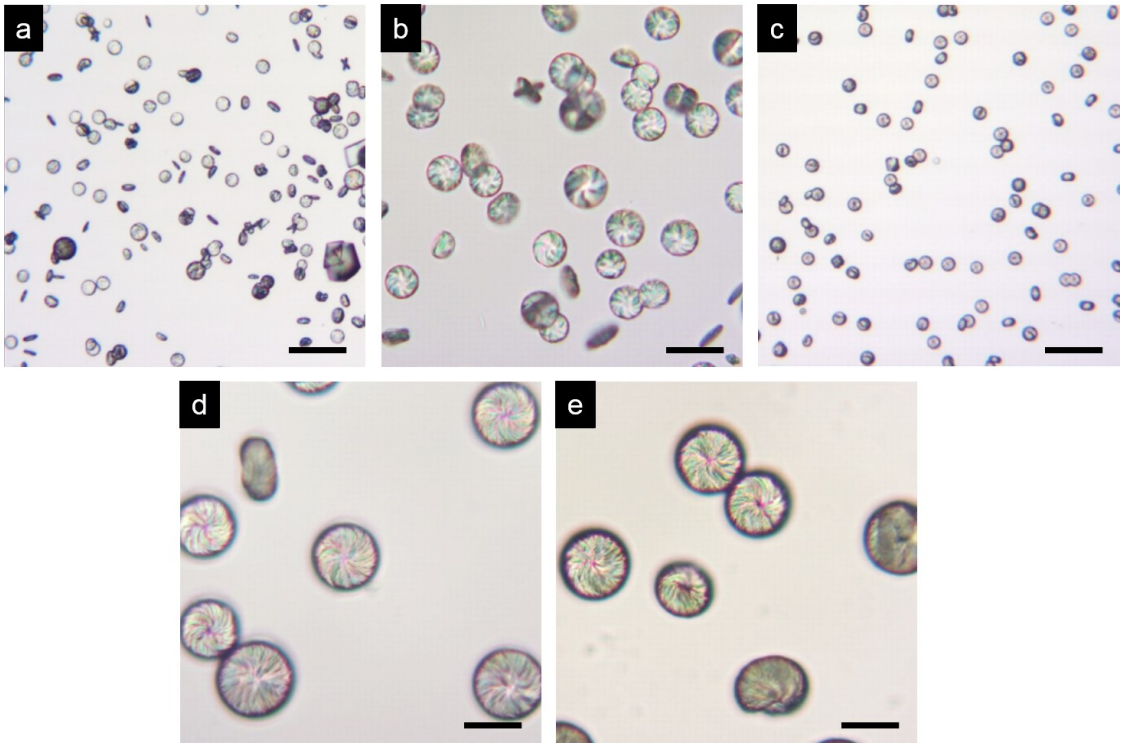

Figure 34. Vaterite toroids grown on glass slides from solutions into which CO_2 was allowed to diffuse, and at varying concentrations of $NaCO_3$, $CaCl_2$ and L-aspartic acid, which were respectively: 1.5, 2.5 and 20 mM after one day (A) and four days (B); 0, 2.5 and 20 mM after one day (C); and 0, 2.5 and 40 mM after one day (D) and four days (E). The scale bars in the images are all 20 microns.

3.2.5. Conclusions

Based on these results, we can conclude that the most promising reaction conditions for the synthesis of chiral vaterite *via* both Jiang *et al.* and the atmospheric CO_2 diffusion methods were obtained when the respective calcium chloride and the sodium carbonate concentrations were 1.5 and 1.5–2.5 mM, and 2.5 and 0 mM, respectively. In comparison, the ammonium carbonate methods either produced chiral vaterite of non-uniform morphologies (room temperature to 60 °C, variation 1), achiral vaterite (60 °C, variation 2) or a mixture of achiral vaterite and a minority of chiral vaterite (room temperature, variation 3). Furthermore, the results underscore the major effect that both pH and sample preparation method have on polymorph selection in calcium carbonate mineralization.

3.2.6. Nucleation of $BaCO_3$ on $CaCO_3$

3.2.6.1. Introduction

The use of chiral additives has no measurable effect directly on the handedness of the silica-carbonate helices. However, we are able to use chiral additives to control the handedness of chiral vaterite. Furthermore, it has recently been shown that $BaCO_3/SiO_2$ double helices can be nucleated specifically on each calcium carbonate polymorp.[96] This now opens an exciting opportunity: can we use chiral vaterite crystals to control the handedness of $BaCO_3/SiO_2$ helices? The ability to control the chirality of these helices could even bring us one step closer to using these silica-carbonate materials to manipulate light.[104] In this work, we present the current state of where we are in terms of attempts to control the chirality of silica-carbonate microstructures with chiral vaterite prenucleated on either glass or aluminium substrates.

3.2.6.2. Results and discussion

3.2.6.2.1. Effect of chiral vaterite on the chirality of silica-carbonate microstructures

In order to investigate the effect of chiral vaterite on silica-carbonate microstructures, helices, in particular, $BaCO_3$ and SiO_2 were precipitated on glass substrates that contained prenucleated chiral vaterite whose synthesis was described above. The reactions were carried out by the CO_2-difussion method in 100 mL beakers at pH 11.2 to facilitate the nucleation and growth

of helices on the substrates over a reaction time of 1.5–2 hours. Typical $BaCl_2 \bullet 2H_2O$ and Na_2SiO_3 final concentrations were maintained at *ca.* 20 and 8.7 mM, respectively.

Figure 35a shows vaterite on the part of the slide that was located above the meniscus of the crystallization solution. The chirality of the vaterite was determined to be right-handed due to the spirals of the toroids tilting in a counterclockwise manner (inset of Figure 35a). To study the effect of growing silica-carbonate helices in the presence of chiral vaterite, the previously submerged section of the slide was also analysed by SEM. The helices mostly nucleated independently of the vaterite, and instead grew directly on the slide where other characteristic morphologies, such as leaves, were also present (Figure 35b). A close-up view of the microstructures revealed that both the structural integrity and the chirality of the vaterite were maintained, as well as the similarity in the dimensions of the vaterite and the base of the helices growing in its vicinity (Figure 35b).

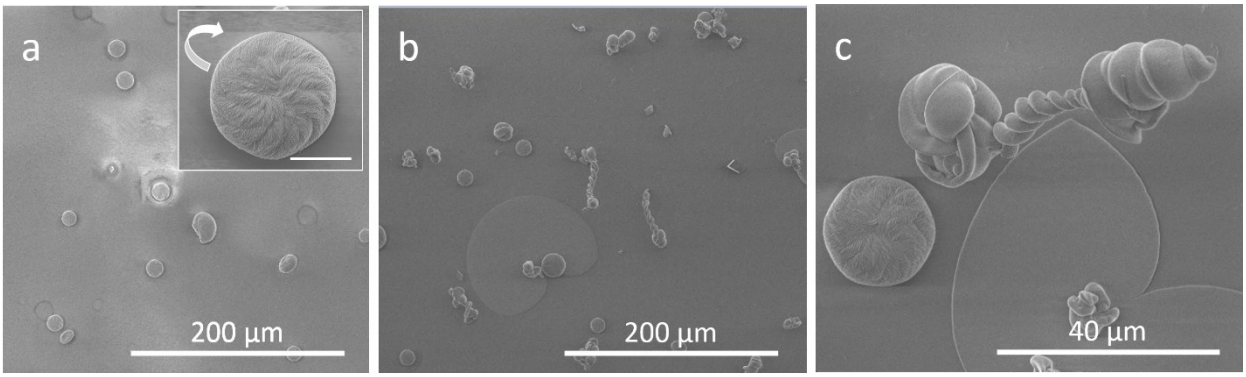

Figure 35. Scanning electron micrographs depicting the crystallization silica-carbonate microstructures in the presence of chiral vaterite after 2 hours: A) right-handed vaterite not exposed to solution; B) helices and vaterite on the section of the slide that was immersed in solution; and C) helices growing in the vicinity of a vaterite toroid.

Figure 36a depicts the growth of a relatively straight double helix on a vaterite toroid, where the actual spiralling behaviour does not immediately start at the original nucleation point. Tracing the origins and deducing the chirality of other hydrid carbonate structures can be slightly more complicated as shown in Figure 36b. Here, the surface coverage of the vaterite toroid by the helices is greater, and it appears to grow towards and then down the side of the toroid before making contact with the substrate. The subsequent growth of the helices is defined by an upward tilt in curvature, and the formation of tighter coils as its bulbous end eventually comes in contact with its elevated base. A spiral-like feature is clearly visible on the tip of the helices, which suggest that

they are also right-handed, since the formation of the former is known to occur with the preservation of chirality. Elsewhere, and in addition to providing direct evidence that these helices do not always start growing from large bases, it is also observed that their growth does not terminate upon making contact with an obstacle, such as vaterite, but instead display a deviation in their growth direction (Figure 36c). Finally, leaves growing on the substrate tended to grow around any vaterite in its direct path (Figure 39d). Other silica-carbonate microstructures grew directly on calcite, either as a helix emanating from a single point (Figure 36e) or a leaf covering the surface of the underlying structure (Figure 36f).

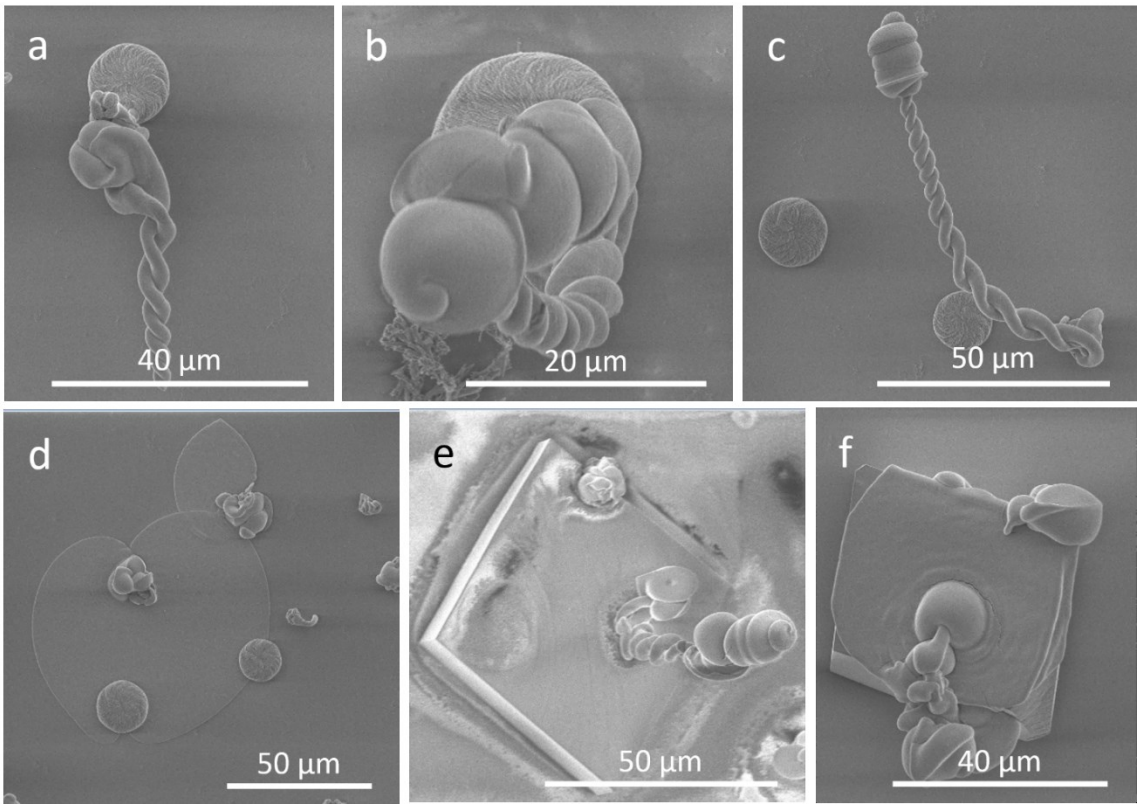

Figure 36. SEM images showing the growth behaviour of various silica-carbonate microstructures including: A–B) helices growing on chiral vaterite; C) change in growth direction of a double helix after it made contact with a vaterite toroid; D) leaves; and E–F) microstructures growing on calcite

3.2.6.3. Conclusions

The abovementioned results indicate that it is quite challenging to gain control over the nucleation of silica-carbonate helices on chiral vaterite, which is in part due to the randomness of nucleation events as well as the inherent unfavourable interstitial energies involved in the alignment of these two different types of carbonate. Moreover, the crystallization solutions might

not have been sufficiently degassed to influence the discrimination in the position of nucleation, similar to that reported by Noorduin *et al.*[96] Another challenge in potentially using chiral vaterite to template the chirality of these helices lies in the distance from the point of nucleation at which their formation starts. It would perhaps be more impactful if the beginning of helix formation closely coincides with nucleation on vaterite, otherwise the chirality of the former would be random. One potential way to achieve a cleaner base for the spirals is to incorporate Chicago Sky Blue dye (CSB) in these reactions; CSB seems to increase the growth rate of leaves as well as decrease the bases of helices (refer to Chapter 4). Our results were not conclusive since the vaterite content on the slides was very low in comparison to calcite.

3.3. Experimental

3.3.1. Materials and method

Analytical grade barium chloride dihydrate ($BaCl_2 \bullet 2H_2O$), and sodium metasilicate (Na_2SiO_3) from Sigma Aldrich and L-aspartic acid from Alfa Aesar were used without further purification. All samples were prepared fresh with distilled water. Microscope slides (75 x 25 x 1 mm) were purchased from Thermo Fisher Scientific. The slides were cleaned by sonicating twice, first in deionized water for *ca.* 5–8 minutes and then in isopropyl alcohol for 5 minutes. The slides were subsequently air dried and stored in a sample boxes.

3.3.2. Experimental conditions for the structures shown in Figures 25–27 (silica-carbonate microhelices)

In the reactions investigated, $BaCl_2$ solution (3 mL, 0.309 mmol, 103 mM) with dissolved L-aspartic acid was added to Na_2SiO_3 (12 mL, 0.127 mmol, 10.65 mM). Typical $BaCl_2 \bullet 2H_2O$ and Na_2SiO_3 final concentrations were maintained at *ca.* 20.6 and 8.7 mM, respectively, while the amino acid concentration was limited to a range of 0–3 mM. For example, 4.433 mL of a 0.12 mol/L NaOH (0.530 mmol) solution was added to L-aspartic acid (0.316 mmol) in a 25 mL vial to obtain a clear solution. This solution of basic additive was combined with $BaCl_2$ and was then divided to give a volume of additive-$BaCl_2$ that was 0.363 mmol in $BaCl_2$ and either 0.023 or 0.045 mmol in additive. The rest of the reaction was conducted at pH 11.2 by the CO_2-diffusion method in 100 mL beakers in the manner described in section 2.5.2. Here, the microstructures were precipitated on glass slides (55 x 25 x 1 mm) over a reaction period of 2 hours.

3.3.3. Experimental conditions for vaterite shown in Figures 28–30

In a 100 mL beaker, 50 mL of a 40 mM aspartic acid solution was added to 0.3 or 0.5 mL of a 500 mM calcium chloride ($CaCl_2 \bullet 2H_2O$) solution. This solution was diluted with 24.5–25 mL deionized water (Solution A). 1.5–2.5 mL of a 100 mM sodium carbonate (Na_2CO_3) solution, diluted with 23.5–25 mL water, was added to solution A. The total reaction volumes were fixed at 100 mL. The final concentrations of Na_2CO_3 and $CaCl_2 \bullet 2H_2O$ were either 1.5 mM or 2.5 mM, while the amino acid had a concentration of 20 mM. The pH of the mixture was subsequently adjusted to either 10.5 or 11 +/-0.2 (Figures 28 and 29, respectively with 1 M NaOH or HCl. The beakers, into which glass coverslips were dropped, were sealed with parafilm and left undisturbed at room temperature. The glass coverslips were subsequently removed at different times, rinsed in deionized water followed by ethanol or acetone, and air dried, before analysis beneath the microscope in order to obtain a time course of the crystallization reaction.

3.3.4. Experimental conditions for vaterite (Figures 31–32, room temperature and/ or 60ºC, Variation 1 & 2)

Several variations to the above protocol (section 3.3.3) were made, where the effect of changes in temperature (room temperature versus 60 ˚C) on the precipitation of calcium carbonate *via* the ammonium carbonate diffusion method was studied at a 1:2.5 mM calcium to carbonate concentration ratios. The progress of the crystallization was followed first at room temperature, then at 60 ˚C for the same solution (variation 1: 1:2.5 calcium to carbonate concentration ratio), entirely at 60 ˚C (variation 2: 1:2.5 calcium to carbonate concentration ratio

In variation 1 (Figure 31, section 3.2.2.1), Na_2CO_3 (13.60 mg in 25 mL water) was added to $CaCl_2 \bullet 2H_2O$ (8.90 mg , 6.05 mmol) dissolved in aspartic acid (25 mL, 40 mM) in a 100 mL beaker. Final concentrations of $CaCl_2 \bullet 2H_2O$, Na_2CO_3, and amino acid were 1, 2.5 and 20 mM, respectively. All the samples were prepared fresh with deionized, degassed water. The beaker, covered with a petri dish to allow the diffusion of gas in through its spout, was then placed in a closed small desiccator (15 cm diameter) along with freshly ground ammonium carbonate (4–6 g) in a 12 mL glass vial. After 12 hours at room temperature, the desiccator was subsequently placed in a 60 ˚C oven overnight in order to speed up the precipitation and growth of calcium carbonate.

Slides were removed from the beaker at different times (6–7 and 12 hours in the oven) and washed prior to analysis by optical light microscopy and SEM.

In Variation 2 the solutions were prepared as described above in a 100 mL beaker, which contained $CaCl_2$ (1 mM), $NaCO_3$ (2.5 mM) and L-aspartic acid (20 mM), and was placed in a closed desiccator (size) with freshly ground ammonium carbonate (Figure 32). The desiccator was immediately placed inside an oven at 60 $^{\circ}$C. The glass slides with the as-grown structures were removed and washed after 13 hours or two days.

3.3.5. Experimental conditions for vaterite (Figures 33, room temperature, Variation 3)

Samples were prepared in 100 mL beakers from stock solutions of L-aspartic acid, Na_2CO_3 and $CaCl_2$ with concentrations of 40, 100 and 500 mM, respectively. Solutions 1 and 2 were prepared by mixing $CaCl_2$ (0.3 mL) with L-aspartic acid (50 mL), followed by deionized water (25 mL). $NaCO_3$ (1.5 mL), diluted with water (23.2 mL), was only added to Solution 2. For Solution 3, the volume of $CaCl_2$ (0.15 mL) was reduced by half before adding L-aspartic acid. Additional water (49.7 and 49.85 mL, respectively) was required to dilute Solutions 2 and 3 to a total volumes of 100 mL. The final concentrations of Na_2CO_3, $CaCl_2$ and L-aspartic were 0, 1.5 1.5, 1.5, and 20 mM (solution 1), 20 mM (solution 2) and 0, 0.75 and 20 mM (solution 3). The pH of the solutions was adjusted to 4.5 with freshly prepared NaOH (1 M) prior to being placed in a small closed desiccator, along with freshly ground ammonium carbonate (5g) in a 20 mL vial covered with parafilm. A needle was used to make several holes in the parafilm in order to allow the diffusion of NH_3 and CO_2 into the solutions. Glass slides, dropped to the bottom of each beaker prior to being placed in the desiccator, were removed after several days and rinsed in 2 separate portions of deionized water, followed by ethanol and were subsequently air dried prior to analysis.

3.3.6. Experimental conditions for vaterite (Figures 34, room temperature, atmospheric CO_2 gas-diffusion method)

Stock solutions of $CaCl_2 \bullet 2H_2O$ (500 mM), Na_2CO_3 (100 mM), and L-aspartic acid (40 mM) were prepared with deionized water and stored as per the method outlined in section 5.2.4. The pH of the solutions was adjusted to 10.5.

$CaCO_3$ was precipitated by preparing three different solutions that contained $CaCl_2 \bullet 2H_2O$, Na_2CO_3, and L-aspartic acid. First, Na_2CO_3 (0.225 mL), diluted with water (7.2 mL,) was added to a $CaCl_2 \bullet 2H_2O$ solution (0.075 mL), containing L-aspartic acid solution (7.5 mL) in a 20 mL beaker. The final concentrations of Na_2CO_3, $CaCl_2 \bullet 2H_2O$ and L-aspartic acid were fixed at 1.5, 2.5 and 20 mM, respectively. The second and third solutions contained only $CaCl_2 \bullet 2H_2O$ (0.075 mL), L-aspartic acid (7.5 and 15 mL, respectively), and additional water (7.42 and 0 mL, respectively). While the final concentration of $CaCl_2 \bullet 2H_2O$ in both solutions was 2.5 mM, the L-aspartic acid concentration of the second and third solutions was 20 and 40 mM, respectively. The total reaction volume was about 15 mL in all cases, while the pH of the mixtures was subsequently adjusted to 10.5 with 1 M NaOH and/or HCl. The beakers were loosely covered with petri dishes to allow the flow of atmospheric CO_2 in through the spouts, and were subsequently left undisturbed at room temperature. Glass slides, which were dropped into the solutions before the beakers were covered, were subsequently removed after one or four day(s). The slides were then rinsed in deionized water followed by acetone, and air-dried before analysis.

3.3.7. Nucleation of silica-carbonate helices on substrates with pre-assembled chiral vaterite architectures (figures 35–36)

In order to investigate whether chiral transfer from vaterite to silica-carbonate microstructures might occur, helices in particular, $BaCO_3$ and SiO_2 were precipitated on glass substrates that contained prenucleated chiral vaterite whose synthesis was described above (section 3.3.3). The reactions were carried out by the CO_2-difussion method in 100 mL beakers at pH 11.2 to facilitate the nucleation and growth of helices on the substrates over a reaction time of 1.5 to 2 hours. Typical Na_2SiO_3 and $BaCl_2 \bullet 2H_2O$ final concentrations were maintained at 8.7 and 20 mM, respectively.

Chapter 4. The growth of silica-carbonate microstructures in the presence of Chicago Sky Blue

4.1. Introduction

Spurred by lessons learnt from the ability of nature to "design" biominerals with a high degree of control over their shape, size, mineral phase and hierarchical assembly over multiple length scales, a multitude of bottom-up research strategies have been geared towards developing self-assembled inorganic materials having superior functionality and complexity.[105-109] Indeed, it is well-known that the physical and chemical properties of a material are intertwined with its function. These materials are expected to have significant ramifications in building devices with nanoscale components for application in optics, electronics and perovskite-based semi-conductors.[104, 110-114] Of particular interest are 3D emergent microstructures, characterized by long-range orientational order and highly curved surfaces, which can be synthesized from the coupled reaction of the carbonates of barium and strontium with silica in alkaline environments (Figure 13).[74] These shapes, coined as biomorphs, include cardioidal sheets/leaves, helicoids, "worms" and flower-like and globular structures. The acid-catalysed mechanism implicated in the formation of bimorphs has largely been based on indirect evidence until recently when Garcia Ruiz *et al.* used a chemical probe to gather evidence which directly supports the autocatalytic nature of the coprecipitation reaction between silica and carbonates.[86] They found that the reaction proceeds with the spatial and temporal oscillation of pH at the growth front, most likely due to carbonate precipitation leading to a reduction of the pH, which subsequently triggers silica precipitation and an increase in pH according to equation 1 and 2:

$$CO_2\,(g) + Ba^{2+}\,(aq) + H_2O\,(l) \rightleftharpoons BaCO_3\,(s) + 2H^+\,(aq) \quad \text{(equation 1)}$$

$$2H^+\,(aq) + SiO_3^-\,(aq) \rightleftharpoons SiO_2\,(s) + H_2O\,(l) \quad \text{(equation 2)}$$

They also found that the growth front of the structures evolves at a rate of *ca.* 0.2 microns/min, while local pH oscillations were calculated to occur up to 2 microns beyond the growth front.[83, 86] In addition, silica precipitation may very well be the rate determining step in the growth of these microstructures, where the barium carbonate nanorods provide confinement of the

diffusing acid. In theory, the protons produced could either be sequestered for the poly-condensation of various large, slow-diffusing siliceous oligomers or, more undesirably, increase the dissolution of the carbonate.

We theorise that the growth/size of the silica-carbonate microstructures could be enhanced by slowing down the diffusion of the as-generated protons away from the growth fronts of the evolving microstructures. One possible way of accomplishing augmented growth is by coupling the coprecipitation reaction to a slow-diffusing catalyst that buffers these protons and concentrates them at the growth front, thus speeding up the precipitation rate of silica and carbonate as well. However, it should be noted that it would be difficult to decouple the influence of this catalyst from slow-diffusing silica oligomers that could theoretically be formed in solution and give rise to a similar effect.

In order for a compound to function as a buffering agent capable of modulating the uptake and release of protons, it would have to possess several key features such as an acidic group(s), solubility in water and an appropriate molecular weight that could slow down the speed of its diffusion. Chicago Sky Blue 6B (CSB; Figure 37) has been identified as a promising candidate, after it was first studied in our labs as an additive for the *in situ* modification of barium carbonate crystals. The incorporation of CSB powder in a solution of sodium metasilicate and barium chloride adjusted to pH 11.2 dramatically increased the size of double helices from 50 μm to over 200 μm (Lukas Helmbrecht and Wim Noorduin unpublished results) in 1.5 to 2 hours. Upon closer inspection of the molecular structure of the dye (Figure 37), we deduced that the presence of its acidic groups that can release and accept protons allow it to function as a slow diffusing buffer, which could explain the reason for the augmented growth of the double helices in *ca.* 1.5-2 h. In support of our buffer theory, Abbott *et al.* reported that the pKa of CSB is 10.50,[115] which would place the dye within the desired buffering range and pH for growing microhelices and leaves. Furthermore, they also reported that the dye is able to form higher order aggregates,[116] which we presume would further slow down the rate of CSB diffusion. CSB has attractive properties such as its solubility in water, due to the presence of its sulfonate groups, which is about 1 mg/mL and its high molecular weight (992 g/mol).

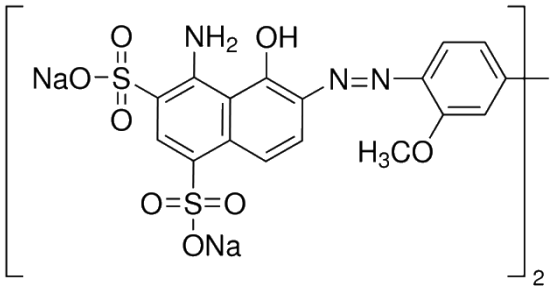

Figure 37. Molecular structure of 2,2'-(4,4'-(3,3'-bis(methoxy)biphenylenebis(azo))bis(8-amino-1-hydroxynaphthalene-5,7-disulfonic acid) tetrasodium salt (Chicago Sky Blue 6B)

In this work, we aim to investigate whether a slow-diffusing buffer in conjunction with the coupled reaction of carbonate and silica can enhance the growth of biomorphs. In doing so, we deduce the role of CSB in the growth of silica-carbonate microstructures. From a theoretical standpoint, if CSB is capable of buffering or positively influencing the reactions at the desired pH (≤11.3), then this will translate to the growth of larger structures relative to those in control reactions without the dye at fixed reaction times. The concept of slow diffusing buffers as catalysts in these precipitation reactions is also of fundamental interest, as these kinds of processes may also play a role in biomineralization, which is quite a paradoxical effect, since it becomes necessary to slow down one process in order to speed up another. Moreover, the ability to control the size, structural morphology, hierarchical texture and composition of high surface area-to-volume materials is of practical importance in fields such as catalysis, optics and electronics.[96, 117-118]

4.2. Results and discussion

4.2.1. Growth of silica-carbonate microstructures in the presence of Chicago Sky Blue (CSB) solution at pH 11.3

Solution pH plays a very important role in the formation of silica-carbonate microstructures, and is regulated locally by the feedback mechanism that exist between silica and carbonate ions. During this regulation process, protons are generated and consumed as a consequence of silica poly-condensation and barium speciation of CO_3^{2-} ions, which are produced by the breakdown of carbonic acid upon the diffusion of CO_2 into a solution of barium and silicate ions. However, as previously mentioned, these protons diffuse away from the growth fronts at a

rate that is faster than the rate at which the as-produced microstructures evolve. Thus, this set of experiments was geared towards studying how the growth of the microstructures might respond if proton diffusion was slowed down by incorporating a compound capable of buffering in the regime of interest.

$BaCO_3$ crystals were grown on glass, stainless steel or aluminium substrates for 1.5–2 h at an initial pH of 11.2–11.3 in silica-rich solutions containing CSB dye at concentrations ranging from 0–0.161 μM (details in section 4.3.3). Optical light microscopy was used to study the as-grown crystals, whose morphologies and alignment of nanocrystals, as inferred by the extinction patterns produced when the samples were viewed between crossed polarizers, were found to be consistent with that of biomorphs. However, it was revealed that at 0.034 μM CSB, the leaves were noticeably larger than those observed in the control experiments without dye, with the leaves being measured along their longest axis (the c-axis). Whereas the long diameter of leaves in control reactions do not usually exceed 80 microns, those crystallized in the presence of 0.034 μM CSB were about twice as large at the end of the reaction (Figure 38a). Even more promisingly, the leaf shown in Figure 38b measures *ca.* 400 microns. As was previously mentioned, it is unusual for silica-carbonate leaves to be this large. A reason to explain how this large leaf arose could be the fusion of two or more smaller leaves, but it becomes readily apparent that there was only one initial $BaCO_3$ crystal nucleus, present in the centre of the circular extinction pattern, from which a single leaf originated. The dye then becomes the most likely candidate to both catalyse and explain these observations concerning enhanced leaf growth. Furthermore, the morphology of this leaf is rather irregular since the leaf either circumvented or grew in an almost spirular manner around barriers/terminated $BaCO_3$ crystals present in its path, while maintaining the alignment of its nanocrystallites. This is perhaps indicative of the reaction-controlled mechanism of silica-carbonate biomorph growth. Furthermore, with increasing CSB concentration, there was a trend towards smaller structures, including leaves (*e.g.* Figure 38c, 0.125 μM) and double helices, with globular structures, a common feature of reactions with a CSB concentration of 0.161 μM. It then becomes clear that the CSB enhances growth up to a certain concentration, but then starts to interfere with the normal interaction of barium and silica. Taking a closer look at the other leaves, some of the crystals were observed to be blue, indicating the incorporation of dye. In conclusion, the results are consistent with our hypothesis that CSB is able to enhance the growth of

microstructures (albeit at lower concentrations), which we believe is achieved by the buffering of protons produced *in situ*, which might augment the precipitation rate of both silica and carbonate. The latter processes could likely serve to supply building blocks to the growing fronts at a faster rate, which would then force the microstructures to grow faster over a fixed reaction time.

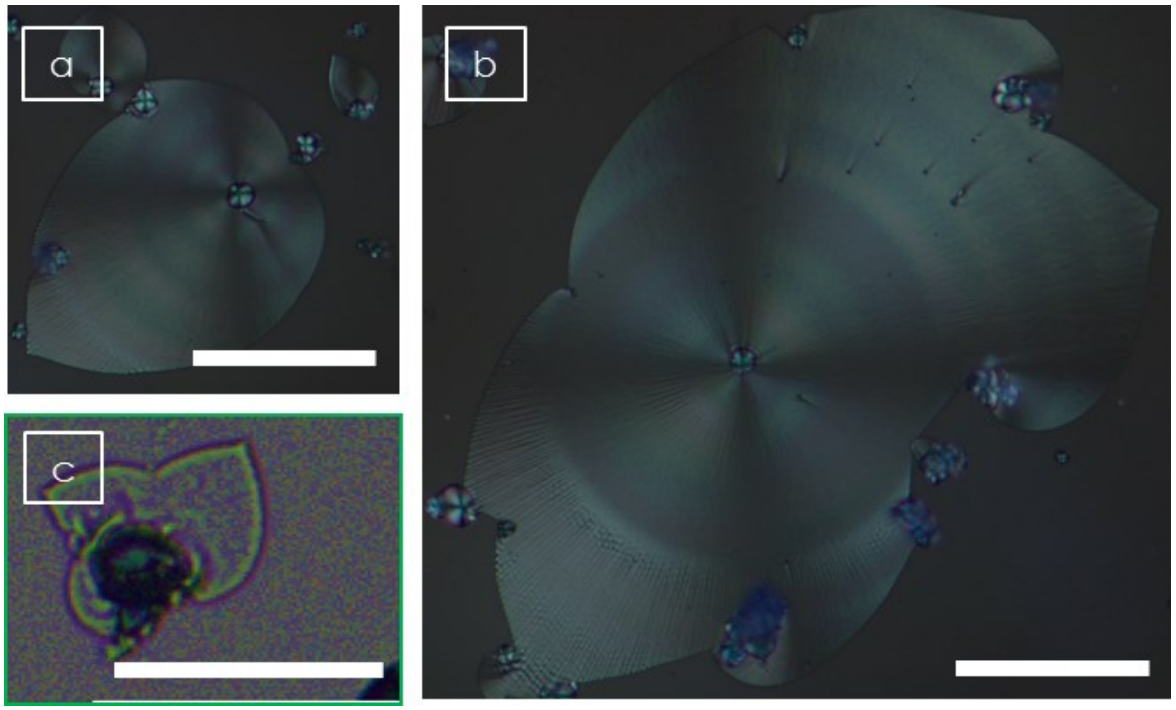

Figure 38. Optical light microscopy images showing the effect of CSB solution at two different concentrations on the growth of silica-carbonate leaves at pH 11.3 in 1.5–2 h: A-B) enhanced leaf growth at 0.034 μM; and C) typical diminutive leaf growth at 0.125 μM. Scale bars in the images are 100 microns (A and B), and (C) 50 microns. The c-axis is denoted by the line in (A).

4.2.2. Direct addition of CSB powder to solutions of barium and silicate at pH 11.3

As previously mentioned, we initially used CSB as a means of dyeing $BaCO_3$ biomorphic crystals prior to their formation in silica-rich environments. The dye in the form of a powder was added directly to a solution containing silicate and barium ions at pH 11.3. This resulted in the formation of super helices that were *ca.* 200 microns in length after 1.5–2 h. Although this is an unconventional addition method for studying the effects of an additive upon the formation of crystals, we then decided to follow up on these interesting results, since CSB is clearly able to enhance the growth rate of silica-carbonate microstructures when added as either an aqueous solution or as a neat powder. Interestingly, preliminary results suggest that the method of addition

of CSB in these reactions seem to influence the super growth of specific morphologies, which are leaves in the case of CSB solution, and helices when CSB powder was used.

Silica-carbonate microstructures were crystallized from mixtures both in the presence and absence (*i.e.* control experiments) of CSB powder at an initial pH of 11.3. After setting the pH of a solution of barium and silicate ions, known amounts of the dye were slowly added to 15 mL volumes of the solution in separate 100 mL beakers with stirring for 1–2 minutes. Even when the mixtures were stirred for longer periods of time, the CSB did not dissolve completely and was dispersed as very fine particles within the mixtures. However, the mixtures became bluer as the amount of added CSB dye was increased, which suggested an increase in the amount of dissolved dye as well. There was an overall increase in the population of leaves in mixtures that contained CSB. When 1.18 mg of the dye was used, both leaves and microhelices were observed (Figure 39a)**.** However, a greater population of leaves were produced when the amount of dye was increased to 2.04 mg (Figure 39b) and 2.64 mg (Figure 39c). The overall increase in nucleation density and polydispersity in leaf size could be due to undissolved dye forming secondary nucleation sites, which presumably grow at a slower rate than primary nucleated structures, since the energy barrier to continue growing/depositing material on surfaces that are already present might be lower when compared to smaller, more recently nucleated sites. Furthermore, since the growth of these microstructures is sensitive to the local diffusion of acid, their sizes are limited to the proximity between neighbouring structures.

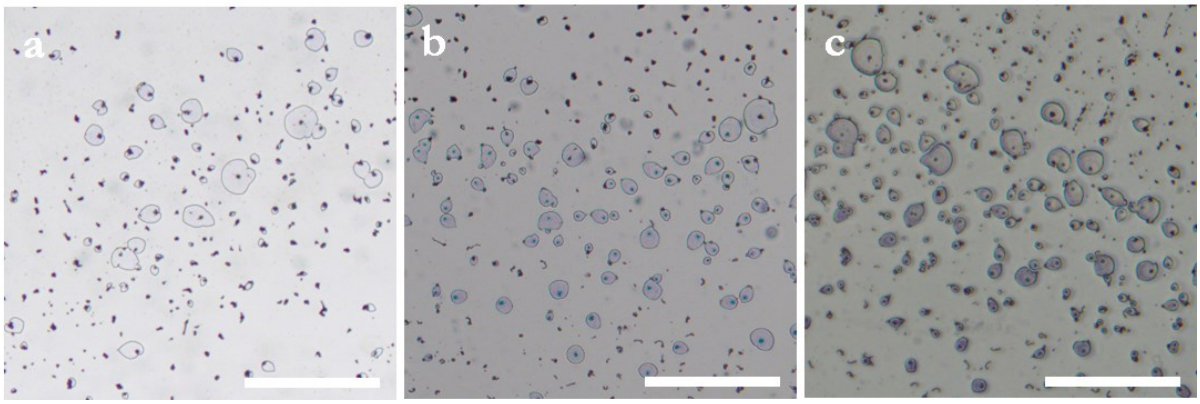

Figure 39. Optical light microscope images of silica-carbonate microstructures that were grown on glass substrates from solutions containing CSB dye: A) 1.18 mg; B) 2.04 mg; and C) 2.64 mg in 15 mL. The scale bars in the images are all 500 microns.

Although a preponderance of leaf-like microstructures was observed in this set of experiments, the same could not be said of the helical microstructures. This could be because the CSB powder affects not only the way the microstructures nucleate and grow, but also how these microstructures interact with the substrate. That is, perhaps the presence of the dye stimulates processes that favour growth on extrinsic surfaces, rather than intrinsically, which occurs when the growth fronts of two helices curl upon each other. Or it could be that lower nucleation densities achieved without CSB are essential for the formation of helices. Nevertheless, it should once again be noted that CSB powder has been proven to catalyse the morphogenesis of super helices in the past, but it appears that such occurrences take place only within some unknown and very narrow window of opportunity. Outside of this timeframe, the apparently delicate balance between the coupling of the dye and the coprecipitation reaction shifts and can no longer be exploited to generate super structures.

4.2.3. Silica-carbonate crystallization reactions with CSB powder at pH 11.9

The inability of CSB to perturb the growth of microstructures in solutions at initial pH 11.9 relative to those at pH 11.2–11.3, under certain conditions, is one possible way of relating the effect of the dye to pH, and thus its ability to influence the outcome of the coprecipitation reaction only when the bulk and/or local pH is within its buffering range. Thus, the morphological evolution of silica-carbonate microstructures as a function of the amount of dissolved CSB at pH 11.9 was also investigated. The microstructures formed in the control reaction without CSB is shown in Figure 40. Close-up views of these structures reveal the formation of typical stems (not shown), flowers (Figure 40e) and vases (Figure 40f), with diameters of about 40 microns. Spike-like features are observed in the flowers, which is indicative of the limited capacity of silica to buffer the acid produced in parts of the structure from which it is isolated. In the presence of 0.067 μM CSB added as a solution (Figure 40b), the microstructures were virtually indistinguishable. Upon adding CSB powder directly into the solutions (Figure 40c–d), similar microstructures to those in the control reaction were observed. However, a CSB concentration of 0.101 μM tended towards mostly vases, which were incompletely formed most likely due to the release and uncontrolled diffusion of acid between neighbouring structures.

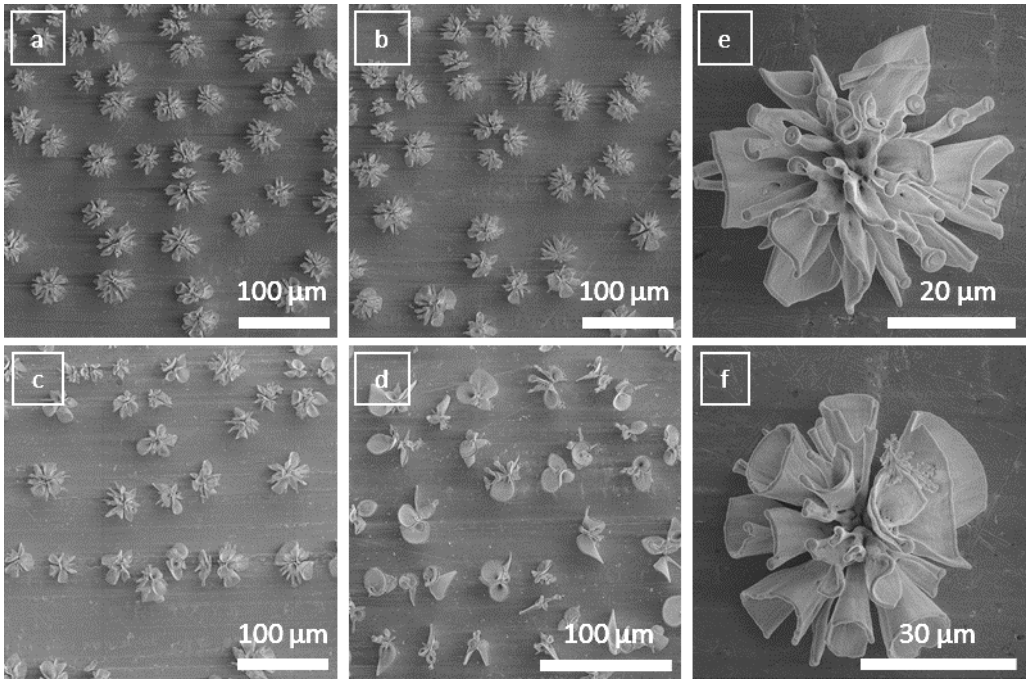

Figure 33. SEM images showing the silica-carbonate microstructures that were grown from solutions at pH 11.9 with CSB dye at different concentrations: A) 0 µM; B) 0.067 µM (1 mL of a 1 mM stock solution); C) 0.071 µM* (1.06 mg); and D) 0.103 µM* (1.54 mg). Close-up view of microstructures from the control solution: E) flower-like barium carbonate; and F) vases. (*apparent concentration)

Taking into consideration the abovementioned results, it is evident that the growth rates of the microstructures were not enhanced and that the diffusion of acid away from the growth fronts was not being controlled in reactions with CSB. This indicates that CSB is not able to buffer acid diffusion locally at pH 11.9, which is logical since its pKa is 10.50.

4.2.3. Crystallization of $BaCO_3$ microstructures in the presence of Chicago Sky Blue (CSB) powder at pH 11.3

So far, the results suggest that it is possible to mediate the crystal growth of silica-carbonate microstructures with CSB, which occurs at pH 11.3 but not at pH 11.9. Here, we think that this is because CSB facilitates the buffering of acid produced locally in these reactions. However, we only have indirect evidence in support of this point, which does not rule out the possibility of other mechanisms/explanations for how the dye is able to influence the crystallization reactions. Moreover, additional verification was required to deconvolute the effect of the dye on the formation of $BaCO_3$ from that of the overall coprecipitation reaction, since it was not known if the dye could replace silica in its role as an initiator of biomorphic shapes. Thus, we excluded silica

from the next set of reactions at initial bulk pH 11.3 in order to explore other means by which the dye may influence $BaCO_3$ growth and assembly.

$BaCO_3$ was first crystallized from mixtures that were prepared by the direct addition of CSB powder (0, 1.18, 1.54, 2.04, and 2.48 mg) to a 15 mL volume solution of barium ions (20 mM) at pH 11.3. SEM was used to visualise the as-formed structures that precipitated on aluminium substrates. Reactions that were performed in the absence of the dye (Figure 41a1) produced crystals in the form of rockets/columns (Figure 41a2), short columns emanating from a central point (Figure 41a3), and branches (Figure 41a5), amongst others. Here, all the observed structures terminated in fine, acicular tips, whereas the corresponding morphologies in the presence of CSB by and large did not contain these features. This can perhaps be attributed to the influence of the dye on crystal shape, which was further evidenced by the transitions to several other different types of morphologies upon the relative increase in dye concentration in the crystallization mixtures. The most noteworthy of these morphologies are dumbbell (Figure 41b4) and closed pseudo-faceted shapes (Figure 41b6), flower-like (Figure 41c3) and flocular (Figure 41c4) aggregates, and randomly stacked rods (Figure 41d4) when the amount of dye was 1.18, 1.54, and 2.04 mg, respectively. It is likely that several of these shapes, including the flowers, originate from the interaction of preformed building units, whose formation and stabilization is perhaps mediated by the dye, as they subsequently go on to stack on-top of each other, thus forming larger aggregates. Perhaps the most interesting example of how the CSB dye is able to exert control over the morphology of $BaCO_3$ crystals can be seen in Figure 41e, where many olivary-like (inset of Figure 41e3) structures that are about 2 microns in length, as well as pseudo-ovoid crystals with triangular excrescences (Figure 41e4), and which measure *ca.* 7 microns in length, and pseudo-hexagonal shapes of rough texture (Figure 41e6) were observed. The miniaturization of the crystals seen here can perhaps be related to a higher dye concentration, and hence an enhanced control over the assembly of building material, which is likely confined to only certain locations and specific arrangements, thus giving faceted crystals.

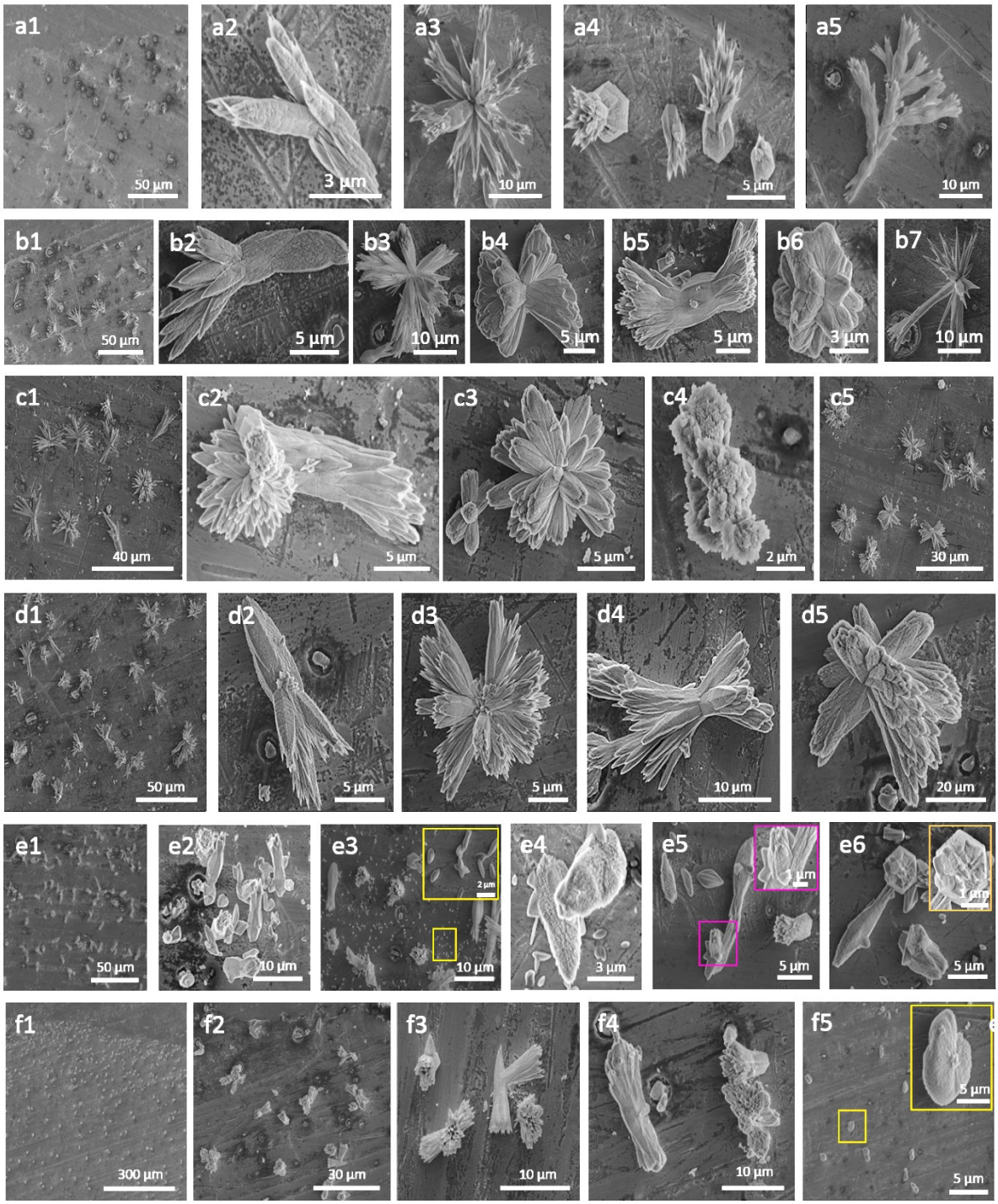

Figure 41. SEM images of various morphologies of $BaCO_3$ crystals formed on aluminium slides upon the diffusion of CO_2 into aqueous $BaCl_2$ solutions (15 mL) without CSB (A) or with CSB powder (B, 0.079 µM*; C, 0.103 µM*; D, 0.137 µM*; E, 0.167 µM*) or with CSB solution (F, 0.067 µM) after *ca.* 1.5 h. (*apparent concentration)

4.2.4. Crystallization of $BaCO_3$ microstructures in the presence of Chicago Sky Blue (CSB) powder at pH 11.9.

Fundamental experiments were conducted without silica at pH 11.9 in order to assess the effect of varying concentrations of CSB dye on the growth of barium carbonate, as well as to see the effect of the dye at a pH far from its pKa. In the control reaction without dye (Figure 42a1–a4), typical morphologies such as stacked crossed-shaped rods, and rods with dendritic growth at one end, and wrapped candy-like microstructures were observed. On the other hand, barium carbonate microstructures were subjected to appreciable modifications in the presence of the dye. In reactions containing 0.067 μM of the dye (Figure 42b1–b4), the barium carbonate crystals were more tapered at the tips. Furthermore, the structure displayed in figure 42b3 might be due to either barium carbonate splitting, or the assembly and subsequent stacking of several crossed-shaped needle-like units, thus forming bundles. Spindle-shaped (Figure 42b3, 5 x 2.5 microns) and pseudo-hexagonal (Figure 42b4, 3 x 3 microns) barium carbonate was also observed at 0.067 μM CSB. These morphologies are consistent with restriction and modification of barium carbonate growth at this dye concentration. Barium carbonate crystals that were formed from solutions containing 1.03 mg (apparent concentration 0.071 μM) (Figure 42c1–c4) of the dye appeared to be less modified than those seen when the final dye concentration was 0.067 μM (from solution). This is expected since the dye does not completely dissolve at the pH of the reaction when added directly as a powder to crystallization solutions. Therefore, the true concentration does not overlap with the apparent concentrations of the dye when added as a powder. The morphologies observed at 1.54 mg of the dye (apparent concentration of 0.103 μM, Figure 42d1–d4) were more compact and/or spherically branched (Figure 42d2) versions of the crossed-shaped and rod-like (Figure 42d3) structures previously mentioned, while floc-like (Figure 42d4) and ball-like (not shown) microstructures were also observed lower down on the substrate. In all cases, there were varying degrees of nucleation and growth of the microstructures with distance along the slides, being greatest at the top and comparatively reduced lower down. This trend correlates well with the availability of atmospheric CO_2 which influxes into the reaction vessel, and hence bulk carbonate supersaturations, also decreases with distance from the solution-air interface.

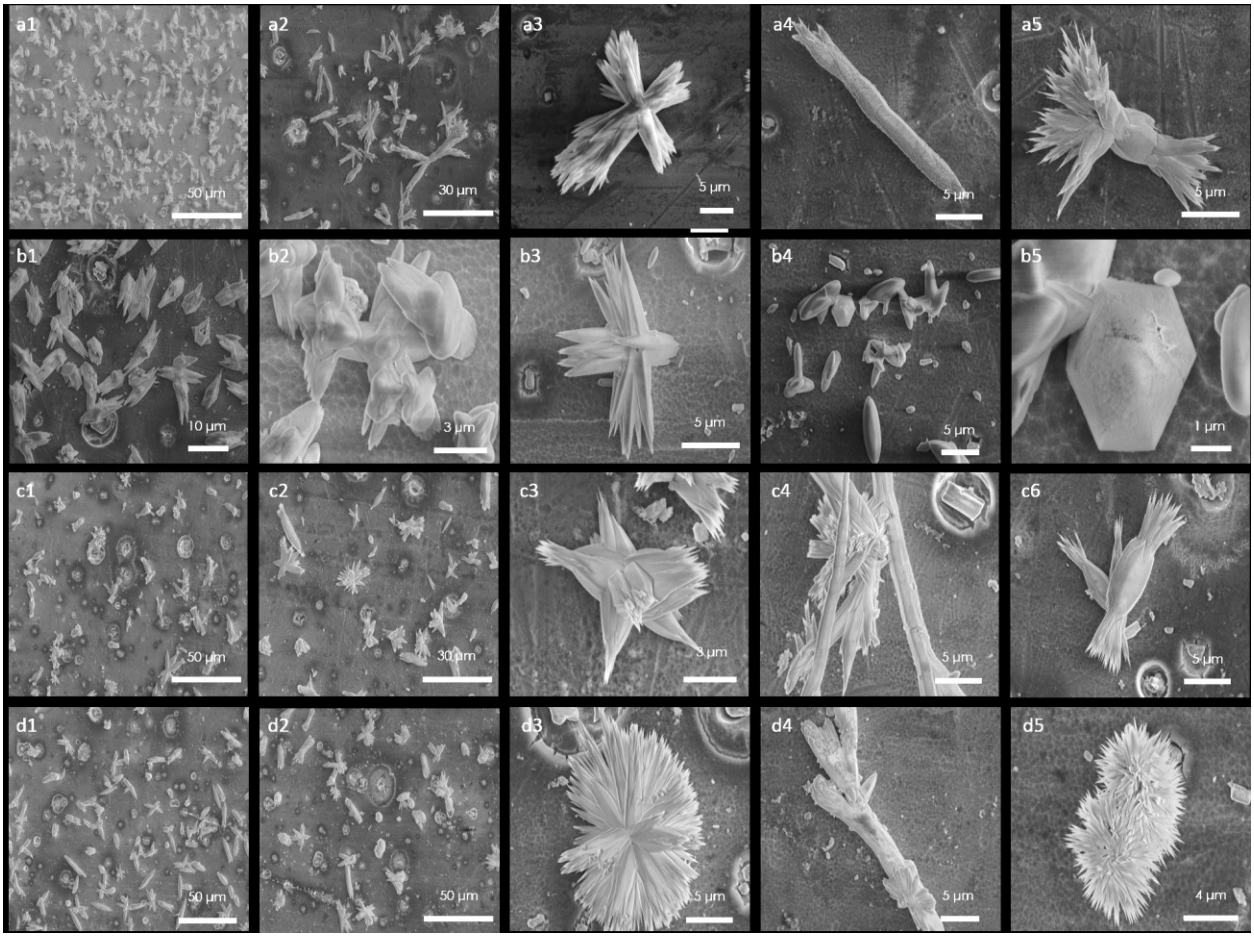

Figure 42. Scanning electron micrograpphs showing the effect of varying the amount of CSB dye added on some of the major morphologies of barium carbonate microstructures that were grown at pH 11.9 on aluminium substrates from 15 mL volumes of solutions. A) 0 µM. B) 0.067 µM (1 mL of a 1µM stock solution). C) 0.071 µM* (1.06 mg). D) 103 µM* (1.54 mg) (*apparent concentration).

Overall, although there is clearly greater modification of barium carbonate with increasing amounts of dye added, the basic morphologies (crossed-shaped and rod-like) are preserved. However, when crystallization is conducted in the presence of 0.067 µM CSB, added as a solution, barium carbonate microstructures are shorter and more spindle-shaped and hexagonal than rod-like. Furthermore, these results suggest that CSB does not enhance the growth of barium carbonate at pH 11.9, which is consistent with our slow-diffusing buffer hypothesis.

4.2.5. Silica-controlled crystallization of $BaCO_3$ microstructures at 37 °C and pH 11.3 in the presence of Chicago Sky Blue (CSB) powder

When the reactions were conducted at 37 °C, the biomorphs exhibited morphologies that were quite different from those observed at room temperature. In the presence of dye amounts of 0.5 mg (apparent concentration 0.034 μM) in a 15 mL volume of solution, the structures resemble sheets having a 3D appearance, and displayed multiple folds along their lengths (Figure 43a–f). Upon closer inspection of these structures, it was revealed that they arise from the nucleation of a spherical core from which short ribbons and sometimes long 3D sheets, growing in space, evolve (Figure 43h–i). The central cores emanating ribbons were flower-like in appearance, and their size appeared to be limited by the proximity to other neighbouring structures (Figure 43i). Furthermore, some of these fibre-like structures had a helical component (Figure 43i).

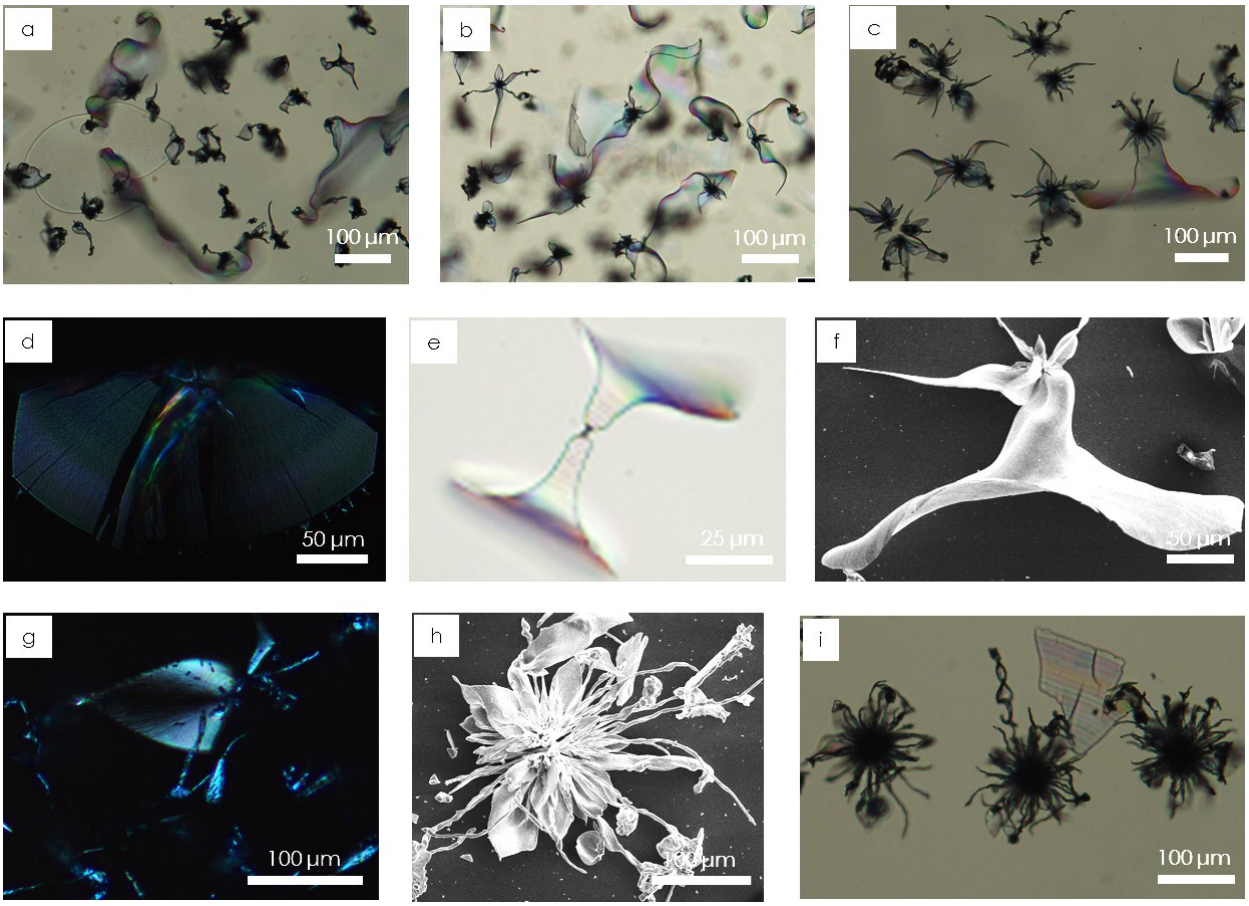

Figure 43. Optical light microscopy and SEM images showing the effect of CSB (0.5 mg; 0.034 μM*) dye on the growth of silica-carbonate microstructures at 37 °C and a pH of that were grown from solutions at pH 11.3. A–F) 3D and trumpet microstructures. G) Blue structures indicating the incorporation of CSB. H–I) Flower-like microstructures sometimes terminated in helices. (*apparent concentration)

At a higher initial amount of the dye (1.5 mg; apparent concentration 0.103 μM), networks of fibres were the dominant feature seen growing on the glass slide (Figure 44a, c). It is believed that these fibres were produced when a $BaCO_3$ crystal nucleated flat side down, then started growing at both ends at approximately the same rate (Figure 44d, h)). In Figure 44b, small sheets that eventually go on to form several filaments around its edges over time, such that neuron-like patterns were created. These filaments, though in very close proximity, appear to be discreet when viewed by SEM (Figure 44c–d). In Figure 44f, it can be seen that two filaments grew orthogonally to each other. At some point during their growth, the filament on the right probably contacted the other filament, causing the sudden precipitation of a small amount of silica, seen on the left of the vertical filament. This suggests that the growth of biomorphs might occur in the wake of a moving acid front.

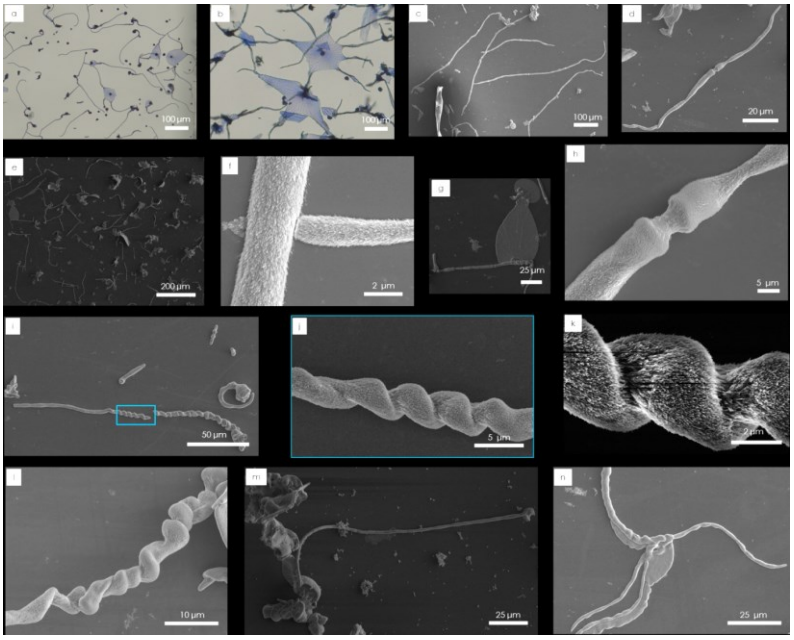

Figure 44. Optical light microscopy and SEM images of silica-carbonate microstructures formed at 37 °C upon the addition of CSB dye (1.5 mg; 0.101 μM*) to a solution of silicate and barium ions that was adjusted to pH 11.3, and covered loosely to allow the influx of CO_2 in through the spout of the 100 mL beaker. A–C) Networks of filaments, some of which exhibit a similar appearance to biological neural networks. D and H) Images of a discrete filament that grew from a central $BaCO_3$ crystal that nucleated flat-side down. E, G and M) Leaf- and 3D sheet-bearing filaments, albeit a less common occurrence than observed at a lower concentration of the dye. F) SEM image possibly depicting further evidence of the acid-catalysed nature of these reactions through the precipitation of a small amount of silica (on the substrate to the left of the vertical filament) when a filament contacted another filament growing orthogonally to it. I–L) Images of single helices, which differ from the double helices and single spirals normally observed at room temperature. H) A propeller-like microstructure which may be the first step towards forming sheets/leaves upon the deposition and space-filling assembly of material between its "tentacles". (*apparent concentration)

Another feature of the above reaction is the formation of filaments in the form of single helices (Figure 44i–l), which to the best of our knowledge have not been reported at or above room temperature. These filaments are initially helical, but can sometimes transition to a straight or less twisted structure at some point during growth, which may represent a fundamental switch in the growth process. For example, there may be different precipitation ratios of silica to carbonate at the start of the reaction compared to the latter stage. This scenario might lend itself to one of the components, likely silica, being more active (*i.e.* dominating growth) as the reaction progresses, and the pH diminishes significantly enough to manifest itself in this abrupt morphological change. Nevertheless, these helices represent true biomorphs as can be seen from the nanocrystallites in the close-up SEM view of one of the structures (Figure 44k).

Although the network of filaments was produced at 37 °C in the presence of 1.5 mg of the dye (apparent concentration 0.101 μM), but not at the aforementioned lower concentration (0,5 mg; apparent concentration 0.034 μM), the trend towards 3D and filament morphologies seem to be a feature of reactions at elevated temperatures. Indeed, Bittarello *et al.*[69] noted that thin filaments and trumpet-like shapes of barium carbonate crystals formed at 50 °C, possibly due to changes in fluid dynamics, transport mechanism and local supersaturation values, while regular sheets and helicoids were always generated under static conditions and in solutions with very high concentration gradients.

4.3. Experimental

4.3.1. Materials and method

Analytical grade barium chloride dihydrate ($BaCl_2 \bullet 2H_2O$), and sodium metasilicate (Na_2SiO_3) from Sigma Aldrich , and Chicago Sky Blue 6B Dye from Alfa Aesar were used without further purification. All samples were prepared fresh with degassed, deionized water. Microscope slides (24 x 24 x 1 mm) were purchased from Thermo Fisher Scientific. Aluminium sheets were purchased from Goodfellow and cut to specific dimensions (20 x 20 x 2 mm). The slides were cleaned by sonicating twice, first in deionized water for *ca.* 5–8 minutes and then in isopropyl alcohol for 5 minutes. The slides were subsequently air dried and stored in dust-free sample boxes.

4.3.2. Base Solution

Sodium metasilicate (0.067 g, 0.55 mmol) was dissolved in degassed, deionized water (37.5 mL) in order to obtain a solution (14.6 mM) contained in a 100 mL beaker. This solution was kept covered to limit exposure to CO_2 and used within 5 to 20 minutes in order to reduce the variation in the growth of silicate species due to polycondensation of silica over time. A solution of barium chloride dihydrate (0.074 g, 0.30 mmol, 50.5 mM) was also prepared in water (6 mL). An aliquot of the previously prepared Na_2SiO_3 solution (9 mL, 14.6 mM) was pipetted into a 100 mL beaker containing the barium chloride solution (6 mL, 50.5 mM). The pH of the resulting solution ([silicate] = 8.76 Mm, $[Ba^{2+}]$ = 20.2 mM) was then adjusted to 11.2–11.3, or 11.8–11.9 using dropwise addition of 1 M HCl and/ or freshly-prepared KOH, in order to induce the growth of double helices or flowers, respectively. Glass or metal substrates were positioned vertically in the sloped slots of a homemade sample holder, which was subsequently placed directly in the reaction solution. The beaker was then loosely covered with a petri dish to allow the flow of atmospheric CO_2 in through the spout, and was left undisturbed at room temperature for 1.5–2 h, unless specified otherwise. After the desired growth period, the sample holder was quickly removed and placed in a beaker of water, and the slides were then individually removed and rinsed in a second beaker of deionized water followed by acetone, then air dried.

4.3.3. Chicago Sky Blue (CSB) solution (with silica, pH 11.3)

CSB stock solutions (0.8 – 1 μM) were prepared by dissolving the dye up to its solubility limit in water, and were then added to the crystallization mixture in a selected concentration range (0.034–0.161 μM) in order to study the effect of the dye on the growth of the as-prepared biomorphs. The masses and volumes mentioned above in section 4.3.2 were scaled proportionally in order to create a base solution of barium (101 mM) and silicate (14.6 mM) ions, which could then be divided amongst several beakers, such that they each contained an equal volume (12 mL), prior to the addition of H_2O (0–3 mL) and/or CSB solution (0–3 mL, 0–1 mM) was added to separate 100 mL beakers containing barium and silicate ions at pH 11.2–11.3, thus setting the total reaction volume to 15 mL. The final concentrations of Na_2SiO_3 and $BaCl_2$ were 8.2 and 20.2 mM, respectively. The reactions were then conducted in the manner described in section 4.3.2.

4.3.4. CSB powder (with silica, pH 11.3)

$BaCO_3$ solution (12 mL, 100 mM) was diluted with water (9 mL) prior to the slow addition of Na_2SiO_3 (36 mL, 14.6 mM) and subsequently adjusted pH to 11.2–11.3. Mixtures with apparent concentrations of 0, 0.079, 0.106, 0.136 and 0.177 μM were prepared by incorporating 0, 1.18, 1.57, 2.03 and 2.63 mg CSB, respectively, into 15 mL volumes of the solution of barium and silicate ions. The CSB powder was not dissolved completely and was dispersed as fine particles throughout the blue mixtures. Although the final concentrations/amounts of dissolved dye were unknown, the mixtures became noticeably bluer with amount of dye added. Final concentrations of Na_2SiO_3, and $BaCO_3$ were 8.78 and 20.2 mM, respectively. The reactions were then conducted in the manner described in section 4.3.2.

4.3.5. CSB powder or solution (with silica, pH 11.9)

In a 100 mL beaker, an aqueous solution was prepared by dissolving Na_2SiO_3 (0.1005 g, 0.823 mmol) in degassed, deionized water (56.2 mL). An aliquot of the Na_2SiO_3 solution (45 mL, 14.6 mM) was added to $BaCl_2{\bullet}2H_2O$ (0.37 g, 25 mL, 60.6 mM) that was prepared with freshly degassed deionized H_2O. The pH of the resulting solution was 11.95 and was not adjusted further. The solution was then divided amongst four 100 mL beakers such that each contained 14 mL of the $BaCl_2$-Na_2SiO_3 solution. Various amounts of water (0–1 mL) and CSB powder (0, 1.06 and 1.54 mg) or CSB solution (1 mL, [CSB stock] = 1 μM) were then slowly added to these mixtures while stirring magnetically. While the volume of the mixtures was fixed (15 mL), the final concentration of CSB, Na_2SiO_3 and $BaCl_2$ were 0, 0.067, 0.071, 0.103, 8.78 and 20.2–mM, respectively. Tape was used to secure one glass slide (Thermo Fisher Scientific 24 x 24 x 1 mm) and one aluminium slide (20 x 20 x 2 mm) inside each beaker, which was then loosely covered with a petri dish and left undisturbed at room temperature for 1.5–2 h. The reactions were then conducted in the manner described in section 4.3.2.

4.3.6. Control reaction 1 (CSB powder or solution, without silica, pH 11.3)

A solution was prepared by dissolving $BaCl_2{\bullet}2H_2O$ (0.444 g, 1.82 mmol) in degassed, deionized water (84 mL). The resulting solution (21.7 mM), with its pH raised to 11.2–11.3 by the dropwise addition of 1 M NaOH, was then divided amongst five 100 mL beakers such that they each contained a volume of 14 mL. Degassed, deionized water (1 mL) was then added to four of

the beakers, which resulted in the same final total reaction volume (15 mL). After this, powdered CSB (0, 1.18, 1.54, 2.04, and 2.48 mg) was slowly added to the $BaCl_2$ solutions (15 mL, 20.2 mM) in the 100 mL beakers while stirring with magnetic stirring. In one of the beakers, CSB solution (1.03 mL), prepared by dissolving CSB powder (1 mg/mL or 0.067 μM in water), was added instead of water. The apparent concentrations of the solutions with CSB powder or solution were 0, 0.079, 0.103, 0.137, 0.167 μM, while the final concentration of $BaCl_2$ in each solution was 20.2 mM. The crystallization of $BaCO_3$ was allowed to take place on glass and aluminium slides for 1.5–2 h, and the remainder of the experiment was conducted in the same manner described in section 4.3.2).

4.3.7. Control reaction 2 (CSB powder, without silica, pH 11.9)

A crystallization reaction was initiated by dissolving $BaCl_2 \bullet H_2O$ (0.37 g, 1.51 mmol, pH 6.63), contained in a 100 mL beaker, in degassed deionized H_2O (70 mL). The solution pH was subsequently adjusted to 11.96 using 1 M KOH. An aliquot of the resulting mixture (55 mL) was then divided amongst four separate 100 mL beakers such that each contained the same volume of $BaCl_2$ solution (14 mL, 21.6 mM). Water was added to bring the total volume of these solutions to 15 ml followed by adding CSB powder (0, 1.18 and 1.51 mg), in a selected concentration range between zero and the solubility maximum with magnetic stirring. CSB dissolved in water (1 mL, [stock] = 1 μM) was added to the rest of the previously prepared barium chloride solution. The apparent concentrations of the solutions with CSB were: 0, 0.067, 0.079, and 0.101 μM. The final concentration of $BaCl_2$ was 20.2 mM. The pH of the mixtures was adjusted a final time to 11.91 by adding 1 M HCl or KOH. Tape was used to secure glass and aluminium slides in each beaker which was left undisturbed at room temperature for 1.5–2 h. To stop the reactions, the slides were removed and rinsed in water, followed by acetone and then air dried.

4.3.8. Silica-controlled crystallization of $BaCO_3$ microstructures at 37°C and pH 11.3 in the presence of Chicago Sky Blue (CSB solution)

In general, the aqueous growth solution was prepared by adding H_2O (9 mL) followed by Na_2SiO_3 (36 mL, 14.64 mM,) to $BaCO_3$ (12 mL, 101 mM), then adjusting the pH to 11.2–11.3 with 1 M HCl/KOH The mixture was then divided amongst four 100 mL beakers such that each contained 14.25 mL. Various amounts of water and CSB (stock concentration was *ca.* 1 μM) were

then slowly added to these mixtures, to obtain a final volume of 15 mL, while stirring. Final concentration of CSB, and Na_2SiO_3, and $BaCO_3$ were 0.034, 0.067, 0.100, and 8.78 and 20.2 mM mM, respectively. A sample holder containing 4 glass or aluminium slides were inserted into each beaker, which was then loosely covered with a petri dish, wrapped in aluminium foil. Controls were left undisturbed at room temperature while the other beakers were either placed in a temperature-controlled room or water bath at 37 ºC for 1.5–2 h, and 4/8 h in other cases. To stop the reactions, each sample holder was quickly removed and placed in a beaker of water, and the slides were then individually removed and rinsed in a second beaker of water followed by acetone, then air dried. In order to eliminate the possibility of structures growing in solution falling onto the substrate during the removal and washing steps, the beakers were alternatively flooded with water until the biomorphs growing on top of the solution were removed and the initial blue solution with CSB became clear and the initial crystallization solution was replaced by water

Chapter 5. Conclusions & Future Work

The search is ever ongoing to create or improve existing materials that aim to meet both today's and future challenges. Yet, for useful new materials to be developed, strategies to control a wide range of physical and chemical properties that can be directly translated to function must be realized. However, the limited scope of current techniques to independently control important aspects, such as shape and composition, poses a fundamental challenge to developing such functional materials. The convergence of old and new research hints at the exciting possibility that the study of silica-carbonate shapes might yet be a new paradigm for assembling new materials *via* a bottom-up approach. In this regard, the work of Noorduin *et al.*[74] is an important milestone in the field, starting with strategies conceptualized to direct the growth of silica-carbonate shapes on substrates, thus taking basic shapes to another dimension where more complex, hierarchical microstructures are possible. More recently, Noorduin and Helmbrecht 2018[104] demonstrated the transformation of silica-carbonate shapes to perovskites, while eliminating shape-composition constraints. Inspired by the work of Noorduin *et al.*,[74] this thesis aimed to explore several aspects of the growth process important to the design of silica-carbonate shapes from solutions at alkaline pH (10–12).

The programming of basic silica-carbonate microstructures into more complex, 3D shapes was conducted by replicating the work of Noorduin *et al.* in Chapter two. First, this involved defining a set of initial conditions (*i.e.* atmospheric CO_2 concentration, pH and temperature) for the growth of particular, basic shapes, which provided nucleation and growth sites for additional shapes in subsequent growth steps. Thusly, we constructed a library of basic and hierarchically-assembled micron-sized shapes that tolerated both barium and strontium ions. Our findings support the conclusion that certain pH regimes are conducive to the formation of distinct classes of microstructures, such as helices at pH 11.2 that yield to flower-like shapes at pH 11.8. This effect is believed to originate from the directionality of growth in such a manner as to minimize any interactions with the local optimum pH zone for the deposition of silica, which is known to passivate growth.

In Chapter three, we attempted to control of the chirality of helical silica-carbonate shapes using chiral molecular (amino acids) and microscale (chiral vaterite) chiral directing agents. Here, double helicoids were allowed to grow from pH-adjusted reaction mixtures to which aliquots of

homochiral aspartic acid were added, or on substrates that contained pre-assemble chiral vaterite. We were eventually able to successfully make chiral vaterite from an existing literature procedure as well as from the novel application of other sub-methods utilised in our labs. This involved the ammonium carbonate method, in addition to the diffusion of atmospheric CO_2 into a solution of $CaCl_2$ ions in the presence of L-aspartic acid. Through these experiments, we were not able to control the handedness of the emergent microhelices with chiral directing agents. The amino acid results suggest we have much to learn about the underlying interactions and reaction mechanisms of these additives, which might be vastly different in composite materials as opposed to single crystals. Furthermore, inventing new strategies to overcome the randomness of nucleation events as well as the inherent unfavourable interstitial energies involved in the alignment of barium carbonate and vaterite present further challenges to directing the chirality of the former with the latter.

Perhaps, the next logical step to address the challenges mentioned above might be the use of larger molecules to control the handedness of silica-carbonate helices, since smaller ones, such as enantiopure aspartic acid, have been unsuccessful. Antifreeze proteins and various biomimetic polymers are interesting candidates for large molecules that could be utilized in these types of studies on chiral control.[30, 119] Moreover, it would also be interesting to grow the microhelices on substrates with higher densities of chiral vaterite which increases the possibility of the double helices growing directly on these chiral crystals.

Finally, the effect of Chicago Sky Blue dye (CSB) on the formation of silica-carbonate microstructures was studied and presented in Chapter 4. We found that CSB was able to accelerate the growth of large structures under certain conditions, an effect that we do not yet have a clear picture of. However, we think that this is perhaps due to the capacity of the dye to function as a slow-diffusing catalyst that slows down the movement of locally-generated acid from the growing fronts of these microstructures. Thus far, follow-up studies with other dyes (Helmbrecht and Ariane, unpublished results) suggest that CSB might be unique in its ability to enhance the growth rates of the as-formed structures. Nevertheless, future investigations could involve synthesizing or screening a wider library of other dyes as candidates to accelerate the growth rate of silica-carbonate microstructures.

Chapter 6. Appendix

Table 1. Space groups of calcium carbonate polymorphs and barium carbonate

Crystal	Crystal system	Space group
Calcite	Trigonal	R3c
Aragonite	Orthorhombic	Pmcn
Vaterite	Hexagonal	$P6_3/mmc$
Barium carbonate	Orthorhombic	Pnma

Notes: A space group describes the complete set of symmetry characteristics of a crystal. These symmetry transformations leave a crystal in an undistinguishable position in 3D space from the original when performed.

In the above space group notations, the first letter (P or R) represents the Bravais lattice type, the first number represents rotation through $360^{\circ}/n$ about a screw axis, the second number in subscript indicates translation about the screw axis following rotation, reflection planes normal to the rotation axis are denoted by the letters m (mirror plane), and a and c (glide planes), while the letter n represents a diagonal glide plane.

Chapter 7. References

1. Thompson, D. A. W., *On Growth and Form*. Cambridge University Press: Cambridge, 1992.
2. García-Ruiz, J. M.; Carnerup, A.; Christy, A. G.; Welham, N. J.; Hyde, S. T., Morphology: An ambiguous indicator of biogenicity. *Astrobiology* **2002,** *2* (3), 353-369.
3. Aquilano, D.; Otalora, F.; Pastero, L.; Garcia-Ruiz, J. M., Three study cases of growth morphology in minerals: Halite, calcite and gypsum. *Prog. Cryst. Growth Charact. Mater.* **2016,** *62* (2), 227-251.
4. St. Laurent, K. Blooming around the world: A story of coccolithophore co-existence. https://oceanbites.org/blooming-around-the-world-a-story-of-coccolithophore-co-existence/ (accessed January 01, 2018).
5. Cölfen, H., Bio-inspired mineralization using hydrophilic polymers. In *Biomineralization II: Mineralization Using Synthetic Polymers and Templates*, Naka, K., Ed. Springer Berlin Heidelberg: Berlin, Heidelberg, 2007; pp 1-77.
6. Lowenstam, H. A., *On biomineralization / Heinz A. Lowenstam, Stephen Weiner*. Oxford University Press: New York, 1989.
7. Driessens, F. C. M., S. Mann, J. Webb, R. J. P. Williams (Eds.): Biomineralization: Chemical and Biochemical Perspectives, VCH Verlagsgesellschaft, Weinheim, Basel, Cambridge, New York, 1989. 541 Seiten, Preis: DM 274.—. *Ber. Bunsenges. phys. Chem.* **1990,** *94* (2), 209-209.
8. Mann, S., *Biomineralization: Principles and Concepts in Bioinorganic Materials Chemistry*. Oxford University Press: 2001.
9. Knoll, A., *Biomineralization and Evolutionary History*. 2003; Vol. 54, p 329-356.
10. *Biomineralization in lower plants and animals: Proceedings of an international symposium held at the University of Birmingham, April 1985 / edited by Barry S.C. Leadbeater, Robert Riding*. Published for the Systematics Association by the Clarendon Press ; Oxford University Press: Oxford [Oxfordshire]: New York, 1986.
11. Gómez-Morales, J.; Falini, G.; García-Ruiz, J. M., 20 Biological Crystallization. In *Handbook of Crystal Growth*, 2015; pp 873-913.
12. Mann, S., The chemistry of form. *Angew. Chem., Int. Ed.* **2000,** *39* (19), 3392-3406.
13. Chen, C. L.; Qi, J. H.; Tao, J. H.; Zuckermann, R. N.; DeYoreo, J. J., Tuning calcite morphology and growth acceleration by a rational design of highly stable protein-mimetics. *Sci. Rep-Uk* **2014,** *4*.
14. Chen, C.-L.; Rosi, N. L., Peptide-Based Methods for the preparation of nanostructured inorganic materials. *Angew. Chem., Int. Ed.* **2010,** *49* (11), 1924-1942.
15. Evans, J. S., "Tuning in" to mollusk shell nacre- and prismatic-associated protein terminal sequences. Implications for biomineralization and the construction of high performance inorganic−organic composites. *Chem. Rev.* **2008,** *108* (11), 4455-4462.
16. Margolis, H. C.; Beniash, E.; Fowler, C. E., Role of macromolecular assembly of enamel matrix proteins in enamel formation. *J. Dent. Res.* **2006,** *85* (9), 775-793.
17. Dey, A.; de With, G.; Sommerdijk, N. A. J. M., In situ techniques in biomimetic mineralization studies of calcium carbonate. *Chem. Soc. Rev.* **2010,** *39* (2), 397-409.
18. Cölfen, H.; Yu, S.-H., Biomimetic Mineralization/Synthesis of Mesoscale order in hybrid inorganic–organic materials via nanoparticle self-assembly. *Mrs. Bull.* **2005,** *30* (10), 727-735.
19. Meldrum, F. C.; Cölfen, H., Controlling mineral morphologies and structures in biological and synthetic systems. *Chem. Rev.* **2008,** *108* (11), 4332-4432.
20. Gotliv, B.-A.; Kessler, N.; Sumerel, J. L.; Morse, D. E.; Tuross, N.; Addadi, L.; Weiner, S., Asprich: A novel aspartic acid-rich protein family from the prismatic shell matrix of the Bivalve Atrina rigida. *ChemBioChem* **2005,** *6* (2), 304-314.

21. Mann, S., Biomineralization: the formidable part of bioinorganic chemistry. *J. Chem. Soc, Dalton Trans.* **1997,** (21), 3953-3962.
22. van Bommel, K. J. C.; Friggeri, A.; Shinkai, S., Organic templates for the generation of inorganic materials. *Angew. Chem., Int. Ed.* **2003,** *42* (9), 980-999.
23. Song, R. Q.; Cölfen, H., Additive controlled crystallization. *Crystengcomm* **2011,** *13* (5), 1249-1276.
24. Herman, A.; Addadi, L.; Weiner, S., Interactions of sea-urchin skeleton macromolecules with growing calcite crystals—a study of intracrystalline proteins. *Nature (London, U. K.)* **1988,** *331*, 546.
25. Falini, G.; Albeck, S.; Weiner, S.; Addadi, L., Control of aragonite or calcite polymorphism by mollusk shell macromolecules. *Science* **1996,** *271* (5245), 67.
26. Mann, S.; Didymus, J. M.; Sanderson, N. P.; Heywood, B. R.; Samper, E. J. A., Morphological influence of functionalized and non-functionalized α,ω-dicarboxylates on calcite crystallization. *J. Chem. Soc., Faraday Trans.* **1990,** *86* (10), 1873-1880.
27. Addadi, L.; Weiner, S., Interactions between acidic proteins and crystals: stereochemical requirements in biomineralization. *Proc. Natl. Acad. Sci. U. S. A.* **1985,** *82* (12), 4110-4114.
28. Mann, S., Molecular recognition in biomineralization. *Nature (London, U. K.)* **1988,** *332*, 119.
29. Dabbs, D. M.; Aksay, I. A., Self-Assembled ceramics produced by complex-fluid templation. *Annu. Rev. Phys. Chem.* **2000,** *51* (1), 601-622.
30. Mitchell, M. J.; Jensen, O. E.; Cliffe, K. A.; Maroto-Valer, M. M., A model of carbon dioxide dissolution and mineral carbonation kinetics. *Proc. R. Soc., London, Ser. A* **2010,** *466* (2117), 1265-1290.
31. Chen, L.; Shen, Y. H.; Xie, A. J.; Huang, B.; Jia, R.; Guo, R. Y.; Tang, W. Z., Bacteria-mediated synthesis of metal carbonate minerals with unusual morphologies and structures. *Cryst. Growth Des.* **2009,** *9* (2), 743-754.
32. Boulos, R. A.; Zhang, F.; Tjandra, E. S.; Martin, A. D.; Spagnoli, D.; Raston, C. L., Spinning up the polymorphs of calcium carbonate. *Sci Rep-Uk* **2014,** *4*, 3616.
33. Ma, Y. F.; Gao, Y. H.; Feng, Q. L., Effects of pH and temperature on $CaCO_3$ crystallization in aqueous solution with water soluble matrix of pearls. *J. Cryst. Growth* **2010,** *312* (21), 3165-3170.
34. Ma, Y.; Gao, Y.; Feng, Q., *Characterization of organic matrix extracted from fresh water pearls*. 2011; Vol. 31, p 1338-1342.
35. Hasse, B.; Ehrenberg, H.; Marxen, J. C.; Becker, W.; Epple, M., Calcium carbonate modifications in the mineralized shell of the freshwater snail biomphalaria glabrata. *Chem. Eur. J.* **2000,** *6* (20), 3679-3685.
36. Ma, H. Y.; Dai, T. G., The first discovery of vaterite in lustreless freshwater pearls of Leidan, Zhejiang. *Acta Mineral. Sin.* **2001,** *21*, 153-157.
37. Heywood, B. R.; Rajam, S.; Mann, S., Oriented crystallization of $CaCO_3$ under compressed monolayers. Part 2.—Morphology, structure and growth of immature crystals *J. Chem. Soc. Faraday T.* **1991,** *87* (5), 735-743.
38. Hazen, R. M.; Downs, R. T.; Jones, A. P.; Kah, L., Carbon mineralogy and crystal chemistry. *Rev. Mineral. Geochem.* **2013,** *75*, 7-46.
39. Weiner, S.; Addadi, L., Design strategies in mineralized biological materials. *J. Mater. Chem.* **1997,** *7* (5), 689-702.
40. Berman, A.; Addadi, L.; Kvick, A.; Leiserowitz, L.; Nelson, M.; Weiner, S., Intercalation of sea-urchin proteins in calcite—study of a crystalline composite-material. *Science* **1990,** *250* (4981), 664-667.
41. Belcher, A. M.; Wu, X. H.; Christensen, R. J.; Hansma, P. K.; Stucky, G. D.; Morse, D. E., Control of crystal phase switching and orientation by soluble mollusc-shell proteins. *Nature (London, U. K.)* **1996,** *381*, 56.
42. Ueshima, R.; Asami, T., Single-gene speciation by left–right reversal. *Nature (London, U. K.)* **2003,** *425*, 679.
43. Grande, C.; Patel, N. H., Nodal signalling is involved in left–right asymmetry in snails. *Nature (London, U. K.)* **2008,** *457*, 1007.

44. Schilthuizen, M.; Davison, A., The convoluted evolution of snail chirality. *Naturwissenschaften* **2005,** *92* (11), 504-515.
45. Kuroda, R.; Endo, B.; Abe, M.; Shimizu, M., Chiral blastomere arrangement dictates zygotic left–right asymmetry pathway in snails. *Nature (London, U. K.)* **2009,** *462*, 790.
46. Zhai, H. L.; Quan, Y.; Li, L.; Liu, X. Y.; Xu, X. R.; Tang, R. K., Spontaneously amplified homochiral organic-inorganic nano-helix complexes via self-proliferation. *Nanoscale* **2013,** *5* (7), 3006-3012.
47. Cartwright, J. H. E.; Checa, A. G.; Escribano, B.; Sainz-Díaz, C. I., Spiral and target patterns in bivalve nacre manifest a natural excitable medium from layer growth of a biological liquid crystal. *Proc. Natl. Acad. Sci. U. S. A.* **2009,** *106* (26), 10499.
48. Barron, L. D., *Molecular Light Scattering and Optical Activity*. 2 ed.; Cambridge University Press: Cambridge, 2004.
49. Cartwright, J. H. E.; Checa, A. G., The dynamics of nacre self-assembly. *J. R. Soc. Interface* **2007,** *4* (14), 491-504.
50. Thomas, J. M.; Renshaw, G. D.; Roscoe, C., Production of dislocation etch pits on calcite using optically active etchants. *Nature (London, U. K.)* **1964,** *203*, 72.
51. Honess, A. P.; Jones, J. R., Etch figure investigations with optically active solvents. *Geol. Soc. Am. Bull.* **1937,** *48* (5), 667-722.
52. Barwise, A. J.; Compton, R. G.; Unwin, P. R., The effect of carboxylic acids on the dissolution of calcite in aqueous solution. Part 2.—d-, l- and meso-Tartaric acids. *J. Chem. Soc., Faraday Trans.* **1990,** *86* (1), 137-144.
53. Orme, C. A.; Noy, A.; Wierzbicki, A.; McBride, M. T.; Grantham, M.; Teng, H. H.; Dove, P. M.; DeYoreo, J. J., Formation of chiral morphologies through selective binding of amino acids to calcite surface steps. *Nature (London, U. K.)* **2001,** *411*, 775.
54. Davis, K. J.; Dove, P. M.; De Yoreo, J. J., The role of Mg^{2+} as an impurity in calcite growth. *Science* **2000,** *290* (5494), 1134-1137.
55. Teng, H. H.; Dove, P. M.; Orme, C. A.; De Yoreo, J. J., Thermodynamics of calcite growth: Baseline for understanding biomineral formation. *Science* **1998,** *282* (5389), 724-727.
56. Teng, H. H.; Chen, Y.; Pauli, E., Direction specific interactions of 1,4-dicarboxylic Acid with calcite surfaces. *J. Am. Chem. Soc.* **2006,** *128* (45), 14482-14484.
57. Mann, S.; Archibald, D. D.; Didymus, J. M.; Douglas, T.; Heywood, B. R.; Meldrum, F. C.; Reeves, N. J., Crystallization at inorganic-organic interfaces—Biominerals and biomimetic synthesis. *Science* **1993,** *261* (5126), 1286-1292.
58. Han, Y.-J.; Aizenberg, J., Effect of magnesium ions on oriented growth of calcite on carboxylic acid functionalized self-assembled monolayer. *J. Am. Chem. Soc.* **2003,** *125* (14), 4032-4033.
59. Kulp, E. A.; Switzer, J. A., Electrochemical biomineralization: The deposition of calcite with chiral morphologies. *J. Am. Chem. Soc.* **2007,** *129* (49), 15120-15121.
60. Jiang, W.; Pacella, M. S.; Athanasiadou, D.; Nelea, V.; Vali, H.; Hazen, R. M.; Gray, J. J.; McKee, M. D., Chiral acidic amino acids induce chiral hierarchical structure in calcium carbonate. *Nat. Commun.* **2017,** *8*, 15066.
61. Ono, S.; Brodholt, J. P.; Price, G. D., Phase transitions of $BaCO_3$ at high pressures. In *Mineral. Mag.*, 2008; Vol. 72, p 659.
62. Yu, S. H.; Cölfen, H.; Tauer, K.; Antonietti, M., Tectonic arrangement of $BaCO_3$ nanocrystals into helices induced by a racemic block copolymer. *Nat. Mater.* **2005,** *4*, 51-55.
63. John, J.; McKetta, J., Encyclopedia of Chemical Processing and Design. CRC Press: 1977.
64. Allen, B. F.; Faulk, N. M.; Lin, S. C.; Semiat, R.; Luss, D.; Richardson, J. T., A continous coprecipitation process for the production of 1-2-3 precursors. *AIChE Symp. Ser.* **1992,** *88*, 76-87.
65. Garcia-Ruiz, J. M., On the formation of induced morphology crystal aggregates. *J. Cryst. Growth* **1985,** *73* (2), 251-262.

66. García-Ruiz, J. M.; Amorós, J. L., Morphological aspects of some symmetrical crystal aggregates grown by silica gel technique. *J. Cryst. Growth* **1981,** *55* (2), 379-383.
67. Garcia-Ruiz, J. M.; Hyde, S. T.; Carnerup, A. M.; Christy, A. G.; Van Kranendonk, M. J.; Welham, N. J., Self-assembled silica-carbonate structures and detection of ancient microfossils. *Science* **2003,** *302* (5648), 1194-1197.
68. Voinescu, A. E.; Kellermeier, M.; Carnerup, A. M.; Larsson, A. K.; Touraud, D.; Hyde, S. T.; Kunz, W., Co-precipitation of silica and alkaline-earth carbonates using TEOS as silica source. *J. Cryst. Growth* **2007,** *306* (1), 152-158.
69. Bittarello, E.; Aquilano, D., Self-assembled nanocrystals of barium carbonate in biomineral-like structures. *Eur. J. Mineral.* **2007,** *19* (3), 345-351.
70. Carnerup, A. M.; Hyde, S. T.; Larsson, A.-K.; Christy, A. G.; Garcia-Ruiz, J. M., Silica-Carbonate biomorphs and the implications for identification of microfossils. In *Life in the Universe. Cellular Origin and Life in Extreme Habitats and Astrobiology,* Seckbach, J.; Chela-Flores, J.; Owen, T.; Raulin, F., Eds. Springer Netherlands: Dordrecht, 2004; pp 221-222.
71. Garcia-Ruiz, J. M., Carbonate precipitation into alkaline silica-rich environments. *Geology* **1998,** *26* (9), 843-846.
72. GarcÍa-Ruiz, J. M., Inorganic self-organisation in precambrian cherts. *Orig. Life Evol. Biosphere* **1994,** *24* (6), 451-467.
73. Hyde, S. T.; Garcia-Ruiz, J. M., Complex materials from simple chemistry: biomorphs and biomaterials. *Actual Chimique* **2004**, 4-6.
74. Noorduin, W. L.; Grinthal, A.; Mahadevan, L.; Aizenberg, J., Rationally designed complex, hierarchical microarchitectures. *Science* **2013,** *340* (6134), 832-837.
75. Hyde, S. T.; Carnerup, A. M.; Larsson, A. K.; Christy, A. G.; Garcia-Ruiz, J. M., Self-assembly of carbonate-silica colloids: Between living and non-living form. *Physica A* **2004,** *339* (1-2), 24-33.
76. Kellermeier, M.; Glaab, F.; Carnerup, A. M.; Drechsler, M.; Gossler, B.; Hyde, S. T.; Kunz, W., Additive-induced morphological tuning of self-assembled silica-barium carbonate crystal aggregates. *J. Cryst. Growth* **2009,** *311* (8), 2530-2541.
77. Terada, T.; Yamabi, S.; Imai, H., Formation process of sheets and helical forms consisting of strontium carbonate fibrous crystals with silicate. *J. Cryst. Growth* **2003,** *253* (1-4), 435-444.
78. Bittarello, E.; Massaro, F. R.; Aquilano, D., The epitaxial role of silica groups in promoting the formation of silica/carbonate biomorphs: A first hypothesis. *J. Cryst. Growth* **2010,** *312* (3), 402-412.
79. Kellermeier, M.; Melero-Garcia, E.; Glaab, F.; Eiblmeier, J.; Kienle, L.; Rachel, R.; Kunz, W.; Garcia-Ruiz, J. M., Growth behavior and kinetics of self-assembled silica-carbonate biomorphs. *Chem-Eur. J.* **2012,** *18* (8), 2272-2282.
80. Kellermeier, M.; Melero-Garcia, E.; Kunz, W.; Garcia-Ruiz, J. M., Local autocatalytic co-precipitation phenomena in self-assembled silica-carbonate materials. *J. Colloid Interface Sci.* **2012,** *380*, 1-7.
81. Eiblmeier, J.; Schurmann, U.; Kienle, L.; Gebauer, D.; Kunz, W.; Kellermeier, M., New insights into the early stages of silica-controlled barium carbonate crystallisation. *Nanoscale* **2014,** *6* (24), 14939-14949.
82. Nakouzi, E.; Ghoussoub, Y. E.; Knoll, P.; Steinbock, O., Biomorph oscillations self-organize micrometer-scale patterns and nanorod alignment waves. *J. Phys. Chem. C* **2015,** *119* (27), 15749-15754.
83. Opel, J.; Hecht, M.; Rurack, K.; Eiblmeier, J.; Kunz, W.; Cölfen, H.; Kellermeier, M., Probing local pH-based precipitation processes in self-assembled silica-carbonate hybrid materials. *Nanoscale* **2015,** *7* (41), 17434-17440.
84. Nakouzi, E.; Knoll, P.; Hendrix, K. B.; Steinbock, O., Systematic characterization of polycrystalline silica-carbonate helices. *Phys. Chem. Chem. Phys.* **2016,** *18* (33), 23044-23052.

85. Nakouzi, E.; Steinbock, O., Self-organization in precipitation reactions far from the equilibrium. *Sci. Adv.* **2016,** *2* (8).
86. Montalti, M.; Zhang, G.; Genovese, D.; Morales, J.; Kellermeier, M.; Garcia-Ruiz, J. M., Local pH oscillations witness autocatalytic self-organization of biomorphic nanostructures. *Nat. Commun.* **2017,** *8*.
87. Opel, J.; Kellermeier, M.; Sickinger, A.; Morales, J.; Cölfen, H.; Garcia-Ruiz, J. M., Structural transition of inorganic silica-carbonate composites towards curved life-like morphologies. *Minerals-Basel* **2018,** *8* (2).
88. Zhang, G.; Morales, J.; Garcia-Ruiz, J. M., Growth behaviour of silica/carbonate nanocrystalline composites of calcite and aragonite. *J. Mater. Chem. B* **2017,** *5* (8), 1658-1663.
89. Nakouzi, E.; Fares, H. M.; Schlenoff, J. B.; Steinbock, O., Polyelectrolyte complex films influence the formation of polycrystalline micro-structures. *Soft Matter* **2018,** *14* (16), 3164-3170.
90. Kunz, W.; Kellermeier, M., Materials science beyond biomineralization. *Science* **2009,** *323* (5912), 344-345.
91. Garcia-Ruiz, J. M.; Melero-Garcia, E.; Hyde, S. T., Morphogenesis of Self-assembled nanocrystalline materials of barium carbonate and silica. *Science* **2009,** *323* (5912), 362-365.
92. Melero-Garcia, E.; Santisteban-Bailon, R.; Garcia-Ruiz, J. M., Role of bulk pH during witherite biomorph growth in silica gels. *Cryst. Growth Des.* **2009,** *9* (11), 4730-4734.
93. Eiblmeier, J.; Kellermeier, M.; Rengstl, D.; Garcia-Ruiz, J. M.; Kunz, W., Effect of bulk pH and supersaturation on the growth behavior of silica biomorphs in alkaline solutions. *Crystengcomm* **2013,** *15* (1), 43-53.
94. Kellermeier, M.; Eiblmeier, J.; Melero-Garcia, E.; Pretzl, M.; Fery, A.; Kunz, W., Evolution and control of complex curved form in simple inorganic precipitation systems. *Cryst. Growth Des.* **2012,** *12* (7), 3647-3655.
95. Kellermeier, M.; Cölfen, H.; Garcia-Ruiz, J. M., Silica biomorphs: complex biomimetic hybrid materials from "sand and chalk". *Eur. J. Inorg. Chem.* **2012,** (32), 5123-5144.
96. Kaplan, C. N.; Noorduin, W. L.; Li, L.; Sadza, R.; Folkertsma, L.; Aizenberg, J.; Mahadevan, L., Controlled growth and form of precipitating microsculptures. *Science* **2017,** *355* (6332), 1395-1398.
97. Imai, H.; Terada, T.; Miura, T.; Yamabi, S., Self-organized formation of porous aragonite with silicate. *J. Cryst. Growth* **2002,** *244* (2), 200-205.
98. Kellermeier, M.; Melero-Garcia, E.; Glaab, F.; Klein, R.; Drechsler, M.; Rachel, R.; Garcia-Ruiz, J. M.; Kunz, W., Stabilization of amorphous calcium carbonate in inorganic silica-rich environments. *J. Am. Chem. Soc.* **2010,** *132* (50), 17859-17866.
99. Bittarello, E.; Massaro, F. R.; Rubbo, M.; Costa, E.; Aquilano, D., Witherite ($BaCO_3$)/alpha-quartz epitaxial nucleation and growth: Experimental findings and theoretical implications on biomineralization. *Cryst. Growth Des.* **2009,** *9* (2), 971-977.
100. Physics, A. I. O. Mind-blowing giant crystals-what can they teach us? https://phys.org/news/2014-08-mind-blowing-giant-crystalswhat.html (accessed June 03, 2019).
101. McCoy, H. N.; Smith, H. J., Equilibrium between alkali-earth carbonates, carbon dioxide and water. *J. Am. Chem. Soc.* **1911,** *33* (4), 468-473.
102. Kids, N. G. Narwhal. https://kids.nationalgeographic.com/animals/narwhal/#narwhal_pod.jpg (accessed January 01, 2017).
103. Addadi, L.; Moradian, J.; Shay, E.; Maroudas, N. G.; Weiner, S., A chemical model for the cooperation of sulfates and carboxylates in calcite crystal nucleation: Relevance to biomineralization. *Proc. Natl. Acad. of Sci.* **1987,** *84* (9), 2732-2736.
104. Holtus, T.; Helmbrecht, L.; Hendrikse, H. C.; Baglai, I.; Meuret, S.; Adhyaksa, G. W. P.; Garnett, E. C.; Noorduin, W. L., Shape-preserving transformation of carbonate minerals into lead halide perovskite semiconductors based on ion exchange/insertion reactions. *Nat. Chem.* **2018,** *10* (7), 740-745.

105. Thiruvengadathan, R.; Korampally, V.; Ghosh, A.; Chanda, N.; Gangopadhyay, K.; Gangopadhyay, S., Nanomaterial processing using self-assembly-bottom-up chemical and biological approaches. *Rep. Prog. Phys.* **2013,** *76* (6), 066501.
106. Friedman, R. S.; McAlpine, M. C.; Ricketts, D. S.; Ham, D.; Lieber, C. M., Nanotechnology: high-speed integrated nanowire circuits. *Nature (London, U. K.)* **2005,** *434* (7037), 1085.
107. Khang, D.-Y.; Jiang, H.; Huang, Y.; Rogers, J. A., A Stretchable form of single-crystal silicon for high-performance electronics on rubber substrates. *Science* **2006,** *311* (5758), 208.
108. López, C., Materials aspects of photonic crystals. *Adv. Mater.* **2003,** *15* (20), 1679-1704.
109. Ozin, G. A.; Hou, K.; Lotsch, B. V.; Cademartiri, L.; Puzzo, D. P.; Scotognella, F.; Ghadimi, A.; Thomson, J., Nanofabrication by self-assembly. *Mater. Today* **2009,** *12* (5), 12-23.
110. Songmuang, R.; Rastelli, A.; Mendach, S.; Schmidt, O. G.; D., H. K.; L., T.; P., D. S.; M., F. P., SiO*x*/Si radial superlattices and microtube optical ring resonators. *Appl. Phys. Lett.* **2007,** *90* (9), 091905.
111. Lee, J.-H.; Koh, C. Y.; Singer, J. P.; Jeon, S.-J.; Maldovan, M.; Stein, O.; Thomas, E. L., 25th Anniversary article: Ordered polymer structures for the engineering of photons and phonons. *Adv. Mater.* **2014,** *26* (4), 532-569.
112. Schumann, M.; Bückmann, T.; Gruhler, N.; Wegener, M.; Pernice, W., Hybrid 2D–3D optical devices for integrated optics by direct laser writing. *Light Sci. Appl.* **2014,** *3*, e175.
113. Ahn, B. Y.; Duoss, E. B.; Motala, M. J.; Guo, X.; Park, S.-I.; Xiong, Y.; Yoon, J.; Nuzzo, R. G.; Rogers, J. A.; Lewis, J. A., Omnidirectional printing of flexible, stretchable, and spanning silver microelectrodes. *Science* **2009,** *323* (5921), 1590.
114. Huang, W.; Yu, X.; Froeter, P.; Xu, R.; Ferreira, P.; Li, X., On-chip inductors with self-rolled-Up SiNx nanomembrane tubes: A novel design platform for extreme miniaturization. *Nano Lett.* **2012,** *12* (12), 6283-6288.
115. Abbott, L. C.; Batchelor, S. N.; Jansen, L.; Oakes, J.; Lindsay Smith, J. R.; Moore, J. N., Spectroscopic studies of Direct Blue 1 in solution and on cellulose surfaces: Effects of environment on a bis-azo dye. *New J. Chem.* **2004,** *28* (7), 815-821.
116. Abbott, L. C.; Batchelor, S. N.; Oakes, J.; Lindsay Smith, J. R.; Moore, J. N., Spectroscopic studies of the intermolecular interactions of a bis-azo dye, Direct Blue 1, on di- and trimerization in aqueous solution and in cellulose. *J. Phys. Chem. B* **2004,** *108* (36), 13726-13735.
117. Polarz, S.; Dilger, S., Chemical architectonics for complex inorganic materials. In *BioInorg. Reac. Mech.*, 2011; Vol. 7, p 27.
118. Studart, A. R., Towards high-performance bioinspired composites. *Adv. Mater.* **2012,** *24* (37), 5024-5044.
119. Davies, P. L., Ice-binding proteins: A remarkable diversity of structures for stopping and starting ice growth. *Trends Biochem. Sci.* **2014,** *39* (11), 548-555.